Design and Construction of Turboexpander based Nitrogen Liquefier

A Thesis Submitted for Award of the Degree of

Doctor of Philosophy

Balaji Kumar Choudhury

Mechanical Engineering Department
National Institute of Technology
Rourkela 769008

Dedicated to my

PARENTS

NATIONAL INSTITUTE OF TECHNOLOGY

ROURKELA, INDIA

Ranjit Kr Sahoo
Professor
Mechanical Engg. Department
NIT Rourkela

Sunil Kr Sarangi
Director
NIT Rourkela

CERTIFICATE

Date: Dec 24, 2013

This is to certify that the thesis entitled "**Design and Construction of Turboexpander based Nitrogen Liquefier**", being submitted by **Shri Balaji Kumar Choudhury** for the award of the degree of **Doctor of Philosophy** in Mechanical Engineering, is a record of bonafide research carried out by him at Mechanical Engineering Department, National Institute of Technology, Rourkela, under our guidance and supervision. The work incorporated in this thesis has not been, to the best of our knowledge, submitted to any other university or institute for the award of any degree or diploma.

(Ranjit Kr Sahoo) (Sunil Kr Sarangi)

Acknowledgement

I am extremely fortunate to be involved in an exciting and challenging research project like "**Design and Construction of Turboexpander based Nitrogen Liquefier**". I have got an opportunity to look at the horizon of technology with a wide view and to come in contact with people endowed with many superior qualities.

At First, I would like to express my deep sense of gratitude and respect to my supervisors Prof. R. K. Sahoo and Prof. S. K. Sarangi for their excellent guidance, suggestions and constructive criticism. I feel proud that I am one of their doctoral students. I will always remember their helping hands and moral support in my good and evil day during this period. The charming personality of Prof. Sarangi has been unified perfectly with knowledge that creates a permanent impression in my mind. I am very much inspired by the patience and confidence of Prof. R. K. Sahoo which will be fruitful throughout my life. He also encouraged and stay with me during the period of testing and commissioning of the plant. Without him I could not get confidence to do experiment. I and my family members also remember the affectionate love and kind support extended by Madam Sahoo and Madam Sarangi during our stay at Rourkela.

I take this opportunity to express my sincere gratitude to the members of my doctoral scrutiny committee – Prof. K. P. Maity (HOD), Prof. A. K. Satatpathy, Prof. S. Murugan of Mechanical Engineering Department and Prof. R. K. Singh of Chemical Engineering Department for thoughtful advice and useful discussions. I am thankful to prof. S. C. Mohanty, Prof. A. Satapathy and my other professors of the Mechanical Engineering Department for constant encouragement and support in pursuing the Ph.D. work.

I am indebted to Mr. Tilok Singh, Mr. Mukesh Goyal, Dr. Anindya Chhakravarty, Mr. Rajendran S. Menon, Mr. Sandeep Nair of Cryogenic Division of Bhabha Atomic Research Centre, Mumbai, for sharing their vast experience and provide kind support regarding liquefaction plant and especially turboexpander. I am very much thankful to Mr. N. Siva Rama Krishna and Mr. A. K. Pradhan of Central Tool Room and Training Center, Bhubaneswar for understanding the requirements for fabricating the turboexpander.

I take this opportunity to express my heartfelt gratitude to Mr. Somnath Das and Mr. Binaya kumar Kar for his cooperation and technical support to build the plant. Beside them I am also grateful towards Mr. Jyana Ranjan Nayak, Mr. Naren Bisoi and Mr. Pradeep kumar Mohanty for providing technical helping hand and Mr. H. Barkey for assistance in official matters.

I record my appreciation and thanks for the helping hand extended by Dr. Sidramappa Alur during my research work. I feel lucky to have Mr. Sachindra Kumar Rout as my co-research fellow. I am also thankful to my friends Sanjay Kumar Swain, Pankaj Kumar, Ajay kumar Gupta for their friendship during my stay at NIT Rourkela.

Thanks goes to my parents Sri Rajmohan Choudhury and Smt. Rajeswari Choudhury, my brother Mr. Saroj kumar Choudhury, my sister in law Mrs. Mamata Choudhury, my sisters and other relatives for their loving support and encouragement for my PhD study. I am most grateful to my beloved wife Mrs. Prachetasi Choudhury for her loving support and coperation. I am happy with my daughter Padmini for not disturbing during my PhD work.

(December 24, 2013) Balaji Kumar Choudhury

Abstract

Cryogenic refrigerators are becoming increasingly popular particularly in the areas of superconducting magnet applications, particle accelerators and medical imaging systems, etc. It has also got wide applications in preservation of live biological materials as well as in scientific equipment. In spite of nearly half a century of R & D experience, our country is still dependent on imports for most of its needs in cryogenic refrigerators and liquefiers. These components are enormously expensive to buy and to maintain. The customers are often forced to buy equipment due to non-availability of proprietary spares. It is imperative that our country develops an indigenous nitrogen liquefier of capacity in the range 10 to 50 litre/hour. With the support from the Department of Atomic Energy, our institute has initiated a programme on development and study of a turboexpander based nitrogen liquefier of intermediate capacity (20 l/h). The focus of this project is to build a turbine based liquid nitrogen generator of capacity 20 l/h using indigenous technology. This technology and expertise will be extended for the liquefaction of helium in future.

The development of the turboexpander based nitrogen liquefier begins with the process design of the cycle. The simulation of the cycles has been done using the software Aspen HYSYS. All the state points are fixed and each equipment specifications are determined. While designing the process, equipment availability, constraints and cost is to be kept in mind. Process design also includes the setting the parameters up to the optimum condition so that maximum amount of liquid will be obtained. After process design the thermodynamics parameters of all the components are available.

As per process the nitrogen gas is compressed in the compressor upto 8 bar. The compressed gas passes through the first heat exchanger. Some amount of the gas is diverted through the turboexpander and remaining gas flow through the second heat exchanger. A JT valve is used to expand the liquid which is collected in the phase separator at a pressure just above ambient (1.2 bar). The vapour comes out of phase separator mixes with the cold gas from the turboexpander and the resultant stream meets at the suction side of the compressor, after passing through the second and first heat exchanger as the reversed stream.

The compressor unit is available in the laboratory which will discharge 336 nm^3/hr of air and maximum working pressure is 10 bar. This is an oil injected twin screw compressor.

Heat exchanger is a necessary component. Due to the requirement of high effectiveness, two number of aluminum brazed plate fin heat exchangers are used. The design of heat exchanger has been done using the software Aspen MUSE and also by using the correlations by Maiti and Sarangi and Manglik and Bergles considering the size and pressure drop as per the need of the process. The fabrication of the plate fin heat exchangers has been done by APOLLO HEAT EXCHANGERS Pvt. Ltd.

The turboexpander is a vital component for the liquefier. Because it helps to further lower down the temperature. A general design procedure is developed which will able to design turboexpander with all pressure ratios. At first the turbine wheel is designed followed by design of nozzles, diffuser, shaft, brake compressor, bearings and other housing components. The fabrication of turbine wheel and brake compressor wheel has been done by TURBOCAM Pvt. Ltd., Goa and rest of components has been done by Central Tool and Training Center, Bhubaneswar.

The JT valve is also necessary for isenthalpic expansion. A suitable modification has been done with a precession needle valve to operate as long stem JT valve. A phase separator is designed and fabricated to separate the liquid nitrogen. All the components are hanged inside a double walled vacuum insulated cold box.

The necessary pressure, temperature and flow measurement instruments are mounted on the node points. Valves and safety devices are mounted on the liquefier. Arrangement has been done to supply the gaseous nitrogen to the liquid nitrogen plant from a liquid nitrogen tank through a LN2 vaporizer and a gas bag. After successful running of the liquefier, for the flow rate 336 nm^3/hr of gaseous nitrogen, it will delivers 17.44 lit/hr of liquid.

Contents

List of Figures

Page No.

List of Tables

Page No.

Nomenclature

a_{ff} = Free flow area/fin (m^2)

a_{fr} = Frontal area/fin (m^2)

a_f = Fin surface area (m^2)

a_s = Heat transfer area/fin (m^2)

a_p = Plate thickness (m)

a_w = Total wall cross sectional area for longitudinal conduction (m2)

A_{fr} = Frontal area available for heat exchanger (m^2)

A_{ff} = Free flow area available for heat exchanger (m^2)

A_s = Heat transfer area of the heat exchanger (m^2)

A_w = Total wall area for transverse heat conduction (m^2)

A = cross sectional area normal to flow direction (m^2)

b = height (nozzle, wheel blade) (m)

b_p = distance between heat exchanger plates (m)

C_n = chord length of nozzle (m)

C = absolute velocity of fluid stream (m/s)

C_0 = spouting velocity (m/s)

C_d = Coefficient of discharge (dimensionless)

C_p = specific heat at constant pressure (J/kg K)

C_s = velocity of sound (m/s)

C_h = heat capacity rate hot side of heat exchanger (W/K)

C_c = heat capacity rate cold side of heat exchanger (W/K)

C_{min} = Minimum of hot and cold capacity ratio (W/K)

C_r = Heat capacity rate ratio (dimensionless)

d = diameter (shaft) (m)

d_s = specific diameter (dimensionless)

D = diameter (m)

D_e = Equivalent diameter of the flow passage (m)

E = Young's modulus (N/m^2)

f_q = vibration frequency (Hz)

f = Fanning friction factor (dimensionless)

f_f = Fin frequency, Number of fins per meter length (fins/m)

G = Core mass velocity (kg/m^{2}s)

h = enthalpy (J/kg)

h_f = Height of fins (m)

h_{conv} = Convective heat transfer coefficient (W/m^2 K)

H_{hx} = No flow height (stack height) of the heat exchanger core (m)

j = The Colburn factor (dimensionless)

k_1 = Pressure recovery factor (dimensionless)

k_2 = Temperature and Density recovery factor (dimensionless)

K_f = Conductivity of the fin material (W/m- K)

K_w = Conductivity of the wall material (W/m- K)

M = Mach number (dimensionless)

$\dot{m}$ = mass of nitrogen delivered from compressor (kg/s)

$\dot{m}_f$ = Rate of mass of liquid nitrogen produced (kg/s)

$\dot{m}_{tr}$ = mass of nitrogen gas diverted through turboexpander (kg/s)

N = Rotational speed (rpm)

n_s = specific speed (dimensionless)

n_l = Total number of layers or total number of fluid passages (dimensionless)

N_{tu} = Number of heat transfer units, $UA / C_{\min}$ (dimensionless)

L_{hx} = Fluid flow (core) length on one side of the heat exchanger (m)

l_f = Fin flow length on one side of a heat exchanger (m)

P = power output of the turbine (W)

p = pressure (N/m^2)

Δp = Pressure drops (Pa)

p_f = Fin pitch (m)

pr = Prandtl number of the fluid (dimensionless)

Q = volumetric flow rate (m^3/s)

Q_H = Heat load (W)

R = Gas constant of the working fluid (J/kg K)

r = Radius (m)

Re = Reynolds number (dimensionless)

Re^* = Critical Reynolds number (dimensionless)

s = Specific entropy (J/kg K)

s_f = Spacing between adjacent fins (m)

t_f = Thickness of fin (m)

T = Temperature (K)

t = Blade thickness (m)

U = Blade velocity (in tangential direction) (m/s)

U_o = Overall heat transfer coefficient ($W/m^2 K$)

x = dryness fraction (dimensionless)

W = velocity of fluid stream relative to blade surface (m/s)

w_n = nozzle width (m)

W_{hx} = Width of the core (m)

y = yield, mass of liquid produced per mass of gas compressed (dimensionless)

Z = number of blades (dimensionless)

Greek symbols

α = absolute velocity angle (radian)

α_t = throat angle (radian)

α_0 = inlet flow angle (radian)

α_{tr} = mass fraction of nitrogen diverted through turboexpander (dimensionless)

β = relative velocity angle (radian)

γ = specific heat ratio (dimensionless)

ε = Effectiveness of heat exchanger (dimensionless)

μ = dynamic viscosity (Pa s)

ρ = density (kg/m^3)

ω = rotational speed (rad/s)

θ = tangential coordinate (dimensionless)

ξ = Inlet turbine wheel diameter to exit tip diameter ratio (dimensionless)

λ_{tr} = Hub diameter to tip diameter ratio (dimensionless)

λ = Longitudinal conduction parameter, dimensionless

σ = Ratio of free flow area to frontal area (dimensionless)

η = Isentropic efficiency (dimensionless)

η_{T-st} = total-to-static efficiency (dimensionless)

η_{T-T} = total-to-total efficiency (dimensionless)

η_f = Fin efficiency (dimensionless)

η_o = Overall surface effectiveness of the extended fin surfaces (dimensionless)

Subscripts

0 = stagnation condition

ad = adiabatic

m = meridional direction

r = radial direction

s = isentropic

t = throat

tr = turbine

θ = tangential direction

w = Wall or properties at the wall temperature

h = Hot fluid side

c = Cold fluid side

i = Inlet

o = Outlet

m = mean

max = Maximum

min = Minimum

hub = hub of turbine wheel at exit

tip = tip of turbine wheel at exit

mean = average of tip and hub

Chapter I

Introduction

1.1 Cryogenic refrigeration and liquefaction

The literal meaning of "cryogenics" is production of icy cold or low temperature. A logical dividing line has chosen by the workers at National Bureau of Standards at Boulder, Colorado for the field of cryogenics is below 123 K. The normal boiling points of the permanent gases, such as oxygen, air, nitrogen, neon, hydrogen, helium lie below 123 K.

In a thermodynamic process when the process fluid absorbs heat at temperatures below that of the environment is called refrigeration. Liquefaction of gases is always accomplished by refrigerating the gas to the temperature below its critical temperature so that liquid can be formed at some suitable pressure below the critical pressure. Thus gas liquefaction is a special case of gas refrigeration and cannot be separated from it. In both cases, the gas is first compressed to an elevated pressure in an isothermal compression process. This high-pressure gas is passed through a countercurrent recuperative heat exchanger to a throttling valve or expansion engine. Upon expanding to the lower pressure, cooling takes place, and leads to formation of liquid. The cold, low-pressure gas returns to the compressor inlet to repeat the cycle. The purpose of the countercurrent heat exchanger is to warm the low-pressure gas prior to recompression and simultaneously it cools the high-pressure gas to the lowest temperature possible prior to expansion. Both refrigerators and liquefiers operate on this basic principle.

There is no accumulation of refrigerant in any part of the system in a continuous refrigeration process. But in a gas liquefying system, the liquid accumulates and is withdrawn. Thus, in a liquefying system, the total mass of gas that is warmed in the

countercurrent heat exchanger is less than that of the gas to be cooled by an amount liquefied, creating an imbalance of mass flow in the heat exchanger. In a refrigerator the warm and cool gas flows are equal, creating a balanced flow in the heat exchanger. The thermodynamic principles of refrigeration and liquefaction are identical. However the analysis and design of the two systems are quite different because of the condition of balanced flow in the refrigerator and unbalanced flow in liquefier systems.

1.2 Methods to produce low temperatures

Based on the method of production of low temperature, cryogenic refrigeration and liquefaction cycles can be grouped under three broad categories.

(i) Process with J-T valve.

(ii) Process with expansion engine or turbine.

(iii) Process with regenerative cycles.

(i) Process with J-T valve

The most usual process for production of low temperature is isenthalpic process by using JT Valves. The operation of JT valve depends upon Joule-Thomson coefficient which is a gas property. It is the effect of change in temperature with change in pressure under constant enthalpy. The Joule-Thomson coefficient can be expressed as,

$$\mu_{JT} = \left(\frac{\partial T}{\partial p} \right)_h \tag{1.1}$$

It is a function of temperature and pressure. The isenthalpic curves are shown in Figure 1-1. The slope of the curve gives the Joule-Thomson coefficients and this may be positive, negative, or zero. When Joule-Thomson coefficient is zero, then that point is called inversion point. The locus of such points different enthalpy forms the inversion curve. The area inside the inversion curve gives cooling effect by isenthalpic expansion while area outside the inversion curve has reverse effect. The Table 1-1 gives the maximum inversion temperature of some cryogenic fluids. Nitrogen has maximum inversion temperature of 622 K which is well above atmospheric temperature. So for nitrogen, JT valve can be used at atmospheric conditions to decrease its temperature. But for neon, hydrogen and helium, the JT valve can only be used if their temperature has cooled below to their inversion temperature by using

other precooling methods. Vapor compression cycle, cascade vapor compression cycle, Mixed refrigerant cascade cycle, Linde cycle etc., are the examples which uses only J-T Valve as expansion device.

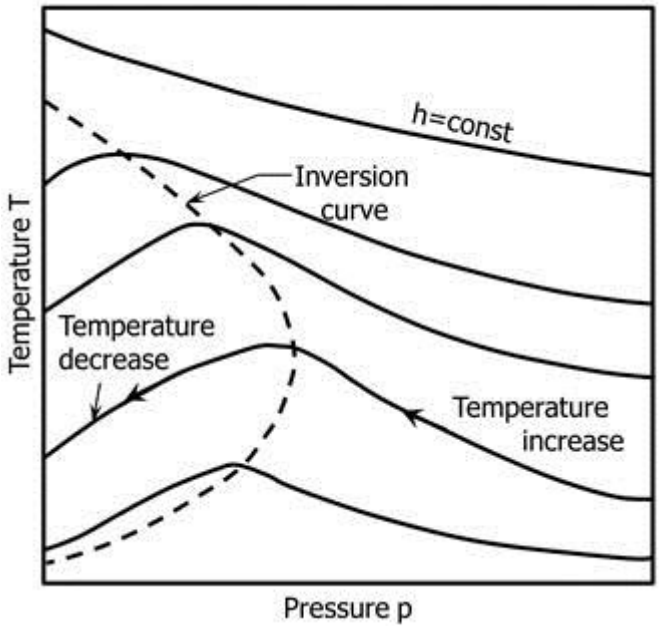

Figure 1-1 Joule Thomson inversion curve [1]

Table 1-1 Maximum Inversion Temperature of Cryogenic Fluids

Fluid	Maximum inversion temperature (K)
Oxygen	761
Argon	722
Nitrogen	622
Air	603
Neon	250
Hydrogen	202
Helium	40

(ii) Process with expansion engine or turbine

Another method of producing low temperatures is the adiabatic expansion of the gas through a work-producing device such as an expansion engine. In the ideal case, the expansion would be reversible and adiabatic and therefore isentropic. In this case, one can define the isentropic expansion

coefficient which expresses the temperature change due to a pressure change at constant entropy. The isentropic expansion process removes energy from the gas in the form of external work, so this method of low-temperature production is sometimes called the external work method.

In any liquefier, the expansion engine or turbine could not be used alone without J-T valve. Because it is difficult to produce wet expansion turbine but a J-T Valve could handle two phase easily. Therefore most cycles use combination of both the expansion methods. Claude cycle, Brayton cycle, Kapitza cycle, Heylandt cycle, Collins cycle are using both J-T valve and expansion turbine for refrigeration and liquefaction.

(iii) Process with regenerative cycles

The Process uses regenerative type of heat exchanger. The regenerative type of heat exchanger has single set of flow passages through which hot and cold fluid passes alternately and continuously. Refrigerators and liquefiers with regenerative heat exchangers are Stirling, Pulse tube, Gifford-McMahon etc. This class of cycle uses working fluid such as helium and a condenser for refrigeration/liquefaction of gases including helium.

1.3 Turboexpander

Generally, the word **"Turboexpander"** is used to define an expander and a compressor as a single unit. It consists two primary components i.e., radial or mixed flow expansion turbine wheel and a centrifugal compressor wheel. Both the wheels are connected by a single shaft as shown in Figure 1-2. The high pressure process gas flows through the turbine wheel to produce power and cause rotation of the shaft by the expense of the kinetic energy. The centrifugal compressor acts as a loading device and is used to extract work output of the turbine. Generally, the shaft is mounted in vertical orientation to reduce the radial load on the bearings. Two number of radial journal and two number of axial thrust bearings are used to keep the shaft in proper alignment and to absorb the radial and axial load.

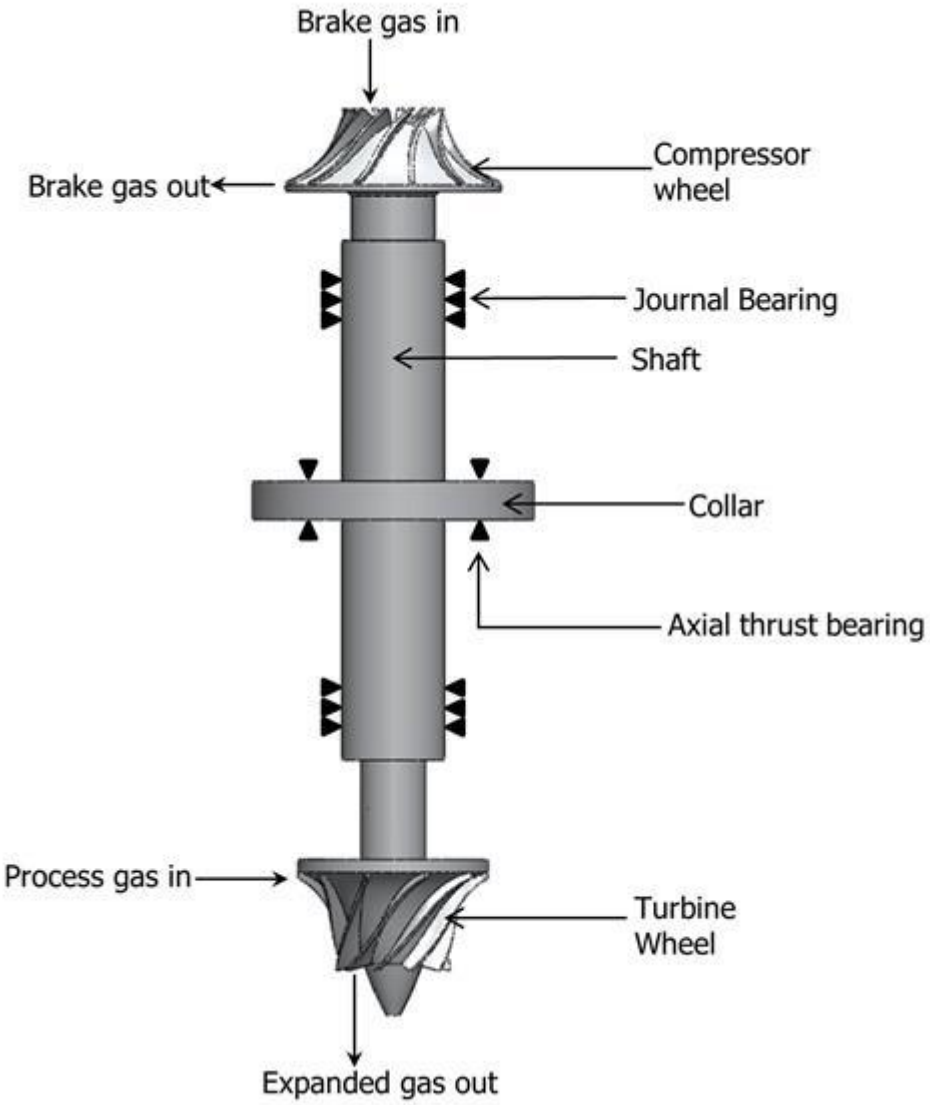

Figure 1-2 Shaft with brake compressor and turbine wheel

1.4 Requirement of liquid nitrogen

In 1772, David Rutherford discovered the chemical element nitrogen. It is a colourless, odourless, tasteless and unreactive gas. It is the most abundant gas in the air and constitutes 78% of air.

The liquid nitrogen have low production cost and relatively higher levels of safety, it is the most common cooling medium in the cryogenic temperature range above 77 K. The application covers such diverse areas as:

(i) Pre coolant: The liquid nitrogen has low temperature up to 77 K. So it is used for precooling the helium to bring the temperature of helium down. After lowering the temperature it is used in any usual cycle to produce liquid

helium. It is not only used for precooling helium but also for other gases like hydrogen, Neon etc.

(ii) Coolant: Due to its very low temperature it is used as a coolant in many industrial, medical and laboratory instruments. In NMR for Medical imaging system it is used as coolant.

(iii) Cryo-treatment: The process of treating the metals at cryogenic temperature is known as cryo-treatment. Metallic components such as hubs, milling cutters, knives, rollers, needles, dies and punches, bearings and precision measuring equipment undergo cryo-treatment for advancement of mechanical properties. The cryo-treatment renders improved mechanical properties, such as longer life, less failure due to cracking, improved thermal properties, better electrical properties with less electrical resistance, reduced coefficient of friction, improved flatness, fine grain structure etc.

(iv) Cryo-Preservation: Preservation of live biological material such as blood, animal and human sperms, embryos, bacterial cultures etc. using liquid nitrogen is known as cryo-preservation. It is the safest method for preservation that can be freezed up to one decade.

(v) Shrink fitting and Press freeing: It is a cost efficient method of assembling and disassembling new and replacement of fine tolerance components. The components with fine tolerance can be assembled by putting the parts inside liquid nitrogen. Due to low temperature it will shrink a little and then it may be fitted with another part.

(vi) When a component is press-jammed, then liquid nitrogen can be used to freeing the jam. It saves the production halt time, money and save the component.

(vii) Cryotherapy: As liquid nitrogen has extreme cold temperature, any cells that are touched by it will be instantly frozen. After freezing cells will die and fall off. This allows liquid nitrogen to be an effective treatment for wart removal or the removal of small skin cancers. Cryosurgery also done by using the liquid nitrogen.

(viii) Food preparation and preservation: There are a number of dishes could be made using liquid nitrogen. Quick ice could be made from liquid nitrogen. The foods are stored using liquid nitrogen.

(ix) Cold trap in vacuum systems and in adsorption pumps

(x) It is used as low temperature dielectric and susceptibility measurement. Due to its inertness property and low temperature, it is used in many chemical applications. Apart from this it has miscellaneous laboratory and industrial applications.

1.5 Objective of the work

Cryogenic refrigeration and liquefaction plants are enormously expensive to buy and to maintain and owners are often forced to buy new plants due to non-availability of proprietary spares. It is the need of our country to develop an indigenous nitrogen liquefier of capacity in the range 10 to 50 litres/hour.

With the support from the Department of Atomic Energy, National Institute of Technology, Rourkela has initiated a programme on development of turboexpander based cryogenic refrigerator and liquefier of capacity in the range of 10 to 50 liters/hour. The objectives of this work are as follows:

(i) Process design and freezing the process parameters based on aspen software.
(ii) Design and fabrication of major components such as plate fin heat exchanger, turboexpander, JT Valve etc.
(iii) Assembly of the nitrogen liquefier by connecting with pipelines and mounting with safety and measuring instruments.
(iv) Commissioning and performance study of the liquefier.
(v) Proper documentation of the components design with fabrication and assembly drawing.

1.6 Organization of the thesis

The thesis has been arranged in eight chapters and appendices. Chapter I deal with a general introduction to cryogenic refrigeration and liquefaction processes. The methods to obtain the cryogenic temperatures along with general cryogenic cycles are described. It shows the properties of nitrogen and focuses the requirement of liquid nitrogen and finally it defines the objective of the present work.

Chapter II is the literature review part of the thesis. It describes history of cryogenic liquefaction and development of turboexpander. It points out some major

suppliers of liquid nitrogen plants. It also focuses on the process design techniques, thermodynamic equations for plant performance.

Chapter III presents process design of the turboexpander based nitrogen liquefaction cycles with optimum state points and component specification. These state points and component specification are used for the design of other components.

Chapter IV includes the design of two plate fin heat exchangers as per the requirement for the nitrogen liquefaction plant. The design of the heat exchangers is made by following a general design procedure using different corelations available in open literature. In addition Aspen MUSE software is used to validate the dimensions and pressure drop.

Chapter V comprises with the design of the turboexpander. It consists of the design of turbine wheel, nozzle, diffuser, shaft, brake compressor, bearings and supporting components.

Chapter VI illustrates the fabrication of remaining components used in the liquefier. It also covers assembly of the fabricated components and instrumentation. Chapter VII shows testing performance of the turboexpander. It also includes operation and performance study of the liquid nitrogen plant.

Chapter VIII presents the concluding remarks and recommendation for future work. And finally references are presented which utilized to develop the turboexpander based nitrogen liquefaction plant. It consists of appendices which contain fabrication drawings and photographs of the turboexpander parts, heat exchanger and other components of the plant.

Chapter II

Literature Review

2.1 Introduction

The chapter describes the innovation of gas liquefaction techniques and focuses on the chronological development of cryogenic liquefaction plants. The commonly used components in the liquefaction plant are turboexpander and heat exchanger. So the development and use of turboexpander in the cryogenic liquefaction plants are described. This chapter also explains the type of heat exchangers used for cryogenic application and their design methods. This chapter also emphasizes on the process cycle design methods and software for process simulation. It also highlights some major cryogenic industries for supplying liquefaction plants.

2.2 Liquefaction of gases

Wolfgang [2] reported the history of liquefaction of common gases as well as the permanent gases. For the first time, at around 1780 Louis Clouet and Gaspard Monge was successfully liquefied a real gas (SO_2) by compressing and cooling. After the liquefaction of SO_2, Ammonia gas was liquefied by Martinus van Marum and Adriaan Paets van Troostwijk in 1787. But Fourcroy and Vauquelin was able to liquefy ammonia at ambient pressure in 1799 and Guyton de Morveau in 1804. In 1823, Michael Faraday published the liquefaction techniques of SO_2, H_2S, CO_2, N_2O , C_2H_2, NH_3 and HCl. Again in 1845, Faraday had published his second paper regarding gas liquefaction. At that time Faraday had much better equipment to compress the gases up to 40 bar and using refrigerating bath to liquefy them to -110 °C. By using this technique he was able to liquefy a number of gases. But he was unable to liquefy CH_4, O_2, CO, N_2, NO and H_2. Those gases were, therefore, called "permanent gases". The Viennese physician

Johannes Natterer tried to liquefy the permanent gases by compressing them up to 360 bar but unable to lower the temperature simultaneously below the critical temperature.

2.3 Cryogenic liquefaction

The general information about the cryogenic liquefaction are available in standard text books [1, 3-5]. A brief history of cryogenics has been described by Scurlock [6] in 1989.

In 1877, Louis Cailletet in Paris and at the same time Raoul Pictet in Geneva attempted to liquefy "permanent" gases. Louis Cailletet had compressed oxygen gas with a hand operated screw jack up to 200 bar and then cooled to -110° C by enclosing the strong walled glass tube apparatus with liquid ethylene. Suddenly it was expanded by releasing the pressure, he observed a momentary fog of oxygen droplets inside the glass tube. Raoul Pictet had used the cascaded refrigeration system to liquefy oxygen. He used sulphur dioxide and liquid carbon dioxide in the heat exchanger to cool the oxygen gas. He used two numbers of compressors to drive sulphur dioxide and carbon dioxide. The gas was expanded by opening the valve at the end of heat exchanger. By doing so a transitory jet of liquid oxygen was formed. But both were unable to collect the liquid oxygen.

In 1883, further improvement Cailletet's apparatus had been done by the Polish scientists Olzewski and Wroblewski, at Cracow. They added an inverted U glass tube and reduced the ethylene temperature to - 136°C by pumping it below atmospheric pressure. These modifications enabled them to produce small quantities of liquid oxygen in the U tube and to liquefy carbon monoxide and nitrogen for a few seconds. But this production of oxygen was discontinuous and the quantities of liquid produced were still very small.

In 1895 the air was liquefied by Carl von Linde in Munich and William Hampson in London. Air was compressed up to 200 bar and cooled to ambient temperature using water cooler. The precooled air was fed into counter flow coiled heat exchanger. Linde has achieved isenthalpic expansion by utilizing the Joule-Thomson effect from a JT-valve. After expansion, liquid was collected but it took three days to cool down the system and achieve steady-state. The yield of the air liquefier is approximately 3 liters per hour. William Hampson had also achieved the success of liquefaction in the same

year in the similar process of Linde. He gave license to Brins Oxygen Company and supplied liquefaction plants to several scientific institutions.

By 1897, Charles Tripler in New York also had built a similar but larger liquefaction plant, which was capable to produced 25 liters per hour [6].He had used a 75 kW steam engine to drive the compressor. In 1898, Sir James Dewar liquefied hydrogen by using the same technique of Linde. He had precooled hydrogen with liquid air. Hydrogen was compressed to 180 bar and cooled with counter-current heat exchanger and finally expanded using a JT-valve.

In 1902, George Claude a scientist of France had improved the Linde process by adding two extra heat exchangers and an expansion engine. This was the first time an expansion engine used in a liquefaction cycle successfully. The expansion engine was reciprocating type.

In 1907, Linde installed the first air liquefaction plant in America. Kamerlingh Onnes build up a cryogenic laboratory at the leiden on the Netherlands in 1895 but in 1908 he was successfully liquefied the Helium gas. There after a lot of liquefaction plants for air, neon, helium were developed for commercial purpose and installed. Another remarkable breakthrough was made when Kapitza developed a rotary expansion engine for helium in 1934. And in 1939 Kapitza modified the basic Claude system by eliminating the third or low temperature heat exchanger. He used the rotary expansion engine instead of a reciprocating expander and a set of valved regenerators instead of recuperators.

Around 1942 Samuel C. Collins developed an efficient liquid helium laboratory facility. He developed Collins helium cryostat resulted to economical and safe production of liquid helium. Furthermore a large liquefaction plants were developed to get large amount of liquid. The capacity of large liquefaction plants was more than 100 ton/day. The increase in the efficiency of the turboexpander and increase in effectiveness of the heat exchanger had lead to the better efficiency of the plant. The basic process cycles remaining same attention was focused to develop and increase the efficiency of the components of the plant, i.e. expansion engines and heat exchangers.

2.4 Turboexpander for cryogenic liquefaction

The fundamental principles and governing equation can be found in several text books and reports of fluid mechanics and Turbo-machinery [7-9]. A detail review on

turboexpander development was presented by Collins and Cannaday [10] and Sixsmith [11]. In 1898, Lord Rayleigh [10] was the first person to introduce the concept of turbine and it could be used to produce low temperature in liquefaction cycles. Considering this suggestion some patents were made on expansion turbine. Among them the patents of Edgar C. Thrupp, Joseph E. Johnson, Charles and Commett, Davis are important. But the commercial development of expansion turbine for gas liquefaction was done by Linde Works in Germany at around 1934 [11]. It was an axial flow single stage impulse turbine. Guido Zerkowitz a scientist of Italy modified the turbine and made it radial flow of impulse cantilever type. The rotational speed of the turbine was 7000 rpm.

In the year 1939, a Russian physicist Peter Kapitza, had made a low pressure cycle with expansion turbine. He made some revolutionary conclusions in paper published in journal of Physics [12]. He proved by giving thermodynamic reason that a low pressure liquefier using an expansion turbine is better than a high pressure liquefier using a reciprocating expander. And the cost of low pressure plant is also very cheap. He also concluded by doing both analytical and experimental studies that a radial inflow turbine would be preferable to an axial impulse type machine. The turbine was rotating at a speed of 40,000 rpm and measured efficiency was 80%.

Swearingen [13] described about a radial inflow, reaction type turbine that was designed by Elliot Company and constructed by the Sharples company in USA. The turbine was supported on ball bearings and design speed is 22,000 rpm. The selection of turbine [14] depends on the parameters like specific speed (n_s) and flow coefficient (ϕ) etc. From this it was concluded that for low flow rate and medium head, the radial inflow configuration gives the maximum efficiency [15] and it became a standard configuration of turbine. Linhardt [16] was also designed a large power output turboexpander and studied the influence of design parameters.

Further much smaller and high speed turbines was made in about 1950 at the University of Reading, England by Sixsmith [17]. The diameter of turbine wheel was 14.28 mm and designed speed was 240,000 rpm. The financial support for the development of this turbine was given by British National Research and Development Corporation. This turbine was employed as a source of refrigeration in a small air liquefier. Based on this design, in 1959 the British Oxygen Company (BOC) manufactured expansion turbines for application in air separation plants. BOC also built

the world's first commercial turbine-based helium liquefier for the Rutherford Laboratory in Oxford. By 1958, the Lucas Company in England had developed a range of gas lubricated radial inward flow turbines for Petrocarbon Development Corporation [18]. The Cryogenic Engineering Division of National Bureau of Standards had followed the work of Reading University and developed a helium expansion turbine. This was used in a helium refrigerator in 1964. The design speed was about 600,000 rpm while it was rotating at about 720,000 rpm and maximum efficiency was 79.8 %.

In Winthertur of Switzerland, Sulzer Brothers [19-21] had constructed a small turbine with gas lubricated bearings. The La Fleur Corporation [22], Lucas Corporation [18] and Linde, Germany had also developed expansion turbine with gas lubricated bearing. The General Electric Company, USA also worked on cryogenic refrigeration systems based on miniature turbomachine [23, 24]. In 1962, L'Air Liquide had developed a radial inflow turbine with high reliability and had high performance having expansion ratios up to 15.

Izumi et. al [25] at Hitachi Ltd., Japan had described the development of a turboexpander for a small helium refrigerator. Yang et. al [26-29] had discussed about the development of miniature turbines at the Cryogenic Engineering Laboratory of the Chinese Academy of Sciences. Naka Fusion Research Centre of Japan Atomic Energy Institute [30-32] had developed large turboexpanders for Helium liquefier. A high expansion ratio (15.3 bar to 1.2 bar) helium turboexpander was developed by Ino et al. [33, 34] for a 70 MW superconducting generator. The turbine impeller was backward swept and was rotating at 230,000 rpm. Further development was continued by Davydenkov [35-37] at around 1990s. Mikrokryogenmash company of Russia [38] had developed small turboexpander for micro-cryogenic systems.

Beasley and Halford [18] had developed a nitrogen turbine supported on gas bearings. Linde Division of Union Carbide Corporation had also developed turbines with gas bearing for large air separation. Kun et. al. [39-41] had described a detailed design methodology which has become a guideline for researchers. In collaboration with NASA/GSFC , Sixsmith et.al. [42] had developed miniature turbines for Brayton Cycle cryocoolers. The turbine had 31.8 mm in diameter and designed to rotate at a speed of 570,000 [42].

In 1985, Central Mechanical Engineering Research Institute (CMERI) Durgapur of India has developed an expansion turbine [43]. It is a radial inflow radial turbine and

is used for the nitrogen plants. They also suggested advantage of rotary expansion engine over reciprocating engine[44].The turboexpander developed was rotating at 30,000 rpm without any vibration. The reliability and machining process had been discussed for the indigenous developed turbine [45].Then further improvements in efficiency had been noticed for cryogenic turboexpander [46, 47].

In 2002, turboexpander was developed and tested at IIT Kharagpur [48], India. They have developed high stabilized gas bearings. The turbine was designed for 140,000 rpm and tested to run at 80,000 rpm. Due to the increase in vibration amplitude above 80,000 rpm they were unable to go beyond that speed.

In 2008, a radial turboexpander was developed at NIT Rourkela [49]. It was designed to work with air or nitrogen to rotate at a speed of 220,000 rpm. Aerodynamic bearings were used for the turboexpander. Recently BARC, Mumbai has developed high speed miniature helium turboexpander [50, 51] which rotates at 2,70,000 rpm. The turbine is tested and found to have efficiency of 65 %.

2.5 Heat exchangers for cryogenic liquefaction

Heat exchangers are the most important and critical components in any cryogenic liquefaction systems. The main function of the heat exchanger is to conserve cold. Using heat exchangers, the heat from the compressed process fluid extracted and transferred to the low pressure stream.

The heat exchangers used for cryogenic liquefaction can be of two types, i.e, recuperative and regenerative. Generally among recuperative type heat exchanger tubular heat exchangers, Giauque-Hampson exchanger, Plate fin heat exchangers, perforated plate heat exchangers are important. The details about the different heat exchanger used for cryogenic application is given by Barron [1, 52].

(i) Concentric tube heat exchanger

For the first time simple tube in tube heat exchanger was used by Linde for liquefaction of air in 1985 [6, 53]. The tube in tube heat exchanger consists of a small inner tube and a co-axial larger tube. In the smaller tube usually high pressure stream flows and in the annular space the low pressure stream flows. The figure of the tube in tube heat exchanger is shown in Figure 2-1. The flow can be parallel or counter type.

Later on the plastic or wire spacer is placed inside tube in tube heat exchanger [Figure 2-2]. By this arrangement better heat transfer occurs due to increase in the heat transfer coefficient. When more than two streams are involved smaller tubes are placed inside a large tube. It is called multi-tube heat exchanger [Figure 2-3].

(ii) Coil wound heat exchanger

Giauque-Hampson exchanger [Figure 2-4] is a coil wound type heat exchanger, one of the most classical heat exchanger used in large liquefaction systems. It consists of small diameter tubes that are wound in several layers over a cylindrical mandrel. The successive layers are wound in opposite direction and provided with spacing strips [54]. The tubes are joined at the ends with a header. All the tubes are covered with an outer casing and the entire unit is insulated. These types of heat exchangers are constructed up to large size which can be transported easily [55]. The major problem with these type of heat exchnagers are expensive and only produces by Linde group and APCI [56] . Prof. Collins [5, 10] had made a special extended type surfaces inside the tubes for his helium liquefier [Figure 2-5].

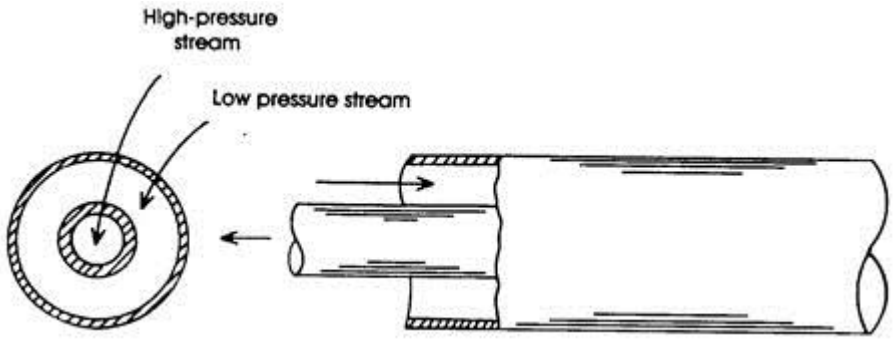

Figure 2-1 Concentric tube heat exchanger [1]

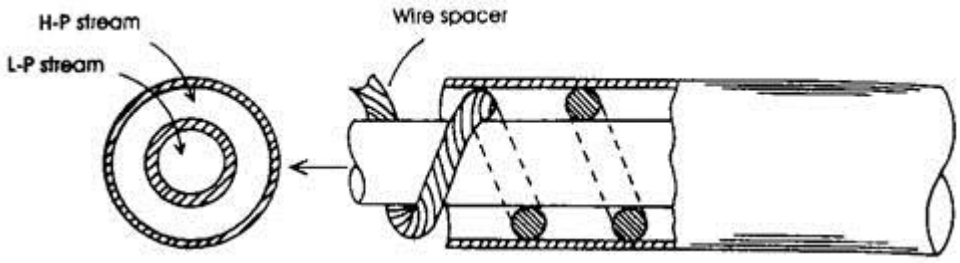

Figure 2-2 Tube heat exchanger with wire spacer [1]

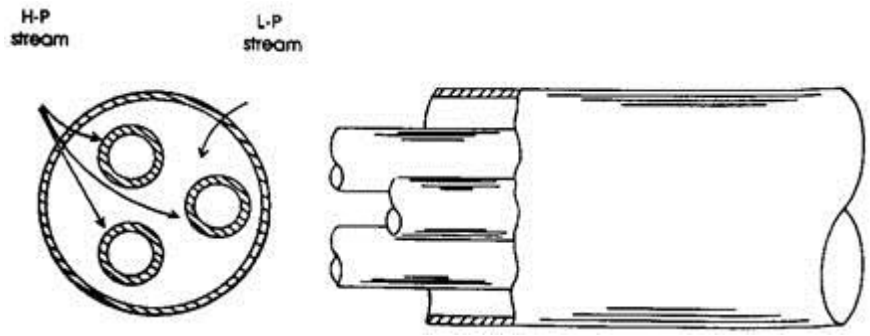

Figure 2-3 Multi tube heat exchanger [1]

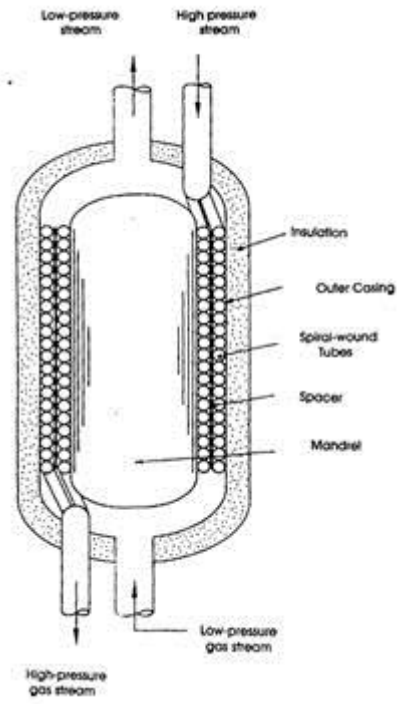

Figure 2-4 The Giauque Hampson heat exchanger [52]

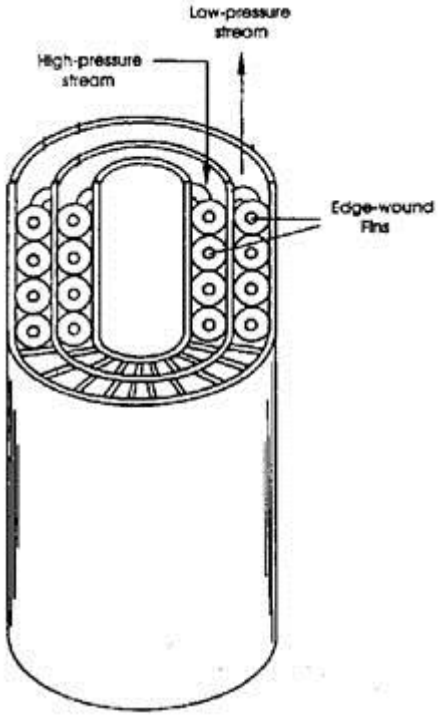

Figure 2-5 The Collins heat exchanger [52]

(iii) Perforated plate heat exchanger

The perforated plate heat exchangers are used in small scale refrigerators and liquefiers. A Schematic diagram of the perforated plate heat exchangers is shown in Figure 2-6 . It consists of a series of parallel perforated plates separated by spacers or gaskets. The spacers are bonded to the plates tightly to prevent leakages. Generally the plates are made of relatively high thermal conductivity material like aluminium for better heat transfer and the spacers with low thermal conductivity material like plastic material to avoid

longitudinal heat conduction. A comprehensive review of the history and applications of perforated plate heat exchanger is given by Venkatarathnam and Sarangi [57] and design and optimization of the plate heat exchanger is given by Venkatarathnam [58, 59].

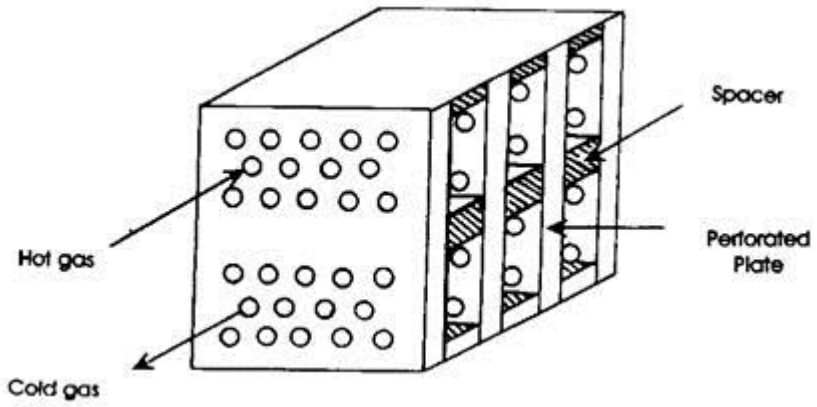

Figure 2-6 Perforated plate heat exchanger [52]

(iv) Plate fin heat exchanger

This type of heat exchanger is used widely because of its high heat transfer area density, compactness, light weight and high effectiveness. It is also much cheaper than the coil wound heat exchanger. It consists of a set of layers of corrugated plates served as fins and these layers are separated by a separating sheet [Figure 2-7]. It is manufactured by many industries around the world grouped in the Brazed Aluminium Plate-Fin Heat Exchanger Manufacturers Association [60]. This associations includes five major brazed aluminium plate fin heat exchanger manufacturers i.e., Chart Energy & Chemicals Inc of USA [61], Fives Cryo [62], Kobe Steel Ltd. of Japan [63] , Linde AG of Germany [64], Sumitomo Precision Products Co. Ltd of Japan.[65].In addition several smaller companies manufacture plate fin heat exchangers such as Appolo Heat exchangers Pvt. Ltd. Several specialized laboratories like Heat Transfer and Fluid Flow Services (HTFS)[33] in England and Heat Transfer Research Inc (HTRI) [34] in USA made significant contribution to the research on plate fin heat exchangers. The growth of these organizations occurs due to the support of many industries and institutions around the world.

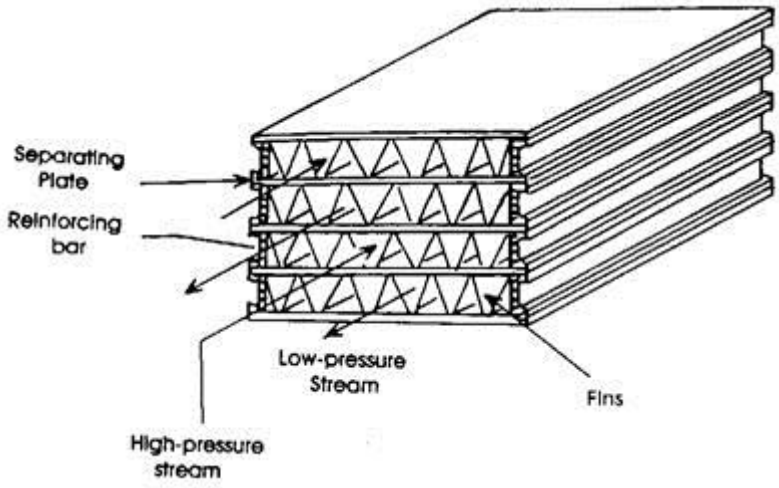

Figure 2-7 Plate fin heat exchanger [52]

2.6 Design Methods of heat exchanger

There are a number of text books [66-71] which describes the heat transfer phenomena and design of heat exchangers. The design and simulation methodology of two streams plate fin heat exchangers are enriched by other books and literatures [72-77]. Pacio and Dorao [78] has classified the design methods as below

(i) Lumped parameters
(ii) Distributed parameters
(iii) Stream evolution

(i) Lumped parameters

This type of design method [79-81] is adopted for two streams with single phase. Sizing and rating can be done by considering the energy balance equation. Lumped parameters model includes five different techniques i.e., Mean temperature difference, ε-NTU [82], P-NTU, ψ-P [83] , P1-P2 [84]. But first two techniques are widely used for designing heat exchangers for cryogenic application. But the drawback with the lumped parameter method is that they consider overall heat transfer coefficient and constant specific heat.

(ii) Distributed parameters

This method involves with dividing the heat exchanger into several zones or elements [85] and applying the lumped parameter method to the individual zones or elements. When phase change occurs inside a heat exchanger then it is divided into zones i.e. single phase vapor, two phase and single phase liquid.

When the heat exchanger divided by considering some definite length of the heat exchanger, each divided part is called element. By dividing the heat exchanger into number of elements, lumped parameter method could be applied and making energy balance at both the ends. In this technique one could consider the variable specific heat which is very important in cryogenic application. If the stream is in different phases then the heat exchanger can be divided into zones and each zone is then divided into several elements [86].

(iii) Stream evolution

This method based on steady state one dimensional mass, momentum and energy balance equations for each individual stream. This can be applied to more complicated geometry and more than two streams. It correlates among the fluid properties, heat transfer and pressure drop characteristics. Aspen MUSE of AspenTech [87] and GENIUS by Linde AG are the software that uses this stream evaluation method.

The plate fin heat exchanger is designed by using commercially available software Aspen–MUSE [88], the simulation software. The software takes care of the various losses occurring in the heat exchanger like flow maldistribution at the headers, longitudinal heat conduction, heat losses to the ambient, pressure losses in the headers etc. It has been accepted as dedicated tool for the design of plate fin heat exchangers in industrial applications.

For the thermal and hydraulic design of coil wound heat exchanger GENIUS proprietary software from Linde is used. This computer program plots the temperature and pressure profiles of the individual streams and calculates the distribution of the tubes to the various layers.

2.7 Process design and simulation

Process simulation is a very essential technique in the design, analysis, and optimization of a cryogenic process plants [89, 90]. Simulations could be done using computer programs or simulation software, that simulate the behavior of the process plants using appropriate mathematical models. Process simulators are used to determine the detailed specifications of all units of a process by considering material balance and energy balance equations. This also helps to troubleshoot startup and shut-

down operations, determine performance under off-design conditions, design and troubleshoot control strategies.

The cryogenic refrigeration and liquefaction processes are different from general processes. This is due to the following reasons

- Large variation in thermo physical properties i.e., specific heat, thermal conductivity etc.
- Use of multistream LNG heat exchangers
- Consideration of pinch point of heat exchanger
- Double distillation columns
- Phase separators

There are a number of software that are used for process simulation i.e., Aspen HYSYS, Aspen Plus, CRYOSIM, ChemCAD etc. They have features that are required for the simulation of cryogenic liquefaction and refrigeration processes.

Process simulation can be done by three methods,

(i) Sequential modular method,
(ii) Equation-oriented method,
(iii) Simultaneous modular method.

(i) Sequential modular method

Sequential modular method [91-94] is widely used to simulate cryogenic refrigeration and liquefaction process. Every component of a process is represented by a mathematical model and a program is written separately as subroutines in these simulators. The mathematical models are developed to give the thermodynamic parameters including pressure, temperature, enthalpy, entropy, etc as output for the given input condition and component specification such as pressure ratio, outlet pressure, efficiency of the equipment, etc. The output of one component will be treated as input to the next component attached with it. The simulation proceeds component by component from the feed to the product streams. When there are recycle loops present in the process, the recycle loops are torn at suitable points and estimated values are assigned to these streams. Recycle loops are sequentially solved until the assumed values of the tear streams match the computed stream information.

(ii) Equation-oriented method

The governing equations like mass balance, energy balance equations and the governing equations of each process unit are solved one at a time, sequentially, in the case of a sequential modular approach. But in equation oriented method the governing equations of all the units are solved together simultaneously in an equation-oriented approach. As all the equations are solved simultaneously there is no need for tearing the streams. Also there is no need for nested iteration loops.

The equation-oriented approach requires a suitable initial guess value of variables for convergence. It is difficult to handle the error and also creates problem at the time adding new unit or component. A robust nonlinear equation solver is required to solve the equations simultaneously. Due to these problems, the process simulation software has both the capabilities. Aspen Plus [95] , Aspen hysys uses both the method; sequential and equation oriented method.

(iii) Simultaneous modular method

When a process has a no. of tear streams with nested loops then this technique is applied. By the sequential method, it takes more time with large no. of iterations. Simultaneous modular method is a combination of sequential and equation oriented method. It is also called two-tier method. Basically the process is solved by sequential method but the nested loops are solved by equation oriented method. A combination of simultaneous and sequential modular approaches is sometimes preferred. The simultaneous modular approach is also used in CRYOSIM [96] for optimization studies.

The dynamic simulation also can be done by the commercially available software like Hysys dynamics [97-100], Cryogenic Process Real-time SimulaTor (C-PREST) [101] etc.

2.8 Major industries supplying liquefaction plants

In some parts of our country, it is possible to buy liquid nitrogen from bulk suppliers at low cost. The steel manufacturing companies are using liquid oxygen plant and liquid nitrogen are waste product for them. So they supply liquid nitrogen at low

cost. But in most cases, including some major metropolitan areas, a laboratory needs to operate its own liquid nitrogen generator.

There are three major international suppliers of nitrogen liquefiers to our country:

- Stirling Cryogenics of Netherlands,
- Linde CryoPlants, UK and
- Consolidated Pacific Industries, USA.
- Air Liquide, France

The liquefier from Stirling Cryogenics [102] of Netherlands is based on the integral Philips-Stirling Cycle, while the latter two use turbine for cold production.

Linde CryoPlant [103] of UK is leading supplier of liquid nitrogen plant. LINIT is a turboexpander based nitrogen liquefier which has starting range of liquid nitrogen production of 25 litres per hour. Also LINIT model with 50 and 100 litres per hour capacity available and they are using gas bearings for the turboexpander.

Consolidated Pacific Industries [104] manufactures liquid nitrogen plant of 1.5 TPD. Liquid nitrogen produced from air by following the cryogenic distillation technology due to different boiling points of oxygen and nitrogen.

Air Liquide of Canada is one of the industries who produce liquid oxygen, nitrogen and hydrogen etc.

Cryomech, Inc. [105] of USA is manufacturers of fully automatic liquid nitrogen plant ranging from 10 to 240 litres per day. It is based on Gifford-McMahon Cycle.

Kelvin International Corporation [106] produced two types of models. M is for small capacity modules and NL for fully assembled industrial models. The ranges starts from 15 to 120 litres per day.

Liquid-nitrogen-plant.com is among one of the leading supplier of Liquid Nitrogen plants incorporating USA-technologies. The liquid Nitrogen is produced by separating the nitrogen from air using membrane technology and then liquefying the gaseous nitrogen using a USA technology built liquid helium refrigerator.

In association with a company named ING. L&A. Boschi of Italy, a liquid nitrogen plant production factory was setup in 1985 in New Delhi. The plants are based on Linde and Claude cycle.

Wuxi Victor Hengsheng Machinery Manufacturing Co., Ltd. is a company from China established in 1999, which produces liquid nitrogen plant. The range of the production is 220 to 2500 litres per hour. Hangzhou Union Industrial Gas-Equipment Co., Ltd. and Hangzhou Kaihe Air Equipment Co.,Ltd. are also dealing with supplying the liquid nitrogen plants.

Chapter III

Process Design of Nitrogen Liquefaction Cycle

3.1 Introduction

A turbo expander based cryogenic refrigerator or cryocooler consists of following parts:

- Compressor
- Heat exchangers
- Turboexpander
- JT valve
- Liquid nitrogen separator along with transfer line
- Cold box
- Piping
- Instrumentation

A screw compressor is installed to provide the compressed nitrogen gas. Heat exchangers are vital components of any cryogenic refrigerator or liquefier. To exchange more amount of heat in small area plate fin heat exchangers are used. The expansion turbine is the heart of the liquefier and it can use for lowering the temperature to desired value adiabatically. J-T Valve is used for isenthalpic expansion. Phase separator is used to separate liquid and gas phases. Piping and other instrumentations are required to connect and to control the systems. The integrated system is kept inside the cold box.

Three types of cycles have been selected for simulation i.e., Claude cycle [89], modified Claude cycle eliminating the third heat exchanger and modified Claude cycle eliminating the first heat exchanger. Out of these three process cycles one process cycle is selected which gives optimum amount of liquid nitrogen. The selected process cycle is further simulated to give optimum parameters like pressure of compression,

effectiveness of heat exchangers, mass fraction diverted through the turboexpander and efficiency of turboexpander. These parameters are utilized in designing the components like heat exchangers, turboexpander etc.

3.2 Description of process cycles

(i) Case-1:

This is a Claude cycle consists of a compressor, a turboexpander, a J-T valve and three numbers of heat exchangers as shown in Figure 3-1. The compressed nitrogen gas passes through HX-1 (first heat exchanger) and a fraction of gas is diverted through the turboexpander, the remaining gas is passes through the HX-2 (second heat exchanger) and HX-3 (third heat exchanger). Then isenthalpic expansion is done by using J-T valve. The phase separators separates liquid and remaining vapour passes through HX-3 as cold stream. The cold stream exits from the HX-3 and mixes with the expanded stream from the turboexpander. It is feed to the compressor through HX-2 and HX-1.

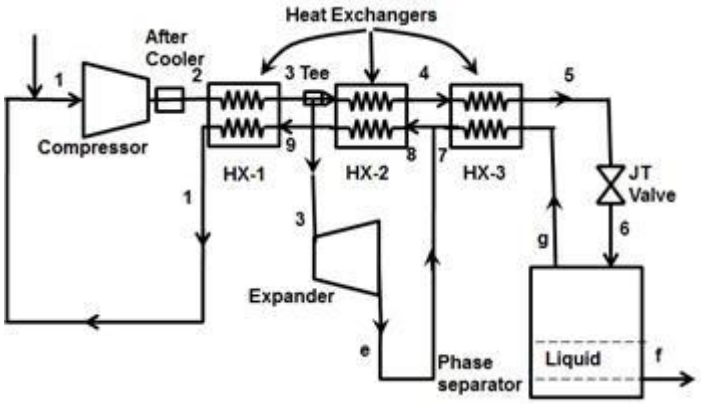

Figure 3-1 Schematic diagram of Claude cycle (Case-1)

(ii) Case-2:

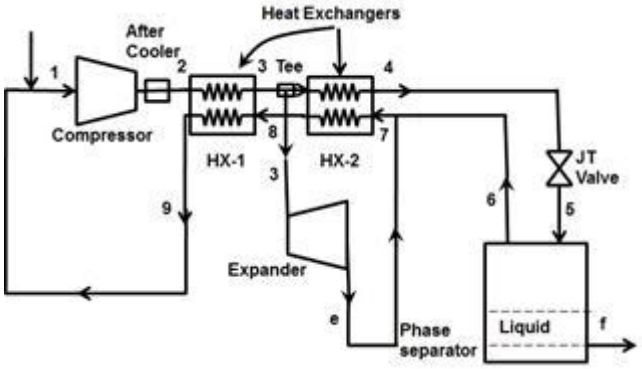

Figure 3-2 Schematic diagram of modified Claude cycle (Case-2)

It is a modified Claude cycles in which placement of all other components remain same as in Claude cycle except the third heat exchanger. The HX-3 is eliminated as shown in Figure 3-2.

(iii) Case-3:

It is also a modified Claude cycle in which all components are same as in Claude cycle except the first heat exchanger. Here HX-1 is eliminated as shown in Figure 3-3. The compressed gas divided into two streams before cooling by any heat exchanger.

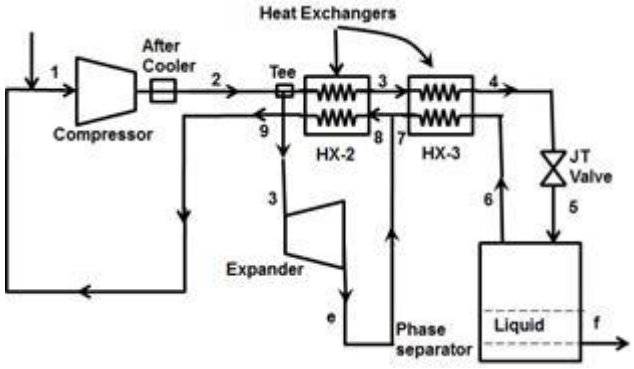

Figure 3-3 Schematic diagram of modified Claude cycle (Case-3)

3.3 Simulation of process cycles

Steady state simulation [89] is done on these three cycles using Aspen Hysys®[107]. Before simulating these cycles the following assumptions are made.

(i) Pressure drop in heat exchangers and pipes are assumed to be negligible.
(ii) No external heat transfer.

Mass flow rate, efficiency of compressor and turboexpander and pinch point of Heat exchangers are kept constant for each process cycles and in every simulation. Yield is estimated for different pressures of compression (10 bar to 100 bar).

The input conditions for the process cycles are

(i) Compressor
- Mass flow rate =1 kg/s
- Inlet temperature = 300 K
- Inlet pressure = 1.1 bar
- Delivery pressure (from 10 bar to 100 bar)

(ii) After Cooler

- Outlet temperature = 300 K

(iii) HX-1 (only for case-1 and case-2)

- Pinch point (minimum temperature difference between two streams of heat exchanger) =5 K

(iv) HX-2

- Pinch point =3 K

(v) HX-3 (only for case-1 and case-3)

- Pinch point =1 K

(vi) Tee (From where diversion occurs to the turboexpander)

- Mass fraction (ratio of mass flow diverted to the turboexpander with compressed mass flow) through Turbo expander (change from 0.5 to 1 to get maximum yield)

(vii) Turbo expander

- Efficiency of turbo expander=50%
- Outlet pressure =1.1 bar

(viii) JT Valve

- Outlet pressure = 1.1 bar

Turboexpander efficiency is taken as 50%. Since the available turboexpander efficiency is limited to this value. The Plate fin heat exchangers have found to give effectiveness of about 0.95 – 0.98. So pinch point is taken as 5 K of HX-1. The maximum yield occurs at a particular mass fraction diverted through the turboexpander.

A graph between yield and pressure at exit of compressor is plotted as shown in Figure 3-4. It shows that under similar operating condition and component specification the yield of case-1 and case-2 is approximately equal. Although yield of all cycles are increasing with the increase in pressure of compression but the yield of case-3 is lowest as compared to the other two process cycles. In case-3 the mass fraction diverted to turboexpander is at higher temperature than the other two cases due to absence of HX-1. The other two heat exchangers HX-2 and HX-3 along with the turboexpander are unable to lower the temperature to produce appreciable amount of liquid.

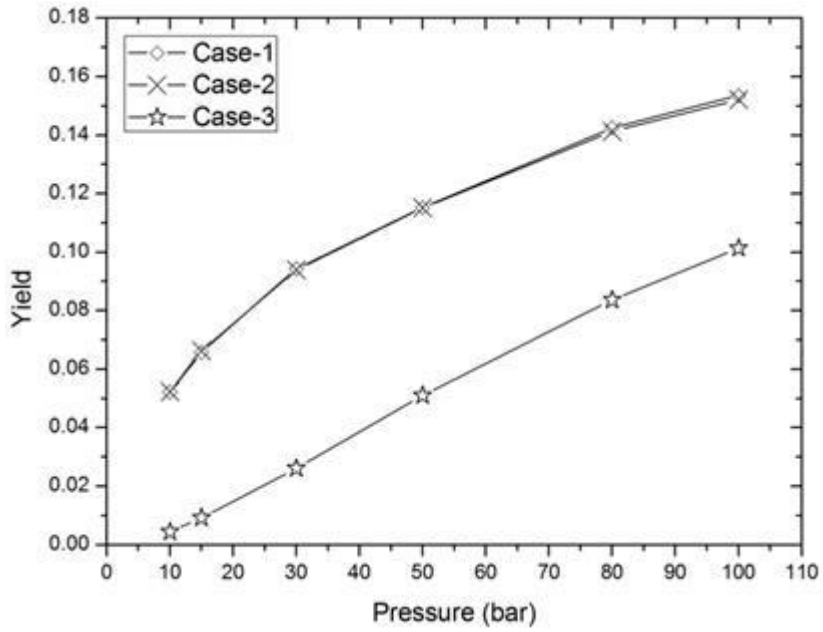

Figure 3-4 Yield at different pressures in the three cases

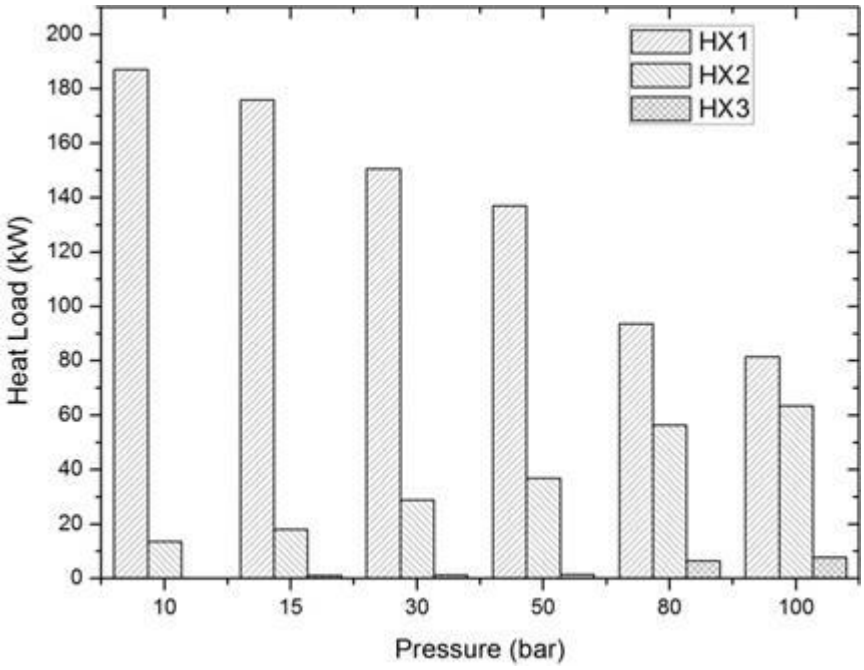

Figure 3-5 Heat load of heat exchangers at different pressures in case-1

A graph has been plotted to compare the amount heat load of three heat exchangers of case-1 with increasing pressure. The heat load of HX-3 in case-1 is found to be very low (1 kW at 15 bar) as compared to the other two heat exchangers (175.9 kW of HX-1 and 18 kW of HX-2) as shown in Figure 3-5. So at pressures (10-50 bar) the

HX-3 can be neglected. If this is eliminated, it will became case-2 i.e., modified Claude cycle with eliminating the last heat exchanger.

Among the three process cycles case-3 has very low yield and at low pressure and case-2 can give yield of case-1 due to negligible load in HX-3 of case-1. So case-2 is selected as the liquefaction cycle [108].

3.4 Calculation of process parameters of selected cycle

The design of process parameters depends on the nodal temperature across the heat exchangers and turbo-expanders. Figure 3-6 shows the process diagram and given below are the set of equations used for the calculation of process parameters.

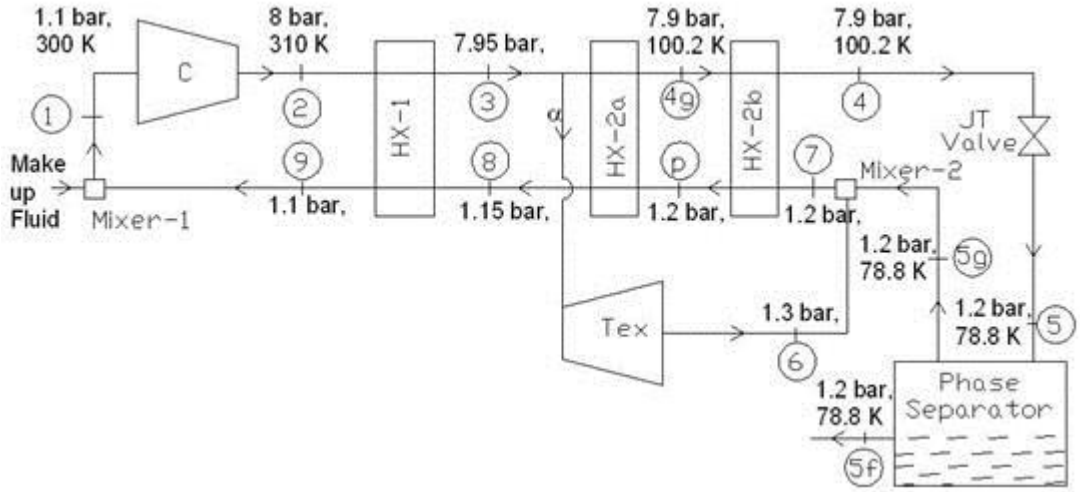

Figure 3-6 Process flow diagram

(i) Input parameters

a. Effectiveness of heat exchanger 1, $\varepsilon_1 = 0.98$

b. Pinch point for heat exchanger 2 =1 K

c. Efficiency of turboexpander, $\eta_{tx} = 0.5$

d. Compressor discharge temperature, $T_2 = 310$ K

e. Mass fraction diverted through turboexpander, $\alpha_{tx} = 0.94$

f. Corresponding property values at saturated liquid and saturated vapor states are taken from property package, ALLPROPS [109].

(ii) Assumptions

a. Pressure drop in the heat exchanger= 0.05 bar.

b. No external heat transfer.

(iii) Component analysis

a. Pinch Point Specification of Heat Exchanger2: Heat exchanger 2 divided into two parts: First part of heat exchanger is used to cool the hot nitrogen gas in the high pressure side up to the saturation temperature of 100.2 K and this stream is condensed in the second part of heat exchanger. The minimum temperature difference occurs at the point where the condensation begins and is called as pinch point. For the specified pinch value of 1K for second heat exchanger gives,

$$T_p = T_{4g} - 1 \tag{3.1}$$

b. Heat Exchanger 1: For the specified value of effectiveness of first heat exchanger and the pinch point specification for heat exchanger 2, the inlet and outlet enthalpies of hot and cold fluids at node points 8, 3 and 9 are calculated. The enthalpies h_8, h_3 and h_9 are calculated from equations(3.4), (3.5) and (3.6) respectively. Since the enthalpy at node point 8 (h_8) requires a prior estimation of y and h_9, initial guess values are provided by equations (3.2) and (3.3) respectively.

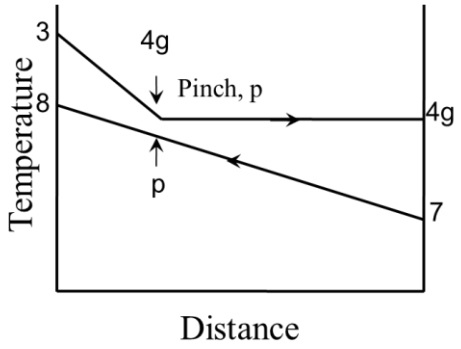

Figure 3-7 Pinch point of HX-2

$$y = (1-\alpha) \ \left(\text{for initial guess}\right) \tag{3.2}$$

$$h_9 = \varepsilon 1 h_2{}' \ \left(\text{for initial guess}\right) \tag{3.3}$$

Considering the energy balance equation between HX-1 and HX-2a,

$$h_8 = \frac{[h_9(1-y)(1-\alpha) - h_2(1-\alpha) + h_{4g}(1-\alpha) - h_p(1-y)]}{[(-\alpha)(1-y)]} \tag{3.4}$$

Now considering energy balance across HX-2a alone,

$$h_3 = \frac{[h_{4g}(1-\alpha) + (1-y)(h_8 - h_p)]}{(1-\alpha)} \tag{3.5}$$

Rearranging the effectiveness equation of HX-1,

$$h_9 = \varepsilon 1 h_2' + (1 - \varepsilon 1) h_8 \tag{3.6}$$

The iterations continued until the two subsequent iterative values of h_9 are within a specified limit (10^{-4} kJ/kg).

c. Turboexpander: In the turboexpander, the process 3-6s is the isentropic expansion and the process 3-6 is the actual expansion. The entropy at node point 3 (s_3) for specified values of h_3 and p_3 is taken from property package [109]. The high pressure stream after the expansion through the turbine is always to be dry which ensures that s_6 is always greater than s_{6g}. The enthalpy at the end of expansion is estimated as,

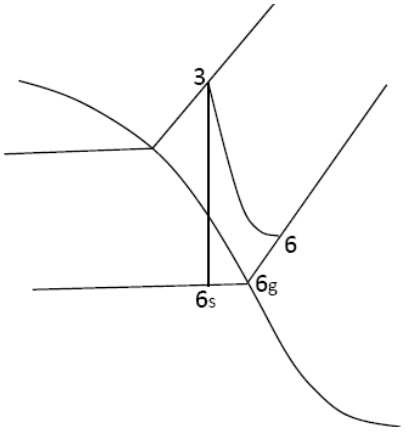

Figure 3-8 Expansion in Turboexpander

$$s_{6s} = s_3 \tag{3.7}$$

$$T_{6s} = T_{6g} \exp\left(-\frac{(s_{6g} - s_3)}{c_p}\right) \tag{3.8}$$

$$h_{6s} = h_{6g} - c_p(T_{6g} - T_{6s}) \tag{3.9}$$

$$h_6 = h_3 - \eta(h_3 - h_{6s}) \tag{3.10}$$

d. Mixer: Applying energy balance equation for the mixer, enthalpy at outlet of mixer is,

$$(1 - \alpha - y) h_{5g} + \alpha h_6 = (1 - y) h_7$$

$$h_7 = \frac{[\alpha h_6 + (1 - \alpha - y) h_{5g}]}{(1 - y)} \tag{3.11}$$

e. Heat Exchanger 2: Enthalpy at outlet of hot fluid is found out by energy balance between hot and cold fluids as

$$h_4 = \frac{[h_3(1-\alpha) - (1-y)(h_8 - h_7)]}{(1-\alpha)} \quad (3.12)$$

f. Throttle Valve: Throttling is an isenthalpic process which yields,

$$h_5 = h_4 \quad (3.13)$$

g. Phase Separator: The dryness fraction, x_5 of the stream entering the phase separator is estimated as

$$x_5 = \frac{(h_5 - h_{f5})}{(h_{g5} - h_{f5})} \quad (3.14)$$

h. Yield: The liquid yield obtained per kg of gas passing through the throttling valve, is $(1-x_5)$. Hence for $(1-\alpha)$ kg of gas passing through the throttling valve, the yield is

$$y = (1-\alpha)(1-x_5) \quad (3.15)$$

To obtain the process parameters the iteration process is repeated starting from equations (3.4) to (3.15) till the tolerance in y is less than 10^{-5}.

3.5 Parametric analysis of selected cycle

Parametric analysis was carried out to optimize the selected process cycle. Following are the key parameters which influences the liquid yield.

(i) Mass fraction diverted through the turboexpander
(ii) Effectiveness of HX-1
(iii) Pinch point of HX-2
(iv) Efficiency of turboexpander
(v) Pressure of compression

(i) Effect of mass fraction diverted through turboexpander

The effect of the variation of mass fraction through turboexpander on the yield at different operating pressures is studied by keeping the values of

turbine efficiency, effectiveness of HX-1 and pinch point of HX-2 constant. From the Figure 3-9, it is found that yield increases with the mass fraction diverted through turboexpander, and after a certain value it starts decreasing [91]. This is because of insufficient amount of fluid in the high pressure side of HX-2.

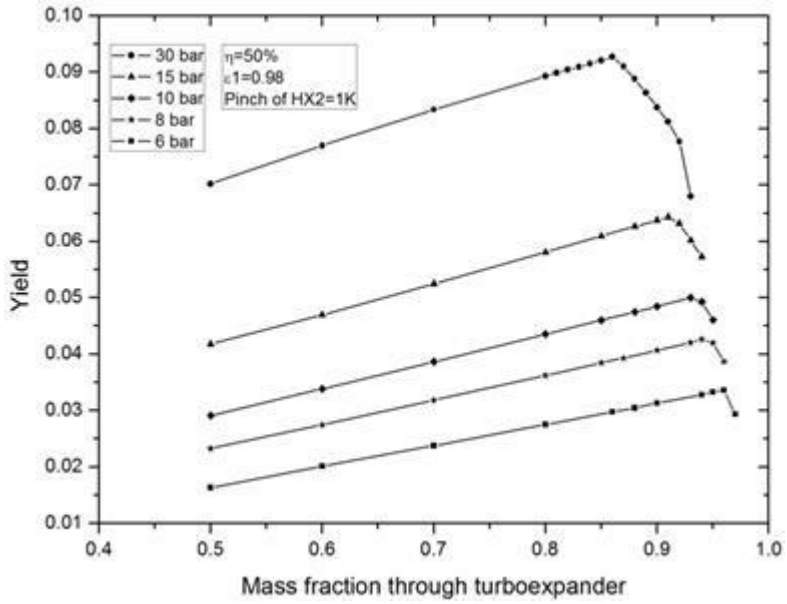

Figure 3-9 Variation of yield with the change of mass fraction through turboexpander at different operating pressures

The yield also increases with increase in pressure. At 8 bar, the maximum yield occurs when 94% of mass diverted through turboexpander. But at 30 bar it occurs when 86 % passed through turboexpander. It means at high pressures, maximum yield can be obtained with less mass fraction diverted through turboexpander.

(ii) Effect of variation of effectiveness of heat exchanger 1

The liquid yield increases in direct proportion with the effectiveness of HX-1, for the given efficiency of turbine, expander flow ratio and pinch point of HX-2. With the increase in effectiveness of HX-1, the temperature at exit of high pressure side decreases. This helps to produce more liquid.

It is also found that liquid yield is not possible, after certain effectiveness of HX-1 as shown in Figure 3-10. The lower limit effectiveness of HX-1 decreases with increasing the operating pressure. At 8 bar the lower limit of effectiveness is 0.88. But at 30 bar it is 0.69. If it is operating at high pressures then a low effectiveness HX-1 can be used.

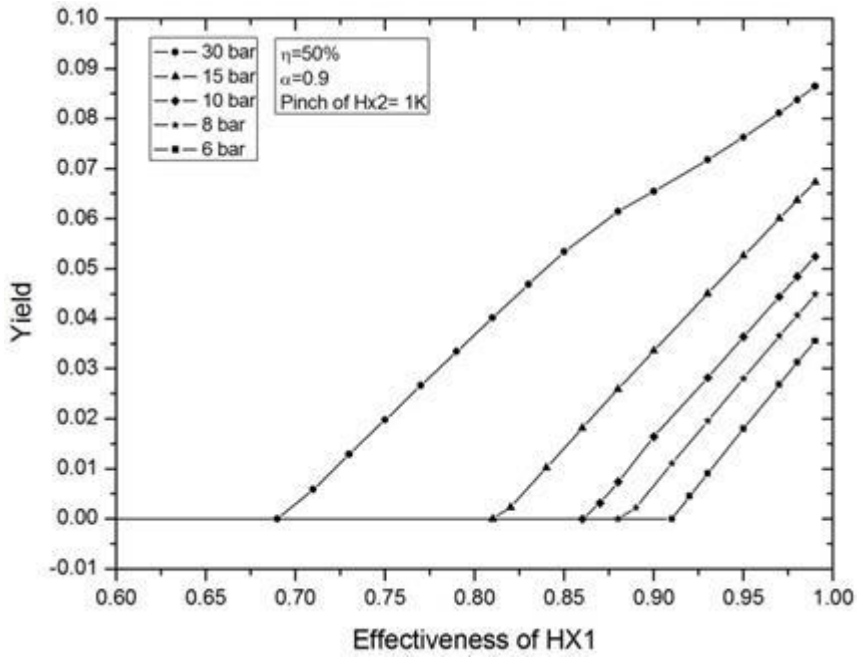

Figure 3-10 Variation of yield with effectiveness of HX-1 at different operating pressures

(iii) Effect of variation of pinch point over the performance of the plant

The liquid yield decreases with increase in pinch point of HX-2, for the given efficiency of turbine, expander flow and effectiveness of HX-1, as shown in Figure 3-11. Thus pinch point of HX-2 has not effect much on the yield but it should be lower as much as possible.

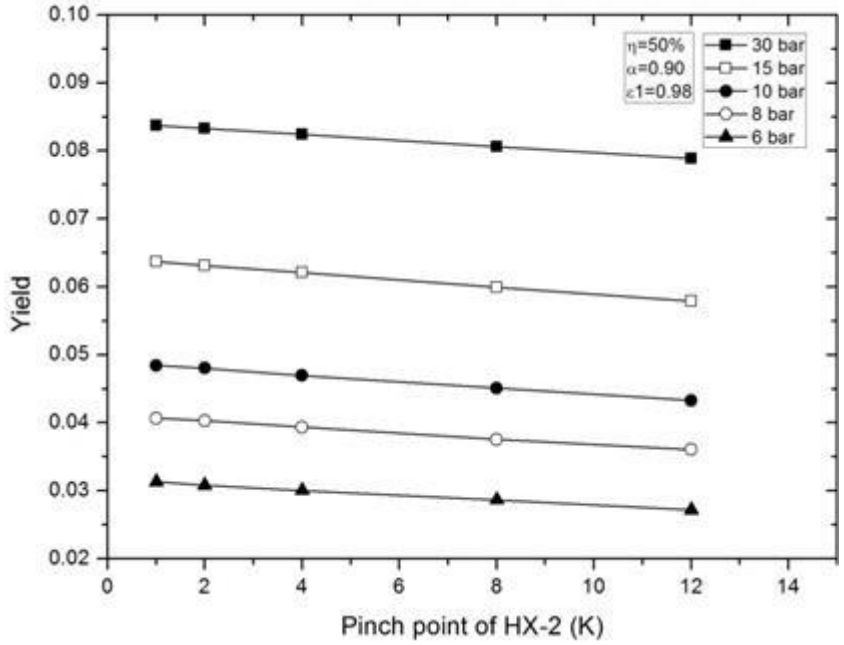

Figure 3-11 Variation of yield with pinch point of HX-2 at different operating pressures

(iv) Effect of efficiency of turboexpander

The effect of turbine efficiency on the liquid yield is shown in the Figure 3-12. For the given effectiveness of HX-1, pinch point of HX-2 the liquid yield increases with the efficiency of turboexpander. With the increase in efficiency of turboexpander the temperature drop in turboexpander increases. This causes to improve the liquid yield. It is observed that the turboexpander with high efficiency can provide a better yield with lesser mass flow rate through it. With increasing operating pressure the yield also increases.

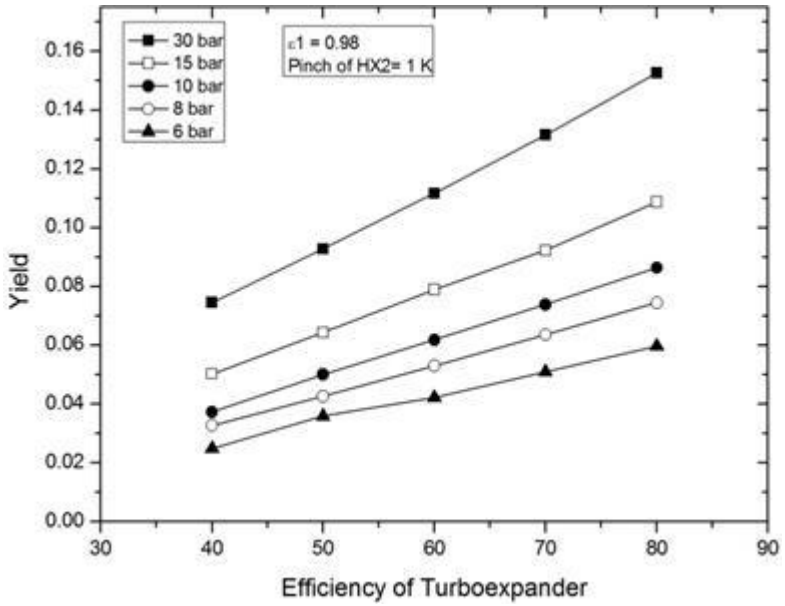

Figure 3-12 Variation of yield with turboexpander efficiency at different operating pressures

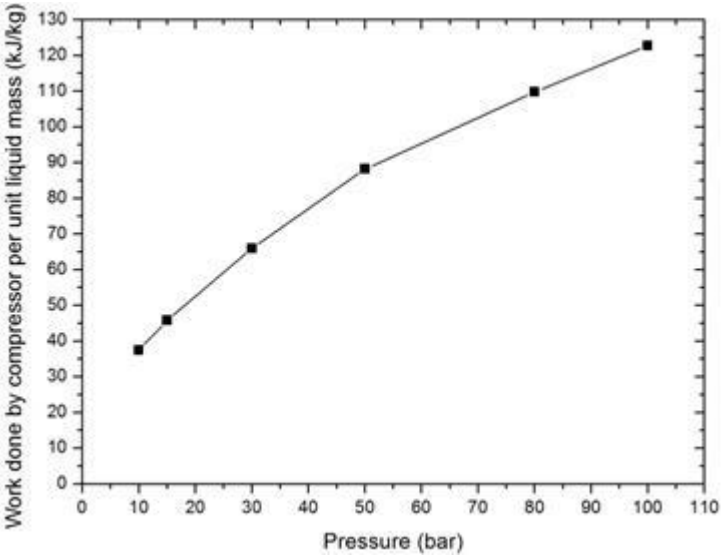

Figure 3-13 Variation of compressor work per liquid mass produced with operating pressure

(v) Effect of pressure of compression

The effects of pressure of compression on yield are shown in Figure 3-9, Figure 3-10, Figure 3-11 and Figure 3-12. Yield increases with increase in pressure of compression. But work required by the compressor to produce unit mass of liquid also increases with increase in pressure as shown in Figure 3-13.

3.6 Performance of nitrogen liquefaction plant

At low pressure (10 bar) the compressor work done per unit mass of liquid is less. Also availability of high effectiveness heat exchangers and difficulties in manufacturing turboexpander at high pressures (above 15 bar), the case-2 cycle should be selected to operate at 8-10 bar. Operating the case-2 cycle at 8 bar, it is found that, the optimum mass fraction to be diverted through turboexpander for the maximum yield is 0.93. For the better performance, the effectiveness of heat exchanger should be as high as possible (0.99), pinch temperature of HX-2 should be as low as possible (1K) and turboexpander efficiency must be as high as possible.

Applying the First Law for steady flow process to the system as shown in Figure 3-6, the liquid yield can be expressed as,

$$\dot{m}h_2 - \alpha\dot{m}h_3 + \alpha\dot{m}h_6 - (\dot{m} - \dot{m}_f)h_9 - \dot{m}_f h_{5f} = 0 \qquad (3.16)$$

Rearranging the equation(3.16),

$$y = \frac{\dot{m}_f}{\dot{m}} = \frac{h_9 - h_2}{h_9 - h_{5f}} + \alpha\frac{h_3 - h_6}{h_9 - h_{5f}} \qquad (3.17)$$

An oil injected twin screw compressor is used to deliver the compressed nitrogen at 8 bar pressure. Seshaiah [110] has done experimental studies on the above compressor and has evaluated calculate flow rate of nitrogen at different pressure ratio. For the required pressure of 8 bar, the compressor will deliver a mass flow rate of 296 kg/hr.

Finally the nitrogen liquefaction plant is fixed with component specifications given in Table 3-1, and the thermodynamics state points given in Table 3-2. As per design it will produce about 13.95 kg/s of liquid nitrogen which is equivalent to 17.44 liters/hr. The yield is calculated to be 4.71 %. The temperature entropy diagram of the selected process cycle is shown in Figure 3-14.

Table 3-1 Basic specifications of liquefier components

Sl. No.	Name of the component	Specifications
1.	Heat exchanger (HX-1)	Effectiveness = 99 %
2.	Turboexpander (Tex)	Efficiency = 50 % Flow through turboexpander = 93 %
3.	Heat exchanger (HX-2)	Pinch temperature =1 K

Table 3-2 Thermodynamic state points of the process cycle

State Points		**Pressure (bar)**	**Temperature (K)**	**Quality**	**Mass Flow Rate (kg/hr)**
1	Compressor inlet	1.1	300.00		296
2	Compressor exit and HX-1 inlet	8	310.00		296
3	HX-1 exit and Tex,HX-2 inlet	7.95	119.66		275.27
4	HX-2 exit and J-T valve inlet	7.9	100.13	0.1125	20.73
5	J-T exit and inside phase separator	1.2	78.78	0.3265	20.73
5f	Liquid produced	1.2	78.78		13.95
6s	Isentropic exit from Tex	1.3	79.49	0.9451	
6	Actual exit from Tex	1.3	90.01		275.27
7	Mixing of phase separator vapor with exit of Tex and LP inlet of HX-2	1.2	89.54		282.05
P	Pinch point in HX-2	1.15	99.13		
8	LP exit of HX-2 and LP inlet of HX-1	1.15	100.93		282.05
9	LP exit of HX-1	1.1	307.89		282.05

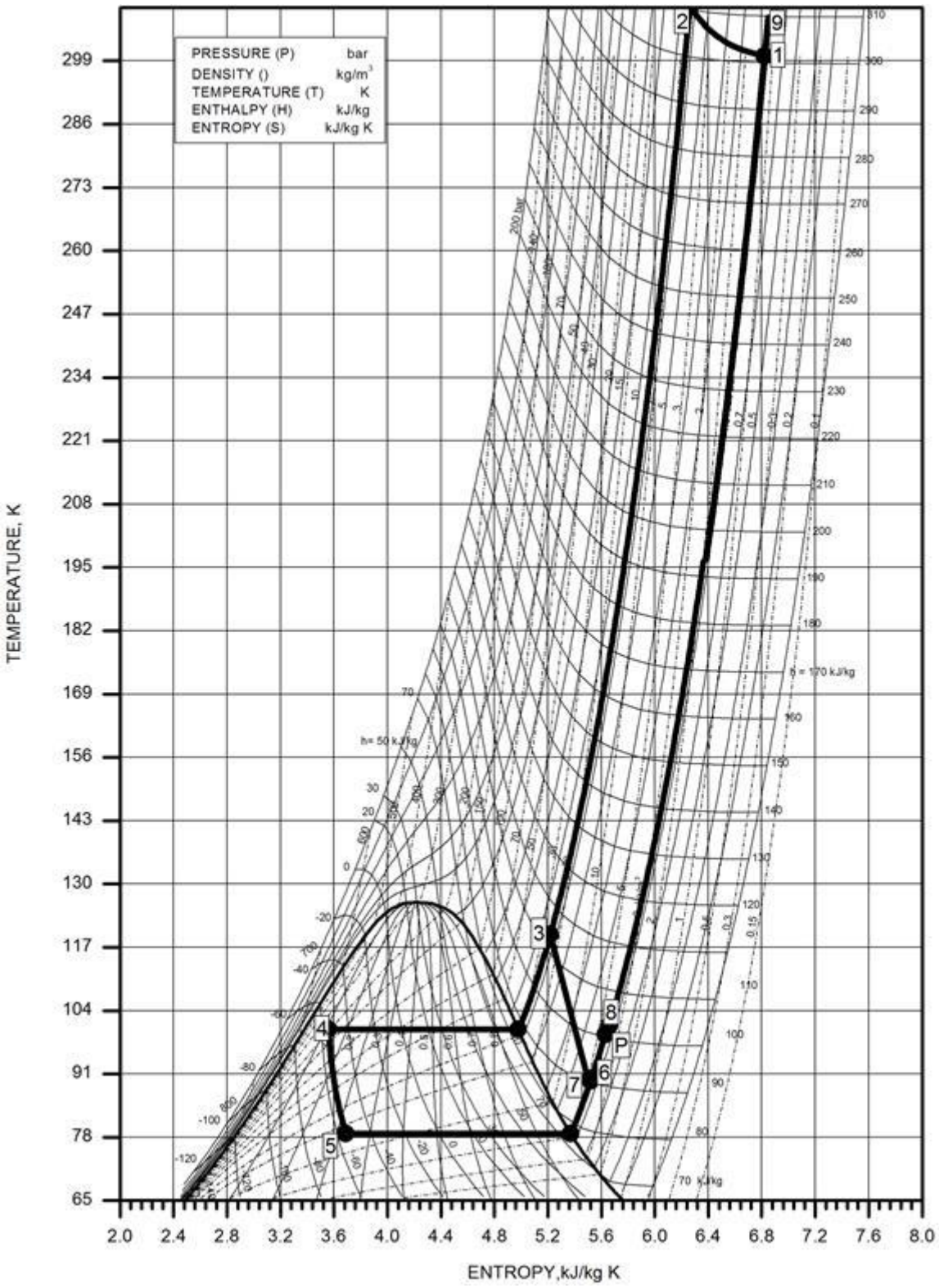

Figure 3-14 Temperature entropy diagram of Nitrogen liquefier

Chapter IV

Design of Heat Exchanger

4.1 Introduction

As per the process design described in chapter-II, the liquefier needs two numbers of heat exchangers. The first heat exchanger should have high effectiveness. So plate fin heat exchangers are to be used which will give high effectiveness up to 0.98. Design or sizing of the heat exchangers consists of determination of the heat exchanger dimensions for the specified heat transfer and pressure drop. The amount of heat transfer and pressure drop is taken from the process cycle state points. The first heat exchanger used is having both streams in single phase but the second heat exchanger under goes a phase change in high pressure stream.

The design of heat exchanger needs the determination of heat transfer coefficients, flow friction which depends on accurate prediction of colburn, j and friction factor, f .Various correlations are available in literature for the determination of colburn, j and friction factor, f . In the present design procedure for the plate and fin heat exchanger is carried out by using the correlations developed by Maiti and Sarangi [111], Manglik et.al [112] and Joshi et.al [113].The heat exchanger is also designed by using commercially available heat exchanger design software, Aspen MUSE [88].

4.2 Plate fin heat exchanger design procedure

The design of heat exchanger needs temperature and pressure at inlet and exit of both the streams along with the mass flow rate and allowable pressure drop in each stream. All properties like density, enthalpy, specific heat, viscosity, prandtl number are determined at mean temperature and pressure. Effectiveness, UA, heat load is also

calculated for the above inlet and exit conditions. As the heat capacity of cold stream is mimimum, effectiveness is found out by the following formula.

$$\varepsilon = \frac{h_{c,o} - h_{c,i}}{h'_{h,i} - h_{c,i}} \tag{4.1}$$

Where, $h_{c,i}$ = Enthalpy at inlet of the cold stream

$h_{c,o}$ = Enthalpy at outlet of the cold stream

$h'_{h,i}$ = Enthalpy at hot stream temperature and cold stream pressure

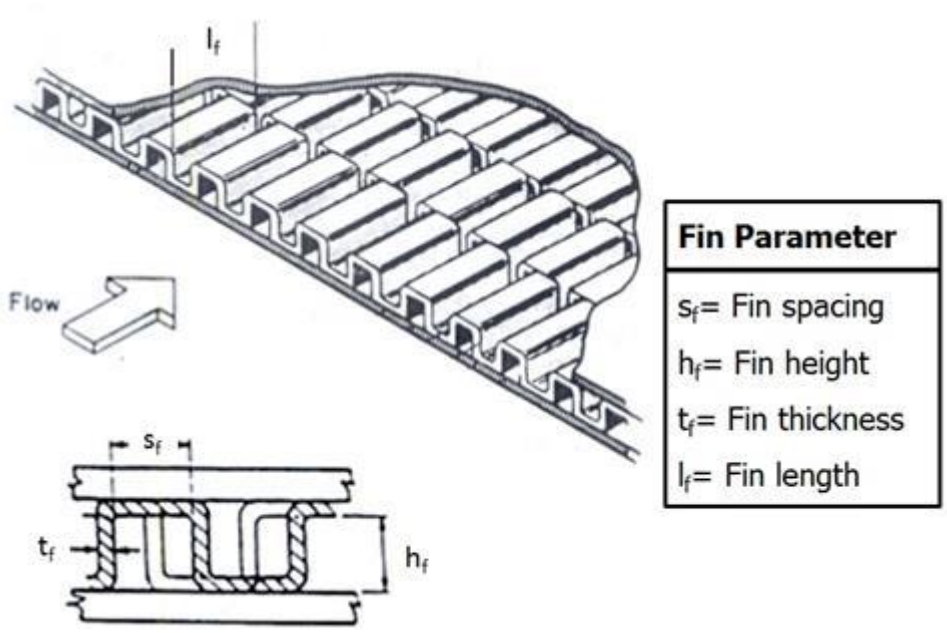

Figure 4-1 Geometry of a typical offset strip fin surface

The dimensions for offset strip fin geometry are shown in Figure 4-1. The input parameters of basic fin specifications for both the streams (i.e. for hot and cold layers) are

(i) Fin frequency, f_f

(ii) Fin thickness, t_f

(iii) Fin length, l_f

(iv) Fin height, h_f

(v) Plate thickness, a_p

The expressions for fin details for both the streams are,

Fin spacing,

$$s_f = \frac{(1 - f_f t_f)}{f_f} \tag{4.2}$$

Plate spacing,

$$b_p = h_f + t_f \tag{4.3}$$

Free flow area per fin,

$$a_{ff} = (s_f - t_f)h_f \tag{4.4}$$

Frontal area per fin,

$$a_{fr} = (s_f + t_f)(h_f + t_f) \tag{4.5}$$

Heat transfer area,

$$a_s = 2h_f l_f + 2h_f t_f + 2s_f l_f \tag{4.6}$$

Fin area,

$$a_f = 2h_f l_f + 2h_f t_f \tag{4.7}$$

Equivalent diameter,

$$D_e = \frac{4 \times \text{total free flow area} \times \text{length}}{\text{total heat transfer area}} = \frac{2(s_f - t_f)h_f l_f}{h_f l_f + h_f t_f + s_f l_f} \tag{4.8}$$

Ratio of fin area with total surface area,

$$= \frac{a_f}{a_s} \tag{4.9}$$

Frontal area ratio,

$$\sigma = \frac{a_{ff}}{a_{fr}} \tag{4.10}$$

Dimensionless parameters for the fin,

$$\alpha = \frac{h_f}{s_f} \tag{4.11}$$

$$\delta = \frac{l_f}{s_f} \tag{4.12}$$

$$\gamma = \frac{t_f}{s_f} \tag{4.13}$$

Assume width of heat exchanger, W and number of layers in hot side and cold side, n_h and n_c.

Total area between plates,

$$A_{fr} = b_p \times n_h \times W_{hx} \tag{4.14}$$

Total free flow area,

$$A_{ff} = \sigma \times A_{fr} \tag{4.15}$$

Core mass velocity,

$$G = \frac{\dot{m}}{A_{ff}} \tag{4.16}$$

Reynolds number,

$$\mathrm{Re} = \frac{GD_e}{\mu} \tag{4.17}$$

Following correlations are used to determine the Colburn, j and friction factor, f .

Maiti and Sarangi correlations :

Critical Reynolds number

$$\mathrm{Re}_j * = 1568.58(\alpha)^{-0.217}(\delta)^{-1.433}(\gamma)^{-0.217} \tag{4.18}$$

$$\mathrm{Re}_f * = 648.23(\alpha)^{-0.06}(\delta)^{0.1}(\gamma)^{-0.196} \tag{4.19}$$

For Re<Re*

$$j = 0.36(\mathrm{Re})^{-0.51}(\alpha)^{0.275}(\delta)^{-0.27}(\gamma)^{-0.063} \tag{4.20}$$

$$f = 4.67(\mathrm{Re})^{-0.70}(\alpha)^{0.196}(\delta)^{-0.181}(\gamma)^{-0.104} \tag{4.21}$$

For Re>Re*

$$j = 0.18(\mathrm{Re})^{-0.42}(\alpha)^{0.288}(\delta)^{-0.184}(\gamma)^{-0.005} \tag{4.22}$$

$$f = 0.32(\mathrm{Re})^{-0.286}(\alpha)^{0.221}(\delta)^{-0.185}(\gamma)^{-0.023} \tag{4.23}$$

Manglik and Bergles correlations :

$$j = 0.6522\mathrm{Re}^{-0.5403}\,\alpha^{-0.1541}\delta^{0.1499}\gamma^{-0.0678}\left[1 + 5.269\times10^{-5}\,\mathrm{Re}^{1.340}\,\alpha^{0.504}\delta^{0.546}\gamma^{-1.055}\right]^{0.1} \tag{4.24}$$

$$f = 9.6243\mathrm{Re}^{-0.7422}\,\alpha^{-0.1856}\delta^{0.3053}\gamma^{-0.2659}\left[1 + 7.669\times10^{-8}\,\mathrm{Re}^{4.429}\,\alpha^{0.920}\delta^{3.767}\gamma^{0.236}\right]^{0.1} \tag{4.25}$$

Where

$$\alpha = \frac{s_f}{h_f} \tag{4.26}$$

$$\delta = \frac{t_f}{l_f} \tag{4.27}$$

$$\gamma = \frac{t_f}{s_f} \tag{4.28}$$

and

$$D_e = \frac{2 s_f h_f l_f}{2\left(h_f l_f + h_f t_f + s_f l_f\right) + t_f s_f} \tag{4.29}$$

After determining the j factor, convective heat transfer coefficient, can be calculated from the formula

$$h_{conv} = \frac{(G \times j \times c)}{(\mathrm{Pr})^{0.667}} \tag{4.30}$$

Fin parameter,

$$M = \sqrt{\frac{(2 \times h_{conv,c})}{(K_f \times t_f)}} \tag{4.31}$$

Fin effectiveness,

$$\eta_f = \frac{\tanh(M l_e)}{(M l_e)} \tag{4.32}$$

Where l_e = effective length of fins

In cryogenic applications, heat loss to the cold fluid stream in the heat exchanger is minimized by placing layers in between two hot fluid layers. The number of layers through which the hot fluid passes will be one unit more than that of cold fluid layer. This arrangement is done to expose the hot fluid layer at both the ends. To take into account of heat losses to the ambient, the fin conduction lengths for the outer layers on the hot side will be taken as b_p whereas for the inner layers of the hot fluid, the conduction length is taken as $b_p / 2$. However for the cold layers placed between the hot layers the fin conduction length is taken as $b_p / 2$ as it present only inner side and adjacent layers share the same lengths.

The overall surface effectiveness of hot side,

$$\eta_{oh} = 1 - \left[\left(\frac{a_f}{a_s}\right) \times (1 - \eta_f) \times \frac{n_h - 2}{n_h}\right] - \left[\left(\frac{a_f}{a_s}\right) \times (1 - \eta_f) \times \frac{2}{n_h}\right] \tag{4.33}$$

and for cold side

$$\eta_{oc} = 1 - (a_f / a_s) \times (1 - \eta_f) \tag{4.34}$$

The ratio of total heat transfer surface area to the separating surface area (wall area) is,

$$A_o / A_w = \frac{1 - Nf_f * t_f}{1 - (A_f / A_o)} \tag{4.35}$$

Overall heat transfer coefficient is,

$$\frac{1}{U_o} = \frac{1}{\eta_{oh} h_h} + \frac{a_p A_o}{K_W A_W} + \frac{(A_{oc} / A_{oh})}{\eta_{oc} h_c} \tag{4.36}$$

Heat transfer area may be calculated as

$$A_0 = \frac{U_0 A_0}{U_0} \tag{4.37}$$

The required length of the heat exchanger is calculated from the equivalent diameter definition, as

$$L = \frac{D_e A_0}{4 A_{ff}} \tag{4.38}$$

The pressure drop is determined using the friction factor calculated from the correlations (4.21) or (4.23) and (4.25).

$$\Delta p = \frac{fLG^2}{2 D_e \rho b_p} \tag{4.39}$$

If the pressure drop obtained is less than allowable pressure drop then calculation is proceed to the estimation of longitudinal conduction of heat. Otherwise the number of layers and fin parameters are modified to get the desired pressure drop.
Frontal area of fin,

$$A_{frt} = W_{hx} \times H_{hx} \tag{4.40}$$

Wall conduction area,

$$A_w = A_{frt} - A_{ffh} - A_{ffc} \tag{4.41}$$

where, A_{ffh} and A_{ffc} are the free flow area of hot side and cold side respectively.

N.T.U required is determined as,

$$N_{tu} = \frac{1}{1 - C_R} \ln\left[\frac{1 - C_R \varepsilon}{1 - \varepsilon}\right] \tag{4.42}$$

Assuming a Factor of safety, $F.S$, NTU (considering longitudinal heat conduction) required is,

$$(N_{tu})_{lc} = (N_{tu}) \times F.S \tag{4.43}$$

and,

$$(UA)_{lc} = (N_{tu})_{lc} * C_{min} \tag{4.44}$$

Area considering longitudinal conduction is,

$$A = \frac{(UA)_{lc}}{U} \tag{4.45}$$

Length of the heat exchanger (considering longitudinal heat conduction) is,

$$L = \frac{D_e \times A_o}{4 \times A_{ff}} \tag{4.46}$$

The effect of longitudinal heat conduction is to reduce the effectiveness of heat exchanger. The decrease in the effectiveness of heat exchanger is found out using Kroeger's equation.

Wall conduction parameter is defined as,

$$\lambda = \frac{K_w A_w}{LC_{min}} \tag{4.47}$$

The effectiveness of heat exchanger with longitudinal heat conduction is,

$$y = \lambda * N_{tu} * Cr \tag{4.48}$$

$$\gamma = \frac{(1 - Cr)}{(1 - Cr)(1 + y)} \tag{4.49}$$

$$\varphi = \gamma(y / (1 + y)^{1/2} \left[\frac{(1 + \gamma)y}{1 - \gamma(1 + \gamma)y} \right] \tag{4.50}$$

$$\phi = \frac{(1 + \varphi)}{(1 - \varphi)} \tag{4.51}$$

$$r_1 = \frac{(1 - C_r) * N_{tu}}{1 + \lambda \times N_{tu} \times Cr} \tag{4.52}$$

Ineffectiveness

$$(1 - \varepsilon) = \frac{(1 - Cr)}{\phi \exp(r_1) - Cr} \tag{4.53}$$

Effectiveness

$$\varepsilon = [1 - (1 - \varepsilon)] \tag{4.54}$$

This calculated effectiveness is to be checked with the previously calculated effectiveness using equation (4.1). If it is less than before then the factor of safety is increased till this effectiveness is greater than or equal to the previous effectiveness. The length obtained is the final length of heat exchanger. And again calculate the pressure drop using the equation (4.39) is calculated for the new length.

4.3 Design of first heat exchanger

The first heat exchanger is designed using the correlations from Maiti and Sarangi [111] and Manglik and Bergles [112]. This design is further rectified by Aspen MUSE software. With the data given in Table 4-1 and Table 4-2, the design is given in Table 4-3 as per design procedure outlined earlier.

Table 4-1 Thermal data for First Heat exchanger

	High Pressure side	**Low Pressure Side**
Inlet temperature	310 K	100.74 K
Outlet temperature	120.45 K	307.89 K
Mass flow rate	82.22 g/sec	78.34 g/sec
Pressure at inlet	8 bar	1.125 bar
Allowable pressure drop	0.05 bar	0.05 bar

Table 4-2 Fin specifications for first heat exchanger

	High Pressure side	**Low Pressure Side**
Fin frequency	714 fins/m	714 fins/m
Fin metal thickness	0.2 mm	0.2 mm
Fin length	3 mm	3 mm
Fin height	6.3 mm	9.3 mm
Separating plate thickness	0.8 mm	0.8 mm

Keeping the core height, core width and number of layers same the length is found out using correlations and Aspen MUSE as shown in Table 4-3. The length of the heat exchanger varies from 1976 mm to 2150 mm. Out of these the length given by Aspen MUSE is selected excluding header length of 90 mm as per Aspen MUSE.

To accommodate a large length of the heat exchanger inside the cold box is difficult. As the cold box has height of 1800mm, the first heat exchanger is divided into two parts of equal length. The divided parts are joined by pipe as shown in.

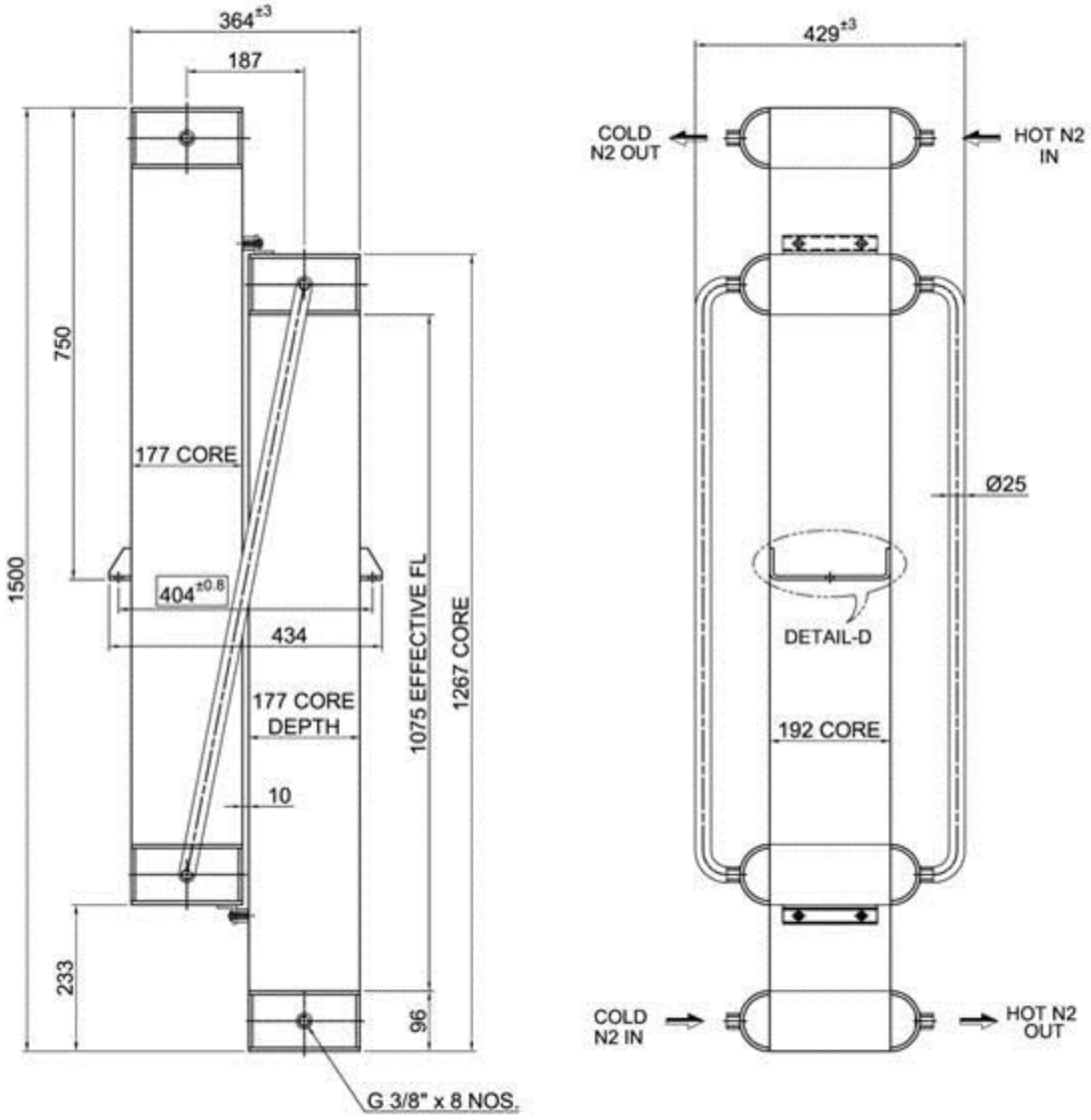

Figure 4-2. Dimension of first plate fin heat exchanger

Table 4-3 Overall dimension of first heat exchanger

	Maiti and Sarangi	**Manglik and Bergles**	**Apen MUSE**
Core length (in mm)	2081	1976	2150
Core width (in mm)	180	180	180
Core Height (in mm)	165	165	165
Number of layers in hot side	10	10	10
Number of layers in cold side	9	9	9

4.4 *Design of second heat exchanger*

As per process design done in Chapter-II the minimum temperature approach is 1 K. The thermal data for the second heat exchanger is given in Table 4-4. Nitrogen gas is cooled to the saturated temperature of 100.45 K at 7.95 bar and then condensation takes place. The heat transfer coefficient on condensation part is high and it is obtained from graph [114] as shown in Figure 4-3. Due to high heat transfer coefficient, the fin frequency in the condensation part of the second heat exchanger is low and this also facilitates the removal of condensed droplets which would otherwise obstruct the flow. The fin specification for the second heat exchanger is shown in Table 4-5. The heat exchanger dimensions are shown in Figure 4-4.

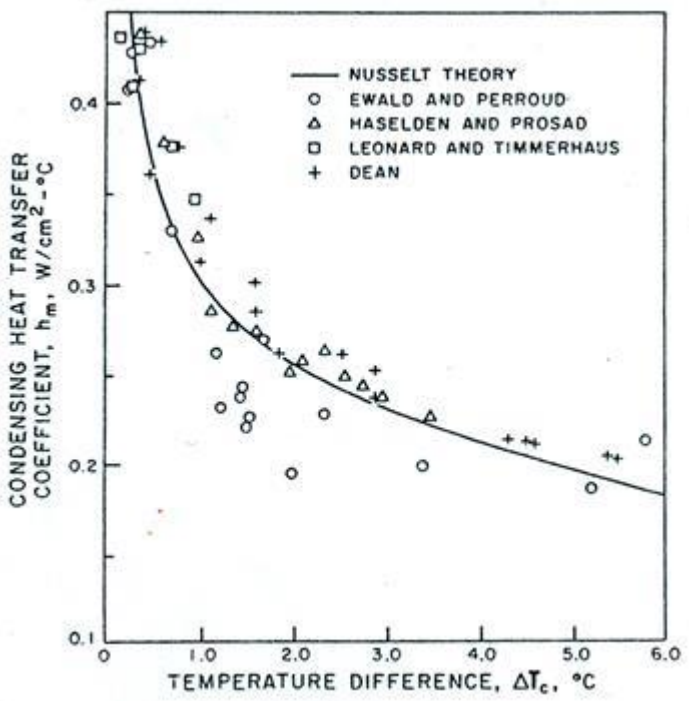

Figure 4-3 Condensing h.t.c for nitrogen as a function of temperature difference [114]

Table 4-4 Thermal data of second heat exchanger

	High pressure side	**Low pressure side**
Inlet temperature	120 K	89.1 K
Outlet temperature	100.45 K	101.2 K
Mass flow rate	5.756 g/sec	78.34 g/sec
Pressure at inlet	7.95 bar	1.2 bar
Allowable pressure drop	0.05 bar	0.05 bar

Table 4-5 Fin specifications for second heat exchanger

	High pressure side	**Low pressure side**
Fin frequency	500 fins/m	714 fins/m
Fin metal thickness	0.2 mm	0.2 mm
Fin length	3 mm	3 mm
Fin height	6.3 mm	6.3 mm
Separating plate thickness	0.8 mm	0.8 mm

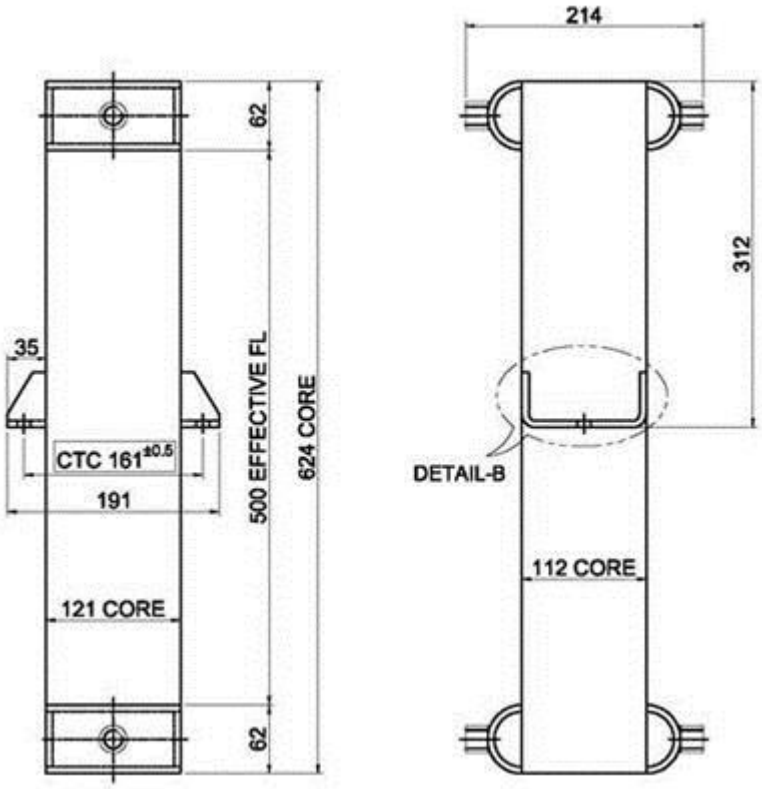

Figure 4-4. Dimension of second plate fin heat exchanger

Chapter V

Design of Turboexpander

5.1 Introduction

The performance of all cryogenic refrigeration and liquefaction plants mainly depends on the efficiency of turboexpander. The turboexpander is an expansion device where the process gas is expanded with reduction of temperature. It is a dynamic system which responds to the variation in process stream parameters. To design the turboexpander a fixed state of process stream parameters or design point is required. The design point is fixed as per the process design done in chapter III. The basic input parameters or design points are given in Table 5-1.

Table 5-1 Basic input values for turboexpander design

Working fluid	Nitrogen
Turbine inlet temperature, T_{in}	124 K
Turbine inlet pressure, p_{in}	7.97 bar
Discharge pressure, p_{ex}	1.2 bar
Mass flow rate, $\dot{m}$	76.46 g/sec

The literatures of design methods for turboexpander [18, 26, 48, 49, 115, 116] are available for low expansion ratio with purely radial turbines. But the above data design point have high expansion ratio (i.e. 6.64). The high expansion ratio is achieved by using backward curved vanes which increases the tangential force on the blades thereby increasing the turbine speed for higher efficiency.

The present design procedure has following characteristics,

(i) Design for any expansion ratio

(ii) Design of radial, backward or forward turbine

The turboexpander consists of a turbine wheel and a brake wheel at the two ends of a vertically placed shaft. The sectional view of the turboexpander is shown in Figure 5-1. The shaft is supported by two number of tilting pad journal bearing and two number of aerostatic thrust bearing. The whole components are place inside a bearing housing. At the lower end of bearing housing, cold end housing is attached. The cold end housing consists of nozzles and diffuser. At the top of bearing housing, warm end housing is present. It consists of a nozzle to the brake compressor.

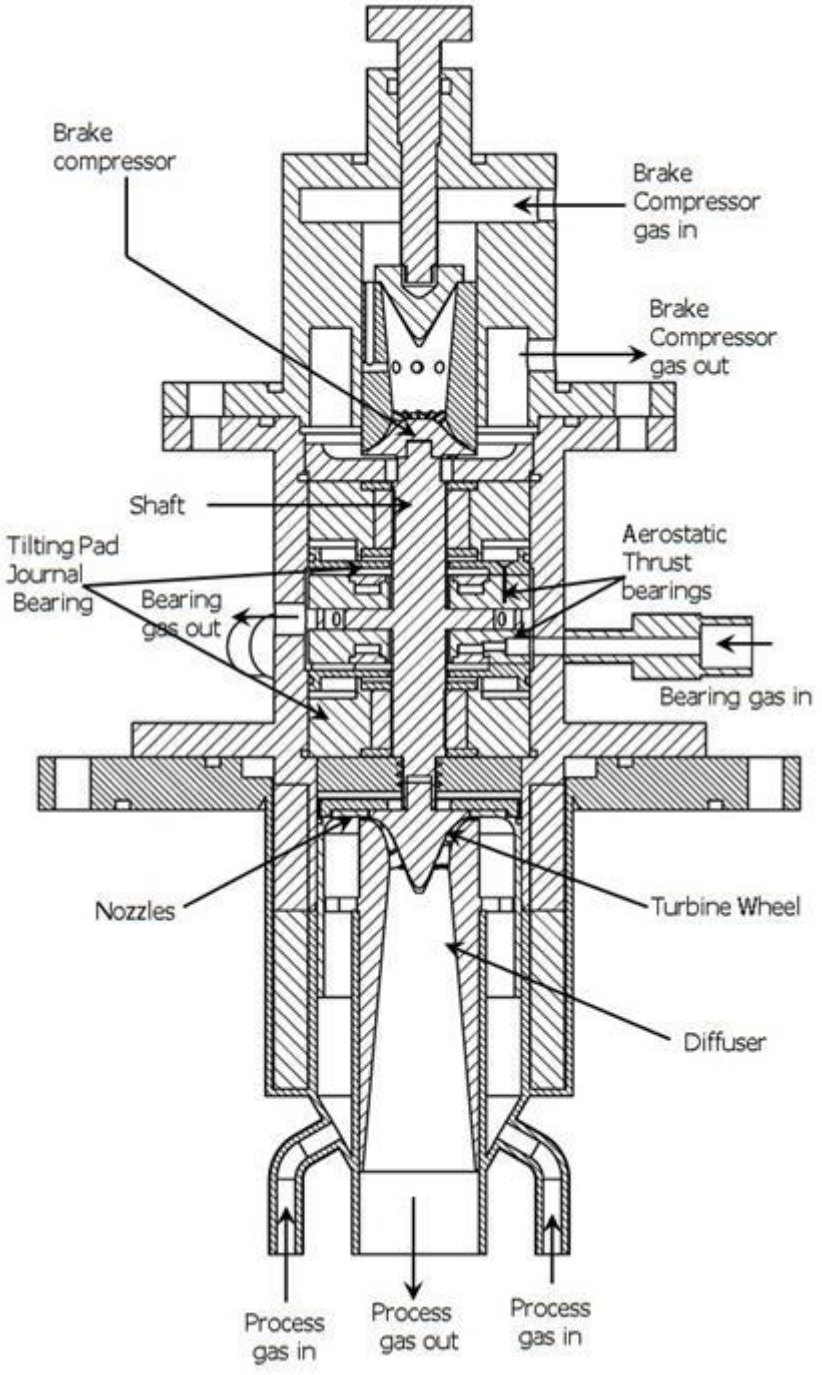

Figure 5-1 Longitudinal section of Turboexpander

The design of turboexpander mainly consists

(i) Design of turbine wheel

(ii) Design of Nozzles

(iii) Design of Diffuser

(iv) Design of Shaft

(v) Design of Brake compressor

(vi) Selection of journal and thrust bearing

(vii) supporting and housing components

(viii) Other turboexpander components

5.2 Design of turbine wheel

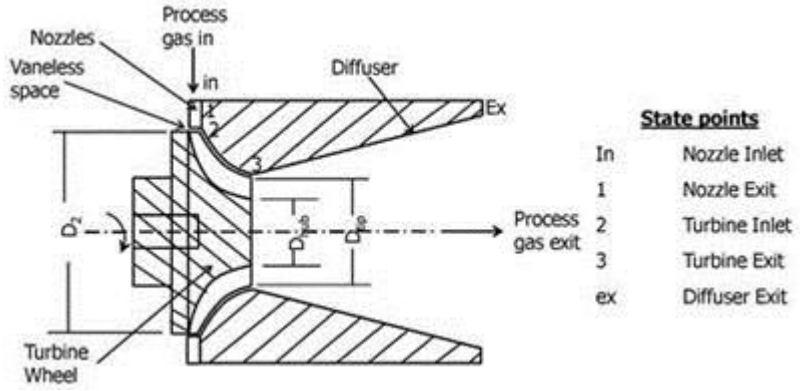

Figure 5-2 State points at nozzles, turbine wheel and diffuser

The two dimensionless parameters, specific speed and specific diameter uniquely determine the major dimensions of the wheel and its inlet and exit velocity triangles.

$$\text{Specific speed, } n_s = \frac{\omega \times \sqrt{Q_3}}{\left(\Delta h_{3,s}\right)^{3/4}} \tag{5.1}$$

$$\text{Specific diameter, } d_s = \frac{D_2 \times \left(\Delta h_{3,s}\right)^{1/4}}{\sqrt{Q_3}} \tag{5.2}$$

Where, Q_3 is the volumetric flow rate at the exit of the turbine wheel and $\Delta h_{3,s}$ is the isentropic enthalpy drop from inlet to the turbine exit. The values of specific speed and specific diameter are chosen so that Mach number of the fluid at the nozzle exit is maintained at or close to unity. If the velocity of fluid exceeds the speed of sound, the flow gets choked leading to the creation of shock waves and flow at the exit of the

nozzle will be non-isentropic. The specific speed and specific diameter are chosen so as to achieve the maximum possible efficiency within the subsonic zone.

Assume $\eta_s d_s = 1.9$

And specific speed $\eta_s = 0.5471$

Then Specific diameter $d_s = \frac{\eta_s d_s}{\eta_s} = 3.4728$

At known p_{in} and T_{in}, h_{in} =118.92 kJ/kg and s_{in} =5.2603 kJ/kg K

As $s_{ex,s} = s_{in}$ and $p_{ex,s} = p_{ex}$, so $s_{ex,s} = 5.2603$ kJ/kg K and $p_{ex,s} = 1.2$ bar

At known $p_{ex,s}$ and $s_{ex,s}$, $h_{ex,s}$ =69.18 kJ/kg

Efficiency of the turboexpander,

$$\eta = \frac{h_{in} - h_{ex}}{h_{in} - h_{ex,s}} \tag{5.3}$$

Reasonable turbine efficiency $\eta_{th} = 75$ % is assumed [49]

Substituting the values in equation(5.3), we get enthalpy at exit of turboexpander as,

$$h_{ex} = h_{in} - \eta(h_{in} - h_{ex,s}) = 81.615 \text{ kJ/kg}$$

Power produced,

$$\mathrm{P} = \dot{m}\ (h_{in} - h_{ex}) = 2.8523 \text{ kW} \tag{5.4}$$

Isentropic enthalpy drop in turboexpander $= h_{in} - h_{ex,s} = 49.74$ kJ/kg

Volume flow rates at diffuser exit, $Q_{ex} = \frac{\dot{m}}{\rho_{ex}} = 0.01480 \text{ m}^3/s$ (5.5)

The states at the exit of the turboexpander are known. But states at turbine exit are not known. There is the difference between the states '3' and 'ex' caused by pressure recovery and consequent rise in temperature and density in the diffuser. The two factors k_1 and k_2 are taken in account.

Where

$$k_1 = \frac{Q_3}{Q_{ex}} = \frac{\rho_3}{\rho_{ex}} \tag{5.6}$$

and

$$k_2 = \frac{h_{in} - h_{3s}}{h_{in} - h_{ex,s}} \tag{5.7}$$

The value of k_1 is assumed to be 1.11 as taken by Ghosh [49] and k_2 value is taken as 1.03 from the suggestion of Kun and Sentz [22, 117]

Substituting the values of k_1 and k_2 in equation(5.6) and (5.7) respectively we get, isentropic enthalpy drop from turbine

$$\Delta h_{3,s} = (h_{in} - h_{3,s}) = k_2(h_1 - h_{ex,s}) = 51.23 \text{ kJ/kg} \quad (5.8)$$

and volumetric flow rate at exit of turbine wheel

$$Q_3 = k_1 Q_{ex} = 0.01643 \text{ m}^3/s \quad (5.9)$$

Again substituting the values of $\Delta h_{3,s}$ and Q_3 in the equations (5.1) and (5.2) gives the speed and diameter of the turbine wheel.

Rotational speed of turbine wheel,

$$\omega = \frac{n_s \left(\Delta h_{3s}\right)^{3/4}}{\sqrt{Q_3}} = 14534.67 \text{ rad/s} \cong 138778 \text{ rpm} \quad (5.10)$$

Inlet diameter of turbine, $D_2 = \frac{d_s \sqrt{Q_3}}{\left(\Delta h_{3,s}\right)^{1/4}} = 29.6 \text{ mm}$ (5.11)

Blade velocity at inlet to the turbine, $U_2 = \frac{\omega D_2}{2} = 215.11 \text{ m/s}$ (5.12)

Spouting velocity, $C_0 = \sqrt{2(h_1 - h_{ex,s})} = 315.4 \text{ m/s}$ (5.13)

Velocity ratio, $V.R. = \frac{U_2}{C_0} = 0.682$ (5.14)

As all radial turbines are found to produce maximum efficiencies over the range of velocity ratio 0.65 to 0.70 [118]. The current velocity ratio from equation (5.14) is within limit.

Rohlik [118] prescribes that, ξ the ratio of eye tip diameter to inlet diameter should be limited to a maximum value of 0.7 to avoid excessive shroud curvature. The value of ξ is taken as 0.6, corresponding to the maximum efficiency within the subsonic zone and for obtaining longer blade passages.

$$\xi = \frac{D_{tip}}{D_2} = 0.60 \quad (5.15)$$

Diameter at the eye tip, $D_{tip} = 0.6 \times D_2 = 0.6 \times 0.0296 = 0.0177 \text{ m} \cong 17.8 \text{ mm}$

Again from reference [41], the exit hub to tip diameter ratio should be limited to a minimum value of 0.4 to avoid excessive hub blade blockage and energy loss. Kun and Sentz [41] have taken a hub ratio of 0.35 citing mechanical considerations. Ino et. al [33] have chosen a value of 0.588. For current design the value of λ is taken as 0.425.

$$\lambda = \frac{D_{hub}}{D_{tip}} = 0.50 \tag{5.16}$$

Diameter at the hub, $D_{hub} = 0.425 \times D_{tip} = 0.00888$ m $\cong 8.9$ mm

Mean outlet diameter of the turbine wheel,

$$D_{3,mean} = \frac{D_{3,hub} + D_{3,tip}}{2} = \frac{0.0089 + 0.0177}{2} = 0.01332 \text{ m} \cong 13.32 \text{ mm} \tag{5.17}$$

$$U_{3,mean} = \frac{\omega \times D_{3,mean}}{2} = 96.801 \text{ m/s} \tag{5.18}$$

$$U_{3,tip} = \frac{\omega \times D_{3,tip}}{2} = 129.359 \text{ m/s} \tag{5.19}$$

$$U_{3,hub} = \frac{\omega \times D_{3,hub}}{2} = 64.679 \text{ m/s} \tag{5.20}$$

Assume absolute meridian velocity C_{m3} is 109.9 m/s. For small turbines, the hub circumference at exit and diameter of milling cutters available determine the number of blades. So number of blades, $Z = 10$ [49], thickness of blades, $t = 0.6$ mm [33] and exit angle α_3 is taken as 95^0 [22].

Absolute velocity at turbine exit,

$$C_3 = \frac{C_{m3}}{\sin \alpha_3} = 110.3198 \text{ m/s} \tag{5.21}$$

Absolute tangential component,

$$C_{\theta 3} = C_3 Cos(\alpha_3) = -9.615 \text{ m/s} \tag{5.22}$$

Relative velocity at turbine exit,

$$W_3 = \sqrt{C_3^2 + U_3^2 - 2C_3 U_3 \cos(\alpha_3)} = 152.978 \text{ m/s} \tag{5.23}$$

$$\beta_{3,mean} = \tan^{-1} \frac{C_3 \sin(\alpha_3)}{U_{3,mean} - C_3 \cos(\alpha_3)} = 45.92^{\circ} \tag{5.24}$$

Flow through turbine

$$Q_3 = C_3 \sin(\alpha_3)\left[\frac{\pi}{4}\left(D_{3,tip}{}^2 - D_{3,hub}{}^2\right) - \frac{Z_{tr} t_{tr}\left(D_{3,tip} - D_{3,hub}\right)}{2\sin\beta_{3,mean}}\right] = 0.01643 \text{ m}^3/\text{s} \quad (5.25)$$

Check the value of Q_3 in equation (5.25) with the previously calculated value from equation (5.9) of Q_3. If they are not equal then change the value of C_{m3}.

Assume incidence angle, α_2 as 26^0. The amount of work can be extracted from a turbine is calculated from change in momentum of the fluid in its passage through the turbine wheel. From the energy conservation equation for turbo machine [22], we get

$$(h_{02} - h_{03}) = C_2 U_2 \cos(\alpha_2) - U_3 C_3 \cos(\alpha_3) \quad (5.26)$$

From equation (5.26), we get

$$C_2 = \frac{1000(h_{02} - h_{03}) + U_3 C_3 \cos(\alpha_3)}{U_2 \cos(\alpha_2)} = 187.386 \text{ m/s} \quad (5.27)$$

$$C_{\theta 2} = C_2 \cos(\alpha_2) = 187.38\cos(26) = 168.42 \text{ m/s} \quad (5.28)$$

$$C_{m2} = C_2 \sin(\alpha_2) = 187.38\sin(26) = 82.145 \text{ m/s} \quad (5.29)$$

$$W_2 = \sqrt{C_{m2}{}^2 + (U_2 - C_{\theta 2})^2} = \sqrt{82.143^2 + (215.113 - 168.42)^2} = 94.487 \text{ m/s} \quad (5.30)$$

$$\beta_2 = \tan^{-1}\frac{C_{m2}}{(U_2 - C_{\vartheta 2})} = \frac{82.145}{(215.113 - 168.42)} = 60.38^{\circ} \quad (5.31)$$

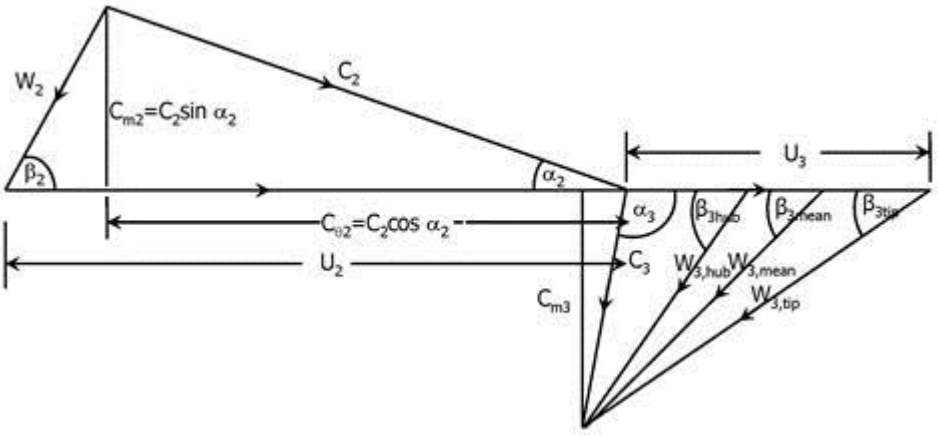

Figure 5-3 Velocity diagrams for turbine

Thermodynamic state at wheel discharge (state 3)

Exit stagnation enthalpy:

$$h_{0ex} = h_{ex} + \frac{C_{ex}^{\ 2}}{2} = 81.615 + \frac{17^2}{2000} = 81.76 \text{ kJ/kg} \tag{5.32}$$

Exit stagnation pressure:

$$p_{0ex} = p_{ex} + \frac{1}{2}\rho_{ex} C_{ex}^{\ 2} = 1.2075 \text{ bar} \tag{5.33}$$

Neglecting the losses in the diffuser, stagnation enthalpy at turbine outlet is $h_{03} = h_{04}$ and static enthalpy at the outlet of turbine is given by

$$h_3 = h_{03} - \frac{C_3^{\ 2}}{2} = 81.76 - \frac{110.32}{2 \times 1000} = 75.674 \text{ kJ/kg} \tag{5.34}$$

$$\rho_3 = \frac{\dot{m}}{Q_3} = \frac{0.07646}{0.01643} = 4.6537 \text{ kg/m}^3 \tag{5.35}$$

Corresponding to h_3 and ρ_3 all the other properties at the turbine outlet are calculated from property calculation software Allprops [109]. Static properties at the turbine outlet are as follows,

$p_3 = 1.020$ bar, $T_3 = 77.373$ K, $C_{s3} = 172.274$ m/s

Relative velocity at eye tip,

$$W_{3,tip} = \sqrt{C_3^2 + U_{3,tip}^2 - 2C_3 U_{3,tip}\cos(\alpha_3)} = 177.17 \text{ m/s} \tag{5.36}$$

$$\beta_{3,tip} = \tan^{-1}\frac{C_3 \sin(\alpha_3)}{U_{3,tip} - C_3\cos(\alpha_3)} = 38.33^\circ \tag{5.37}$$

Highest Mach number at eye tip = $\frac{W_{3tip}}{C_{s3}} = \frac{177.17}{172.274} = 1.0284$

Where C_{s3} is the velocity of sound for the corresponding state point 3.

Similarly Relative velocity at hub,

$$W_{3,hub} = \sqrt{C_3^2 + U_{3,hub}^2 - 2C_3 U_{3,hub}\cos(\alpha_3)} = 132.65 \text{ m/s} \tag{5.38}$$

$$\beta_{3,hub} = \tan^{-1}\frac{C_3 \sin(\alpha_3)}{U_{3,hub} - C_3\cos(\alpha_3)} = 55.94^\circ \tag{5.39}$$

Mach number at hub = $\frac{W_{3hub}}{C_{s3}} = \frac{132.65}{172.274} = 0.77$

Thermodynamic state at wheel inlet (state 2)

For computing the thermodynamic properties at wheel inlet (state 2, Figure 5-2), the efficiency of the expansion process till state 2 is assumed. The nozzle efficiency η_s needs to be between 0.9 and 0.95. So nozzle efficiency $\eta_s = 0.93$ is assumed. Assuming isentropic expansion in the vaneless space, the efficiency of the nozzle along with the vane less space is defined as

$$\eta_n = \frac{h_{in} - h_2}{h_{in} - h_{2s}} \tag{5.40}$$

Since $h_{02} = h_{01} = h_{0in} = h_{in} = 118.92$ kJ/kg

$$h_2 = h_{in} - \frac{C_2^2}{2} = 118.92 - \frac{187.386^2}{2 \times 1000} = 101.363 \text{ kJ/kg} \tag{5.41}$$

$$h_{2s} = \frac{h_{01}\eta_n - h_{01} + h_2}{\eta_n} = 100.04 \text{ kJ/kg} \tag{5.42}$$

Also $s_{in} = s_1 = s_{2s} = 5.2603$ kJ/kg

Knowing h_{2s} and s_{2s} the other properties at the point 2 are calculated as,

$p_{2s} = p_2 = 4.319$ bar

$T_2 = 104.57$ K, $\rho_2 = 15.0194$ kg/m^3, $s_2 = 5.273$ kJ/kg K, $C_{s2} = 199.6$ m/s

From continuity equation, the blade height at entrance to the wheel is computed as:

$$b_2 = \frac{\dot{m}_{tr}}{(\pi D_2 - Z_{tr} t_{tr})\rho_2 C_{m2}} \tag{5.43}$$

$$= \frac{0.07646}{\left(\pi \times 0.0296 - 10 \times 0.6\right) \times 15.0914 \times 82.144} = 0.709 \text{ mm}$$

Absolute Mach number at the exit of nozzle or turbine wheel $\frac{C_2}{C_{s2}} = \frac{187.38}{199.6} = 0.9388 < 1$

The absolute Mach number at exit of the nozzle should be less than 1.

Blade Profile of Turbine wheel:

The blade profile of the turbine wheel is determined by following the computational procedure described by Hasselgruber [119] by assuming pressure balanced flow path. This technique gives three dimensional contours of the blades and simultaneously determines the velocity, pressure and temperature profile in the turbine wheel.

Figure 5-4 Turbine wheel

The turbine wheel was made with Aluminum alloy (i.e. Al-6160-T6). The photograph of the turbine wheel is shown in Figure 5-4.

5.3 Design of nozzles

Thermodynamic state at the throat and vane less space, a convergent type of nozzle, which gives subsonic flow at nozzle exit, is desired. The Figure 5-5 shows the schematic diagram of nozzle ring with nozzle dimensions. If D_t is nozzle throat circle diameter and C_{mt} the meridian component of the nozzle throat velocity, then considering the mass balance equation,

$$C_{mt} = \frac{\dot{m}}{\pi D_t b_t \rho_t} \tag{5.44}$$

Where, b_t is the height of the nozzle. It is usually somewhat smaller than the turbine inlet blade height. This allows some margin for expansion in annular space and also to accommodate the axial misalignment. So it is taken as 0.8 times of the turbine inlet blade height.

$b_t = 0.8 \times b_2 = 0.567$ mm

Following Reference [41] D_t is 1.08 times of D_2, but in the current design it is taken as 1.068 times of D_2 to decrease the vane less space.

$$D_t = 1.068 \times D_2 = 0.0316 \text{ m } = 31.6 \text{ mm}$$

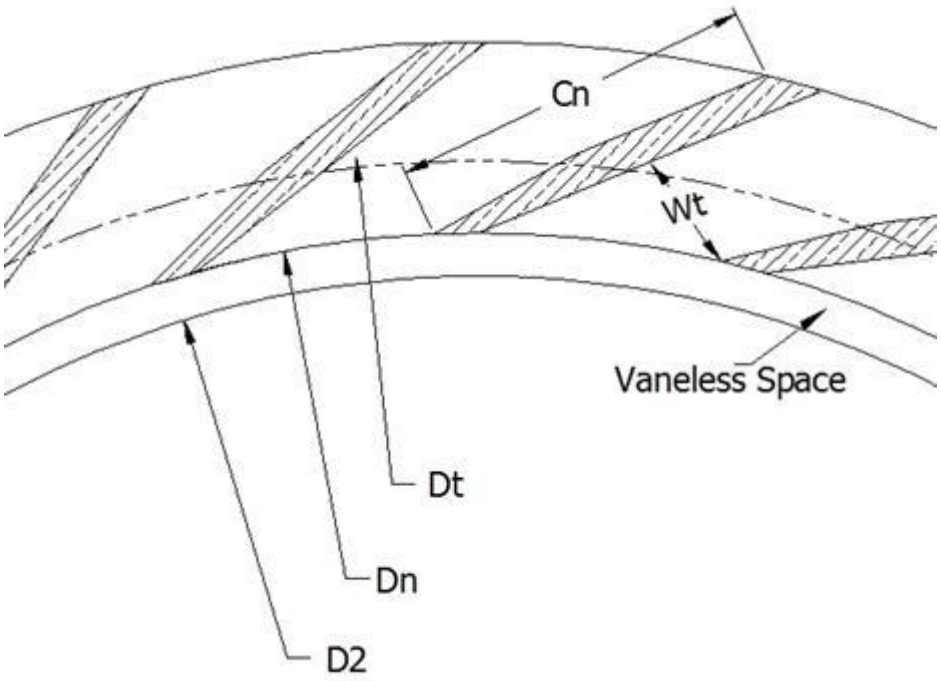

Figure 5-5 Major Dimensions of Nozzle

The velocity at exit of the throat consists of two components, C_{mt} and $C_{\theta t}$. The meridian component is perpendicular to the nozzle throat circle diameter, which determines the mass flow rate whereas the other component $C_{\theta t}$ is tangential to the throat. From conservation of angular momentum in free vortex flow over the vaneless space, the tangential component of the throat velocity,

$$C_{\theta t} = \frac{C_{\theta 2} D_2}{D_t} \tag{5.45}$$

Assuming isentropic expansion in the vane less space, $s_t = s_2$

Corresponding to the assumed value of pressure at the throat, $p_t = 4.525$ bar and $s_t = s_2 = 5.273$ kJ/kg K the properties at the throat are found from the properties package are as follows

$T_t = 106.01$ K, $\rho_t = 15.61$ kg/m^3, $h_t = 102.71$ kJ/kg, $C_{st} = 200.97$ m/s

Substituting the values of the properties, the velocities at the throat are found as follows

$C_{mt} = 86.95$ m/s; $C_{\theta t} = 157.698$ m/s and $C_t = 180.08$ m/s

The enthalpy at the throat is given by

$$= h_{01} - \frac{C_t^2}{2}$$

$$= h_{01} - \frac{C_{mt}^2}{2} - \frac{C_{\theta t}^2}{2}$$

$$= 118.92 - \frac{86.95^2}{2\times 1000} - \frac{157.698^2}{2\times 1000} = 102.71 \text{ kJ/kg}$$

The value of enthalpy at the throat obtained from equation matches with that obtained from the assumed value of the pressure, hence pressure at the throat, $P_t = 4.525$ bar .

Mach number at the throat, $M_t = \frac{C_t}{C_{st}} = \frac{181.767}{200.66} = 0.906$

This leads to subsonic operation with no loss of energy which may be due to aerodynamic shocks.

Sizing of the nozzle vanes

The correct throat angle for finite trailing edge thickness of nozzle is estimated using the conservation of momentum & continuity of flows [40] . Aerodynamically, it is desirable to make the trailing edge as thin as mechanical design consideration will allow. Using the continuity equation and the density at the throat, the throat width W_t and the throat angle α_t are calculated as follows.

Assuming the number of nozzles, $Z_n = 23$

Width at the throat

$$w_t = \frac{m_{tr}}{Z_n b_t \rho_t C_t} = \frac{0.07646}{23\times 0.5672\times 15.61\times 180.081} = 0.00208 \text{ m} = 2.08 \text{ mm} \quad (5.46)$$

and the throat angle,

$$\alpha_t = \tan^{-1}\left(\frac{C_{mt}}{C_{\theta t}}\right) = 28.87^o \quad (5.47)$$

It may be noted that the throat outlet angle is different form the turbine blade inlet angle and the discrepancy is due to the drifting of fluid in the vane less space.

The blade pitch length, p_n is estimated as,

$$p_n = \pi D_t / Z_n = 3.142\times 31.6 / 23 = 4.318 \; mm \quad (5.48)$$

α_t is the angle between the perpendicular to the throat width w_t and the tangent to the throat circle diameter. From Figure 5-5, the inner diameter of the nozzle ring is calculated as,

$$D_n = \sqrt{D_t^2 + w_t^2 - 2w_t D_t Cos\alpha_t} = 29.8 \text{ mm} \tag{5.49}$$

Where α_t is angle between D_t and w_t.

In cascade theory, blade loading and cascade solidity are defined as:

$$\delta u = \frac{\Delta V_u}{C_{mn}} = \cot\alpha_t - \cot\alpha_0 \tag{5.50}$$

$$\sigma_n = \frac{Ch_n}{S} \tag{5.51}$$

From cascade notation, $\cot\alpha_t = \cot\lambda_\infty - \frac{\delta u}{2}$ and $\cot\alpha_0 = \cot\lambda_\infty + \frac{\delta u}{2}$

The separation limit in an approximate way is expressed by a minimum required solidity. Its value is found from the aerodynamic load coefficient ψ_z defined as the ratio of actual tangential force to ideal tangential force, also known as Zweifel number. The optimum value for the aerodynamic load coefficient is about 0.9. Thus the chord length of nozzle can be found from the equation of solidity and expressed as

$$Ch_n = \frac{2s\left(\cot\alpha_t - \cot\alpha_0\right)\sin^2\alpha_t}{\psi_z \sin\lambda_s} = \frac{2\,\delta u \times S}{\psi_z\left[1 + \left(\cot\lambda_\infty + \frac{\delta u}{2}\right)^2\right]\sin\lambda_s} \tag{5.52}$$

Where

S = tangential vane spacing = $\frac{\pi D_n}{Z_n} = 4.07$ mm

λ_∞ = cascade angle or mean vector angle

$$\lambda_\infty = \cot^{-1}\left(\frac{\cot\alpha_t + \cot\alpha_0}{2}\right) = 44.627^0 \tag{5.53}$$

λ_s = stagger angle = $\lambda_\infty + \alpha_m$ and

Nozzle inlet angle, α_0 is taken as 78° [33]

Stagger deviation angle curve from the Figure 5-6 [120] gives α_m as a function of $\Delta\lambda = \left(\alpha_0 - \alpha_t\right)$ for various values of λ_∞, yields α_m = -2.4°, leading to:

$\delta_u = 1.6011$, $\lambda_\infty = 44.6274$, $\lambda_s = 42.2274$ and $Ch_n = 5.02$ mm

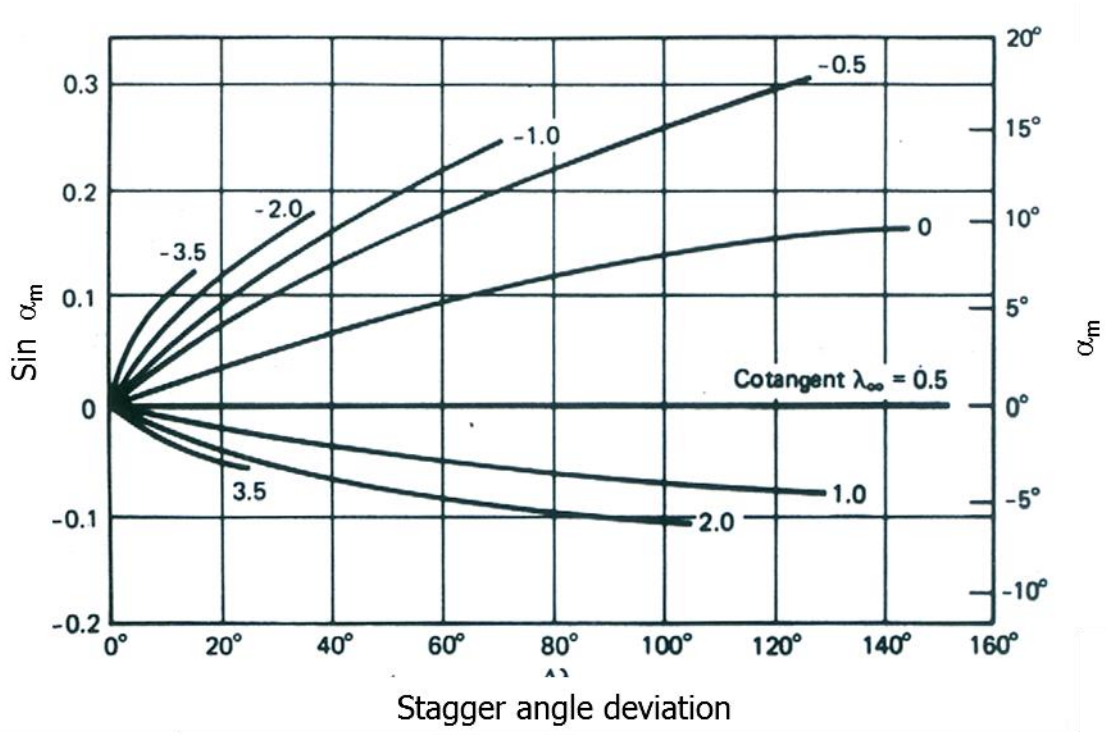

Figure 5-6 Stagger angle deviation graph for different cascade angle [120]

5.4 *Design of diffuser*

Kinetic energy at the rotor outlet should be recovered using a diffuser. The best suited diffusing angle $\left(= \tan^{-1} \frac{exit\ \ diameter - throat\ \text{diameter}}{2 * length\ \text{of the diffuser}}\right)$ which minimizes the loss in pressure recovery is 5°-6° and the aspect ratio is maintained, 1.4 to 3.3. Diameter of the diffuser at inlet is equal to the turbine wheel inlet diameter with recommended radial clearance of 2% of the turbine exit radius, which is approximately 0.1 mm for wheel. Diffuser outlet diameter is equal to the outlet piping diameter which gives the length of the diverging section as 87.4 mm. The volume flow rate at the exit from the diffuser is calculated from the equation(5.5).

$$A_{ex} = \frac{Q_{ex}}{C_{ex}} = \frac{0.0148}{17} = 0.00087 \text{ m}^2 \qquad (5.54)$$

Assuming radial clearance 0.1 mm

Diameter at inlet of diffuser, $D_{d,in} = D_2 + 2 \times$ radial clearance=29.8 mm

Area at the inlet of diffuser, $A_{d,in} = \frac{\pi}{4} \times D_{d,in}{}^2 = 0.00069746 \text{ m}^2$

Diameter at exit of diffuser, $D_{ex} = \sqrt{\frac{4 \times A_{ex}}{\pi}} = 0.0333\text{m}=33.3 \text{ mm}$

Diameter at throat of diffuser, $D_{d,th} = D_{3,tip} + 2 \times$ radial clearance = 18 mm

Taper angle of the diverging section, $\Psi_d = 5^0$

The length of the diverging section of the diffuser is given by

$$L_d = \frac{(D_{ex} - D_{d,th})}{2\tan(\psi_d)} = \frac{0.0333 - 0.018}{2\tan(5)} = 87.4 \text{ mm} \qquad (5.55)$$

The length of the converging section depends on the height of the turbine wheel and the turbine wheel height depends on blade profile program.

The nozzle and the diffuser are combined to make one component as shown in Figure 5-7. In the Figure 5-8, the nozzle is covered with the nozzle cover and its bottom part is the difusser.

Figure 5-7 Nozzle Diffuser

Figure 5-8 Nozzle cover

5.5 Design of shaft

The dimensions of the shaft based on data from comparable installations by other workers are verified for maximum stress, critical speed and heat conduction. Ino et. al. [33] have chosen a shaft diameter of 16 mm for their helium turbine rotating at 2,30,000 r.p.m, while Yang et al [26] have chosen 18 mm for their air turbine rotating at 180,000 r/min. The shaft diameter 16 mm, length 108 mm with collar diameter 44 mm have been taken as design input for this work. The Figure 5-9 shows the fabricated shaft.

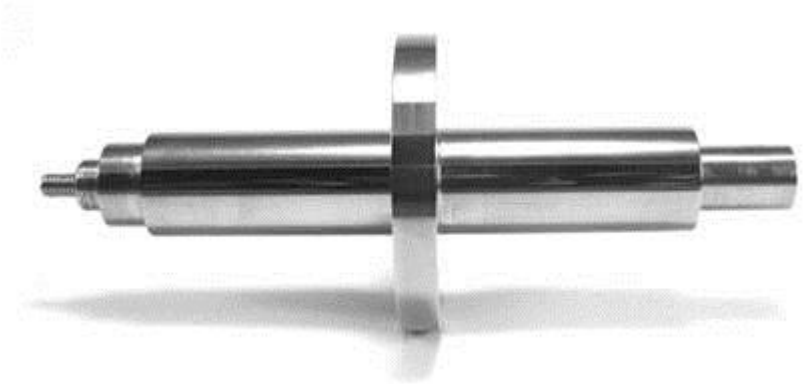

Figure 5-9 Shaft

The peripheral speed on the shaft surface is computed to be

$$V_{surf} = \frac{\omega d}{2} = \frac{14534.67 \times 16}{2000} = 116.27 \text{ m/s} \qquad (5.56)$$

and that on the tip of the collar is 319.76 m/s.

Taking density of Monel K-500 material as 8440 kg/m^3, a preliminary calculation considering the collar as a solid disk gives [121]

$$\sigma = \frac{1}{3}\rho_{ss} V^2_{surf} = \frac{1}{3} \times 8440 \times 290.693^2 = 287.65 \text{ MPa} \qquad (5.57)$$

This value is less than recommended design stress of 790 MPa for Monel K-500.

Shaft speed is generally limited by the first critical speed in bending. This limitation for the given diameter determines the shaft length. The overhang distance into the cold end, strongly affects the conductive heat leak penalty.

The first bending critical speed for a uniform shaft is given by the formula [120]

$$f = 0.9\left(d/l^2\right)\sqrt{\frac{E}{\rho}} \text{ Hz} \qquad (5.58)$$

Where d is the diameter of the shaft, l is the length, E is the Young's modulus and ρ is the density of the material. Considering the shaft to be monel K-500 of diameter 16 mm and length 108 mm, the bending critical speed is

$$f = 0.9\left(d/l^2\right)\sqrt{\frac{E}{\rho}} = 0.9\left(0.016/0.1^2\right)\sqrt{\frac{1.8\times10^{11}}{8440}} = 6650.09 \text{ Hz} = 399{,}005.4 \text{ rpm}$$

This is well above the operating speed of 1, 38,777 rpm.

5.6 Design of brake compressor

The shaft power generated by the turbine is transferred by using brake compressor which is mounted on the shaft. Hence the brake compressor is designed to transfer 2.852 kW of power.

The design inputs for design of brake compressor are given in Table 5-2.

Table 5-2 Basic input parameters for design of brake compressor

Process gas	Air/nitrogen
Power to be dissipated, P	2852 W
Angular speed, ω	14534.67 rad/s (1, 38,777 rpm)
Inlet total pressure, p_{04}	4.1 bar
Inlet total temperature, T_{04}	300 K (ambient temperature)
Expected efficiency, η_b	60%

To determine the compressor discharge pressure and flow rate, an estimate of the static thermodynamic properties at the inlet is needed.

Stagnation density at 4.1 bar and 300 K is 4.61 kg/m^3
Let static density at inlet be,

$$\rho_4 = 0.96\rho_{04} = 0.96\times4.61 = 4.4256 \text{ kg/m}^3 \qquad (5.59)$$

From the $\eta_s - d_s$ diagram for a single stage centrifugal compressor, the operating point is chosen in order to achieve proper velocity triangles within the constraints of available power and rotational speed. The operating conditions are $\eta_s = 1.95,\ d_s = 2.9$.

Where specific speed,

$$\eta_s = \frac{\omega\sqrt{Q_4}}{\Delta h_s^{3/4}} \tag{5.60}$$

and specific diameter,

$$d_s = \frac{D_5 \Delta h_s^{1/4}}{\sqrt{Q_4}} \tag{5.61}$$

Δh_s is the isentropic static head drop across the compressor and D_5 is the diameter of the impeller. Balje [120] has pointed out that mixed flow geometry is necessary to obtain the highest efficiency at these values of η_s and d_s

Assume, $\Delta h_s = 7504.4$ J/kg;

From equation(5.60), volume flow rate at the inlet of compressor

$$Q_4 = \left[\frac{\eta_s(\Delta h_s)^{3/4}}{\omega}\right]^2 = \left[\frac{1.95\times(7504.4)^{3/4}}{14534.67}\right]^2 = 0.0117 \text{ m}^3/\text{s} \tag{5.62}$$

From equation(5.61),

$$D_5 = \frac{d_s\sqrt{Q_4}}{(\Delta h_s)^{1/4}} = \frac{2.9\sqrt{0.0117}}{(7504.4)^{1/4}} = 0.0337 \text{ m=33.7 mm} \tag{5.63}$$

Mass flow rate through the compressor,

$$m_b = \rho_4 Q_4 = 4.4256\times 0.0117 = 0.05179 \text{ kg/s} \tag{5.64}$$

Assuming zero swirls at inlet, Power input,

$$P = \phi\sigma_{sf} m_b U_5^2 \tag{5.65}$$

Where, $\phi =$ power input factor $= 1.02$ [122]

$\sigma_{sf} =$ Slip factor $= 0.9$ [122]

$U_5 =$ Peripheral speed at exit $= \frac{\omega D_5}{2}$

$m_b =$ Mass flow rate through compressor $= \rho_1 Q_1$

Substituting the values in equation(5.65), we get

$$P = \frac{1.02\times 0.9\times 0.05179\times 14534.67^2\times 0.0337^2}{4} = 2852.4 \text{ W}$$

This agrees with the power to be dissipated.

Hence static enthalpy drop across the compressor is $\Delta h_s = 7504.4$ J/kg

Power dissipated,

$$P = \frac{m_b \Delta h_{0s}}{\eta_b} = \frac{\rho_4 Q_4 \Delta h_{0s}}{\eta_b} = 2852 \text{ W} \qquad (5.66)$$

here Δh_{0s} is the total isentropic head drop across the compressor.

Substituting the value of Q_1 in equation(5.66)

Total isentropic head drop, $\Delta h_{0s} = \frac{2852.4 \times 0.60}{4.4256 \times 0.0117} = 33047.72$ J/kg

Peripheral speed at exit, $U_5 = \omega D_5 / 2 = \frac{14534.67 \times 0.0337}{2} = 244.94$ m/s

Assuming exit to inlet diameter ratio, $\frac{D_5}{D_4} = 2.25$

and blade height to diameter ratio at inlet as $\frac{b_4}{D_4} = 0.2$

Inlet diameter, $D_5 = D_4 / 2.25 = 0.0337 / 2.25 = 0.015$ m = 15 mm

Inlet blade height, $b_4 = 0.2 \times D_4 = 0.2 \times 0.015 = 3$ mm

Number of blades of brake compressor

There are several empirical relations for determining the optimum number of blades. Well known among them are

$$\begin{aligned} &\text{Eck} && : z_b = 8.5 \sin\beta_5 (1 - \frac{D_4}{D_5})^{-1} \\ &\text{Pfleirderer} && : z_b = 6.5 \left(\frac{D_4 + D_5}{D_5 - D_4} \right) \sin\left(\frac{\beta_4 + \beta_5}{2} \right) \\ &\text{Stepanoff} && : z_b = \frac{1}{3}\beta_5 \text{ with } \beta_5 \text{ given in degrees.} \end{aligned} \qquad (5.67)$$

The equations(5.67) give 17, 16 and 18 blades respectively for the impeller. A choice of 12 numbers of blades and thickness of 0.75 mm are assumed from the present design point of view.

Inlet velocities

Assuming number of blades, $z_b = 12$ and a uniform thickness $t_b = 0.075$ mm, the radial absolute velocity C_{m4} (which is also equal to the absolute velocity C_4 in the absence of inlet swirl) is given as:

$$C_{m4} = C_4 = \frac{Q_4}{(\pi D_4 - Z_b t_b) \times b_4)} = 102.309 \text{ m/s}$$

The peripheral velocity at inlet is computed to be:

$$U_4 = \frac{D_4 \omega}{2} = 109.01 \text{ m/s}$$

The inlet blade angle β_4 and the inlet relative velocity W_4 are computed from the inlet velocity triangle shown as,

$$\beta_4 = \tan^{-1} \frac{C_{m4}}{U_4} = 43.18^o,$$

$$W_4 = \sqrt{U_4^2 + C_4^2} = 149.5 \text{ m/s}$$

The relative Mach number at inlet,

$$M_{W4} = W_4 \Big/ \sqrt{\gamma R T_4} = 0.422.$$

This value indicates that the flow is subsonic in nature.

Thermodynamic variables at inlet and exit

Static temperature at inlet:

$$T_4 = T_{04} - \frac{C_4^2}{2C_p} = 294.99 \text{ K} \tag{5.68}$$

Inlet static pressure:

$$p_4 = p_{04} \left(\frac{T_4}{T_{04}} \right)^{\frac{\gamma}{\gamma - 1}} = 3.868 \text{ bar} \tag{5.69}$$

γ being the specific heat ratio 1.41. The density at inlet is calculated as

$$\rho_4 = \frac{p_4}{RT_4} = 4.4235 \text{ kg/m}^3 \tag{5.70}$$

This is close to the assumed value equation (5.59) of 4.4256 kg/m^3.

The rise in stagnation temperature through the compressor can be obtained from the power expended and the mass flow rate through the compressor. Thus

$$T_{05} = T_{04} + \frac{P}{\dot{m}_b C_p} = 300 + \frac{2852.3}{0.05179 * 1045.29} = 352.688 \text{ K} \tag{5.71}$$

The exit stagnation temperature for an isentropic compressor with isentropic efficiency, $\eta_b = 0.6$ is estimated as,

$$T_{05s} = T_{04} + \frac{\eta_b P}{\dot{m}_b C_p} = 331.73 \text{ K} \tag{5.72}$$

The corresponding stagnation pressure is found to be:

$$p_{05} = p_{04}\left(\frac{T_{05s}}{T_{04}}\right)^{\frac{\gamma}{\gamma-1}} = 5.80 \text{ bar} \tag{5.73}$$

The absolute exit velocity:

$$C_5 = \sqrt{2\left(h_{05s} - h_{5s}\right)} = 279.08 \text{ m/s} \tag{5.74}$$

Absolute Mach number at the outlet of the compressor,

$$M_5 = \frac{C_5}{C_{st}} = \frac{339.62}{368.78} = 0.921 \tag{5.75}$$

Using the value of 0.9 for the slip factor, the tangential velocity:

$$C_{\theta 5} = 0.9\, U_5 = 220.44 \text{ m/s} \tag{5.76}$$

$$C_{m5} = \sqrt{C_5^2 - C_{\theta 5}^2} = 171.14 \text{ m/s} \tag{5.77}$$

The exit blade angle:

$$\beta_5 = \tan^{-1}\left(\frac{C_{r5}}{U_5 - C_{\theta 5}}\right) = 81.85^o \tag{5.78}$$

and the absolute exit angle :

$$\alpha_5 = \tan^{-1}\left(\frac{C_{m5}}{C_{\theta 5}}\right) = 41.104^o \tag{5.79}$$

The relative velocity at exit:

$$W_5 = C_{m5}\cos ec(\beta_5) = 172.88 \text{ m/s} \tag{5.80}$$

Relative mach number at outlet,

$$M_{w5} = \frac{W_5}{C_{s5}} = \frac{172.88}{368.779} = 0.4767$$

Exit temperature

$$T_5 = T_{04} + \frac{\Delta h_{adst}}{C_p} = 315.22 \text{ K} \tag{5.81}$$

and exit pressure:

$$p_5 = p_{04}\left(\frac{T_5}{T_{04}}\right)^{\frac{\gamma}{\gamma-1}} = 4.45 \text{ bar} \tag{5.82}$$

Density at exit:

$$\rho_5 = \frac{p_5}{RT_5} = 4.757 \text{ kg/m}^3 \tag{5.83}$$

The required blade height at exit,

$$b_5 = \frac{\dot{m}_b}{(\pi D_5 - Z_b t_b)\rho_5 C_{m5}} \tag{5.84}$$

After obtaining all the dimensions the brake compressor has been fabricated. Figure 5-10 shows the photograph of the brake compressor.

Figure 5-10 Brake compressor

5.7 Selection of journal and thrust bearing

Successful working of a turboexpander strongly depends on the performance of the bearings and their protection systems. The main functions of the bearings are,

i) To support the rotor in the correct position relative to the static parts of the machine.
ii) To permit the rotor to run stably up to the design speed.
iii) To withstand the axial and radial force imposed on the rotor by the working fluid. Thrust bearing supports the axial thrust load comprises of the rotor weight and the difference of force due to pressure between the turbine and the compressor ends. The radial load arises primarily due to rotor imbalance and is taken up by a pair of aerodynamic journal bearing.

For the turboexpander gas lubricated bearings are used, i.e., aerostatic thrust bearings and the aerodynamic tilting pad journal bearings. The main advantages of these bearings are

i) Complete absence of oil contamination because the process gas (Nitrogen) can be used for lubrication.
ii) It can accept a wide range of operating temperature.

iii) Extremely high speed can be achieved.

iv) Heat in flow can be minimized.

v) High stability to self-excitation and external dynamic load.

(i) Pivot-less tilting pad journal bearing

Two number of pivot less tilting pad journal bearings are used at the two ends of the shaft as shown in Figure 5-1. A pivot-less tilting pad bearing consists of three pads floating around the journal, within the pad housing, surrounded by gas films on all sides. Each pad basically consists of a front face that forms the bearing surface, and its back face, consists of the network of three holes. High pressure from the bearing surface is communicated to the back face of the pad through the holes. This generates a pressure profile at the back face. The forces coming into picture are the aerodynamic load on the pad, the frictional force on the bearing surface and the force due to pressure distribution at the pad back face. The normal forces developed in the bearing clearance and at the back face, along with the frictional force due to rotor motion, determine the equilibrium of pad tilt. This type of tilting pad bearings is especially suited for supporting small rotors.

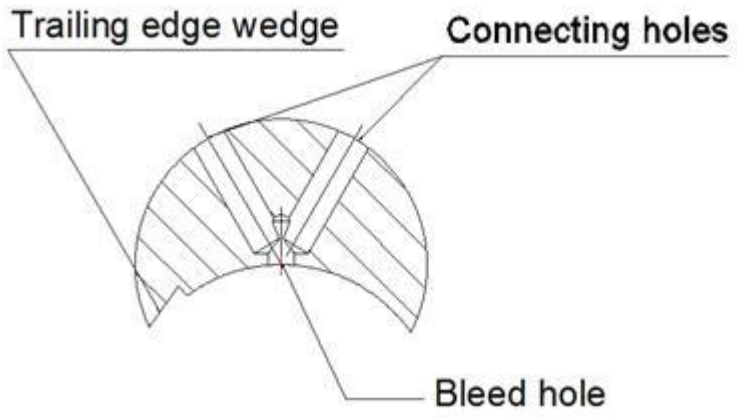

Figure 5-11 Pad

The dimensions of the tilting pad journal bearings are determined by the following the procedure of Chakraborty [123], the basic input parameters are

i) Bearing gas (Air /Nitrogen)

ii) Ambient conditions (i.e. Pressure and Temperature)

iii) Shaft diameter

iv) Rotational speed

Apart from these basic input parameters, some other additional input parameters are required for the pad geometry as shown in Table 5-3. The calculation of pad geometry is shown in Table 5-4.

Figure 5-12 Pivot less tilting pad journal bearing

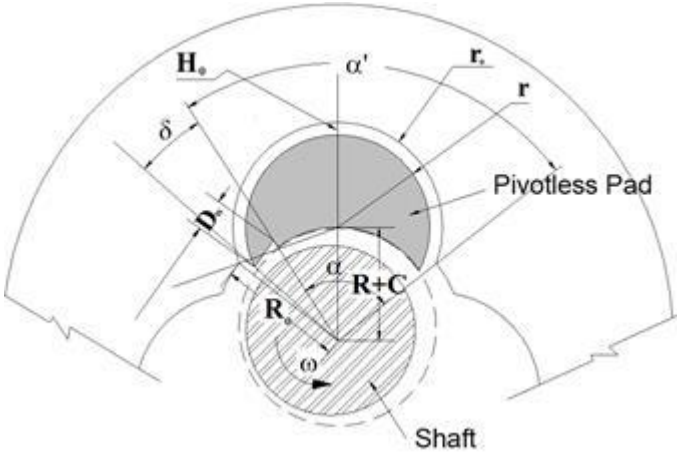

Figure 5-13 Pad and Rotor geometry

Table 5-3 Input parametrs to determine pad geometry

Length to diameter ratio	1
Pad clearence with rotor,C	0.015 mm
Pad angle ratio,γ	1.25
Clearence with pad housing,H_o	0.005 mm
Wedge depth, Δ	1 mm
Total pad angle,α'	111°
Connecting hole diameter, d_{con}	1.75 mm
Bleed hole diameter,d_{bleed}	1.3 mm
Included angle between connecting holes, θ_{holes}	60°

Table 5-4 Pad geometry

Pad radius,r	7.4638 mm
Pad housing radius, r_o	7.505 mm
Corrected Total pad angle,α'_c	111.59°
Angular extent od pad trailing edge wedge,δ	22.318°
Wedge width, D_w	3.1023 mm
Angular extent od pad trailing edge wedge,δ_c	28.9°
Pad angle ratio,γ_c	1.3495
Effective pad angle, α	82.69°

(ii) Aerostatic thrust bearing

Two number of aerostatic thrust bearing are used at the two sides of the collar as shown in Figure 5-1. As the thrust load of the aerostatic thrust bearings is unidirectional, that's why a double thrust bearing is always provided as a stop in case of accidental thrust reversal. The shaft is vertically oriented and runs at high speed.

The aerostatic thrust bearing dimensions are checked by following the procedure of Chakraborty [123] , for the 50 N of load with the conditions and dimensions shown in Table 5-5. The aerostatic thrust bearing has three supply gas lines. At the backside of the bearing there is a gas plate which collects the exhaust gas comes out of the bearing.

Table 5-5 Aerostatic thrust bearing input parameters

Supply Gas Pressure, p_0	8 bar
Exhaust Pressure, p_a	1.2 bar
Ambient Temperature , T	300 K
Number of feed holes, n	18
Outer diameter of thrust bearing,d_1	44 mm
Inner diameter of thrust bearing,d_2	18 mm
Feed hole pitch circle diameter,d_0	30 mm
Total bearing clearance, h_t	0.03 mm
Feed hole coefficient of discharge, C_d	0.8
Hole diameter upper side, d_{hu}	0.8 mm
Hole diameter lower side, d_{hl}	0.4 mm

Table 5-6 Aerostatic thrust bearing clearance at load and no load

	Bearing clearance at no load	Bearing clearance at on load
Upper side	17.57 μm	16.47 μm
Lower side	12.43 μm	13.53 μm
Total	30.00 μm	30.00 μm

Figure 5-14 Aerostatic thrust bearing

Figure 5-15 Exhaust gas plate

5.8 Supporting structures

The supporting structure of the turboexpander can be divided into 3 parts.

(i) Cold end housing

(ii) Bearing housing

(iii) Warm end housing

(i) Cold end housing

The cold end housing is the lower most part which is capable to hold the Teflon insulation rings so that the heat could not enter into it. It contains the nozzle diffuser centrally. It takes the process gas inside and cooled gas comes out centrally from the diffuser.

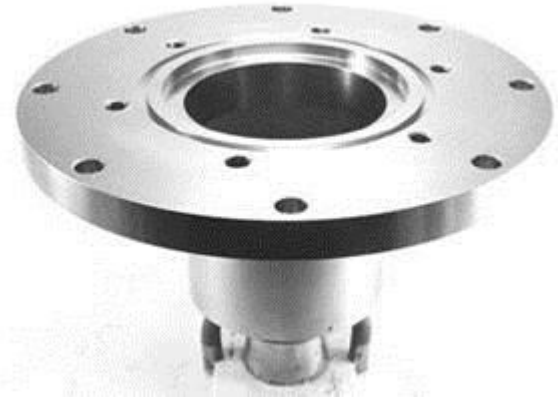

Figure 5-16 Cold end housing

(ii) Bearing housing

The bearing housing is the central component providing support to the two journal bearings and the two thrust bearings. It contains total six inlet tubes for supply of bearing gas to the aerostatic thrust bearings. And an exit hole for exhaust of the bearing gas. Two lock nuts are provided, one in turbine side and another on compressor side to set all the bearings and insulator inside the housing. Flanges are provided at the both ends of the housing to attach the warm end casing and cold end casing.

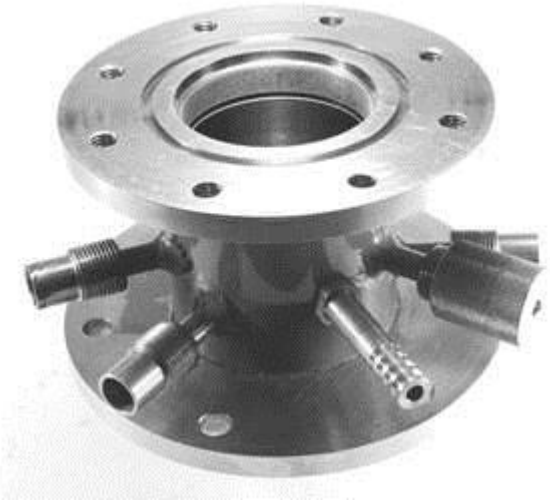

Figure 5-17 Bearing housing

(iii) Warm end housing

The warm end housing has a nozzle to the brake compressor which is fitted above brake compressor by shrink fit operation. There is an inlet and exit tube through which air is sucked in and compressed air goes out. At the top of the warm end housing there is a controller to control the gas inlet. The warm end housing is made up of Aluminum alloy material.

Figure 5-18 Warm end housing

5.9 Other turboexpander components

(i) Labyrinth seals

For each succeeding stage the pressure increases and therefore it is necessary to seal the interface between the dynamic and the stationary components. The simplest of these inter-stage seals is the labyrinth seal that work by creating turbulence in the cavities and thereby restricting flow from the high pressure side to the low pressure side. Seals of this type are favorable because there is no contact between the stationary and the moving parts; hence there is no mechanical friction or wear. The principle is shown in Figure 5-19. It is made up of Teflon.

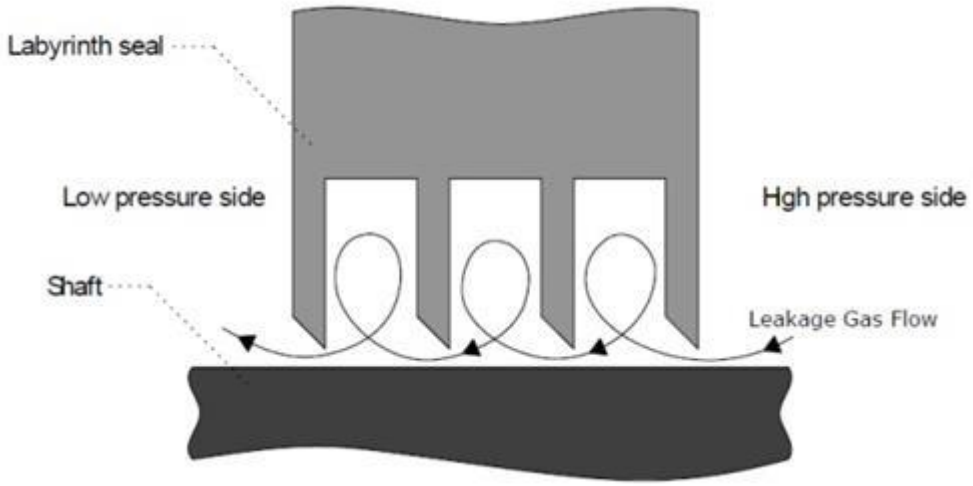

Figure 5-19 Principle of Labyrinth Sealing

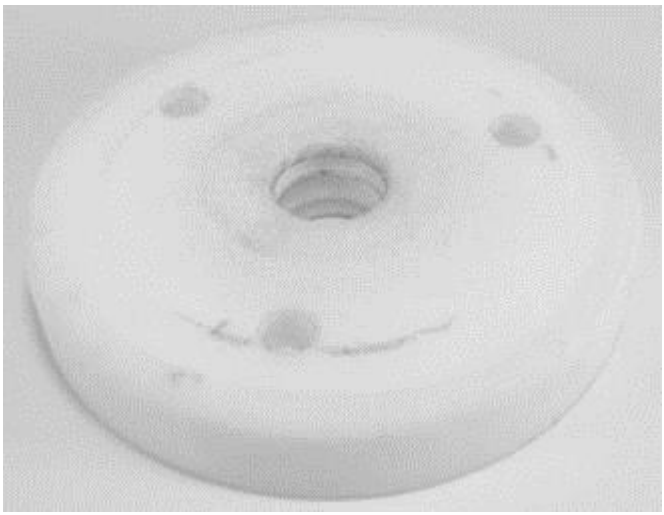

Figure 5-20 Labyrinth Seal

(ii) Thermal Insulations

The thermal insulators are required to separate the inlet process gas from the expanded cold gas. Two number of nylon insulation rings are provided.

(iii) Spacer

There is a spacer required to maintain the distance between the two thrust bearings. The width of the space plays an important role. It depends on the total thrust bearing clearance between the thrust bearing and the collar width of the shaft. The holes are provided along the circumference of the space. The function of the holes is to outlet the bearing gases from the thrust bearing. Another function is

to insert the probe through any of the holes so that it will reach near to the collar of the shaft to measure the rotation of the shaft.

Figure 5-21 Thermal Insulation

Figure 5-22 Spacer

(iv) Locknuts

Two number of locknuts are provided to keep the all the bearings along with the shaft inside the bearing housing. One is kept on turbine side, while other one is on the brake compressor side. Threads are provided on their circumference for fastening in the bearing housing. Two numbers of holes are provided for tightening.

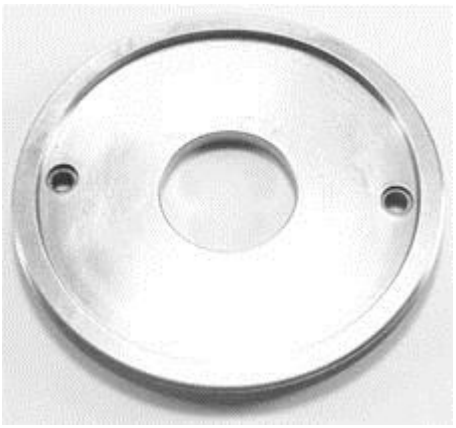

Figure 5-23 Lock Nut turbine Side

Figure 5-24 Lock Nut compressor Side

Chapter VI

Assembly and Instrumentation

6.1 Available equipment

(i) Compressor

The compressor is available in our laboratory. The compressor is a Kaerser make oil injected twin screw compressor. The specifications of the available compressor are given in the Table 6-1. The compressor has the capacity to deliver 336 m^3/h of air at maximum working pressure. The flow rate requirement for the liquefaction plant is fulfilled by the compressor. The photograph of the compressor is shown in Figure 6-1. The compressor runs automatically and takes care of the pressure range set for the operation. Beside the compressor there is an arrangement to control the flow and regulate the delivery air pressure. The pipe line and instrumentation diagram for compressor is shown in the Figure 6-2.

Table 6-1 Specification of the compressor

Make	Kaeser (Germany)
Model	BSD 72
Profile of screw	Sigma
Free air delivery	336 m^3/hr (at 10 bar of working pressure)
Suction pressure	Atmospheric
Maximum Pressure	11 bar
Motor	37 kW, 74 amps, 3 Φ, 50 Hz, 415V±10%, 3000 rpm (direct coupled)
Oil capacity	24 L
Cooling	Air

Figure 6-1 Photograph of the compressor

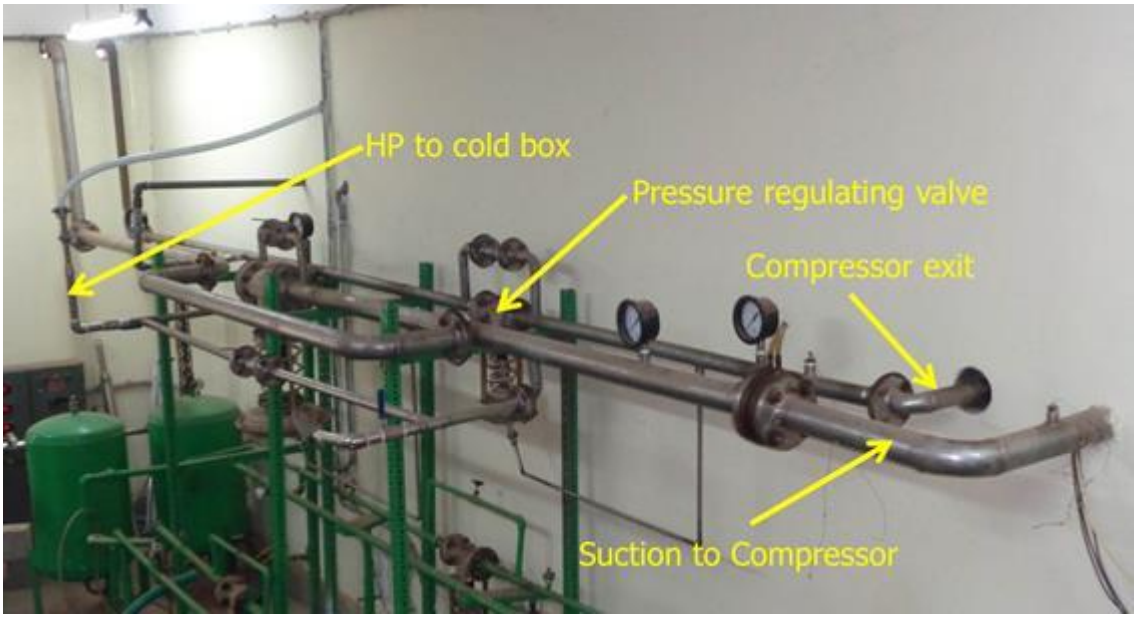

Figure 6-2 Arrangement for regulating the pressure and flow rate

6.2 Fabricated components

(i) Heat exchangers

As per design discussed in Chapter-IV, two numbers of brazed aluminum plate fin heat exchangers are fabricated by APOLLO HEAT EXCHANGERS Pvt. Ltd, Thane, Maharastra, India. At the inlet and exit end of the heat exchanger transition joints are welded. The transition joints are procured from THEVENET + CLERJOUNIE of France. Photographs of the first and the second heat exchanger are shown in Figure 6-3 and Figure 6-4 respectively.

Figure 6-3. Photograph first heat exchanger

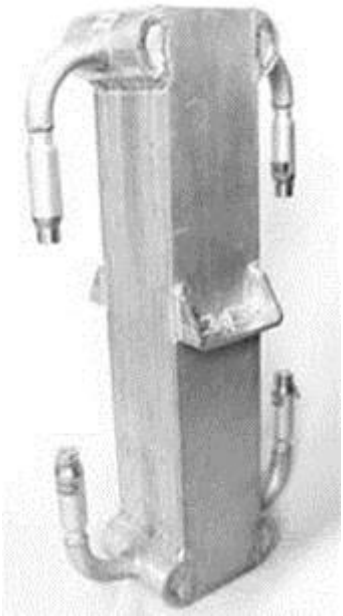

Figure 6-4. Photograph second heat exchanger

(ii) Turboexpander

Two set of turboexpander fabricated according to the dimensions determined in chapter V. The turbine wheel and brake compressor have been manufactured at TURBOCAM India Pvt., Goa, India Ltd. by using 5-axis CNC machine. The turboexpander housing and other components of the turboexpander have been manufactured at Central Tool and Training Centre, Bhubaneswar. The production drawings of the turboexpander parts are given in appendix A.

The shaft of the turboexpander rotates at a high speed about 1, 40,000 rpm. The clearance between the bearing and the shaft is also very small. So a precise dynamic balancing of the shaft is required [124]. The dynamic balancing was done by Schenck Ro Tec Gmbh make hard bearing type precision balancing machine at BARC, Mumbai. The balancing machine is meant for small rotors and able to balance less than 10 mg per plane. The residual unbalance after balancing of by removing weight from the shaft is mentioned in Table 6-2.

Table 6-2 Balancing report of shaft

Shaft No.		Before balancing	After balancing	Speed (rpm)
1	Turbine Side	1.16 mg 135°	2.30 mg 23°	2111
	Brake wheel side	37.9 mg 6°	3.43 mg 73°	
2	Turbine Side	11.3 mg 50°	2.29 mg 25°	2310
	Brake wheel side	126 mg 236°	4.45 mg 162°	

The assembly of the turboexpander components need to be done in a very clean and dustless environment. Before proceed for the assembly of turboexpander the shaft, the thrust bearing surface and the tilting pad bearing have been polished to get mirror surface finish. At first the labyrinth seal is inserted inside the bearing housing. Then lower tilting pad bearing is inserted. The lower thrust bearing is inserted by taking care of the bearing gas feed holes of the bearing and housing are matching. Then the shaft is inserted followed by the spacer, upper thrust bearing and upper tilting pad bearing. Now both the ends of the housing are tightened by using the locknuts. The turbine wheel is fitted in the lower side while brake wheel is fitted on the upper side of bearing housing. The bearing housing is ready to assemble with cold end housing. The nozzle diffuser is fitted inside the cold end

housing. Then it is covered with nozzle cover. The thermal insulator rings are inserted inside the annular space in the cold end housing. The turbine end is taken inside the cold end housing and bolted with placing an O-ring. The upper end flange of the bearing housing bolted with the hot end housing. A nozzle for the brake compressor is shrink-fitted inside the hot end housing.

(iii) J-T expansion valve

The Swagelok make needle valve is suitably modified to be used as expansion valve. To operate it from the top of the cold box, a long stem is attached with the valve along with a metering handle to know the percentage opening of the valve. The long stem is made rigid and leak proof so that the valve can be operated from the top without any leakages. The assembly diagram of the long stem handle is shown in Figure 6-5 and the photograph of the expansion valve assembly is shown in Figure 6-6.

(iv) Phase separator

The phase separator is a cylindrical container with rounded lower end and a circular flange with eight numbers of holes at the upper end as shown in Figure 6-7. On the both sides of the phase separator two no. of brackets are welded which will help to hang the container. The container is designed with 25 litres of capacity by volume. So it could accommodated easily inside the cold box and able to contain liquid nitrogen for an hour. The phase separator is made up of stainless steel (SS304).

There is a cover plate over the phase separator. The cover plate has a vapour nitrogen outlet hole, a liquid-vapour nitrogen inlet hole, a liquid nitrogen outlet hole and a feed through hole for temperature measurement. The cover plate has holes to match with phase separator flange an it fitted with the nuts and bolts by placing a Teflon sheet in between as gasket to prevent leakage. The cover plate diagram is shown in Figure 6-8.

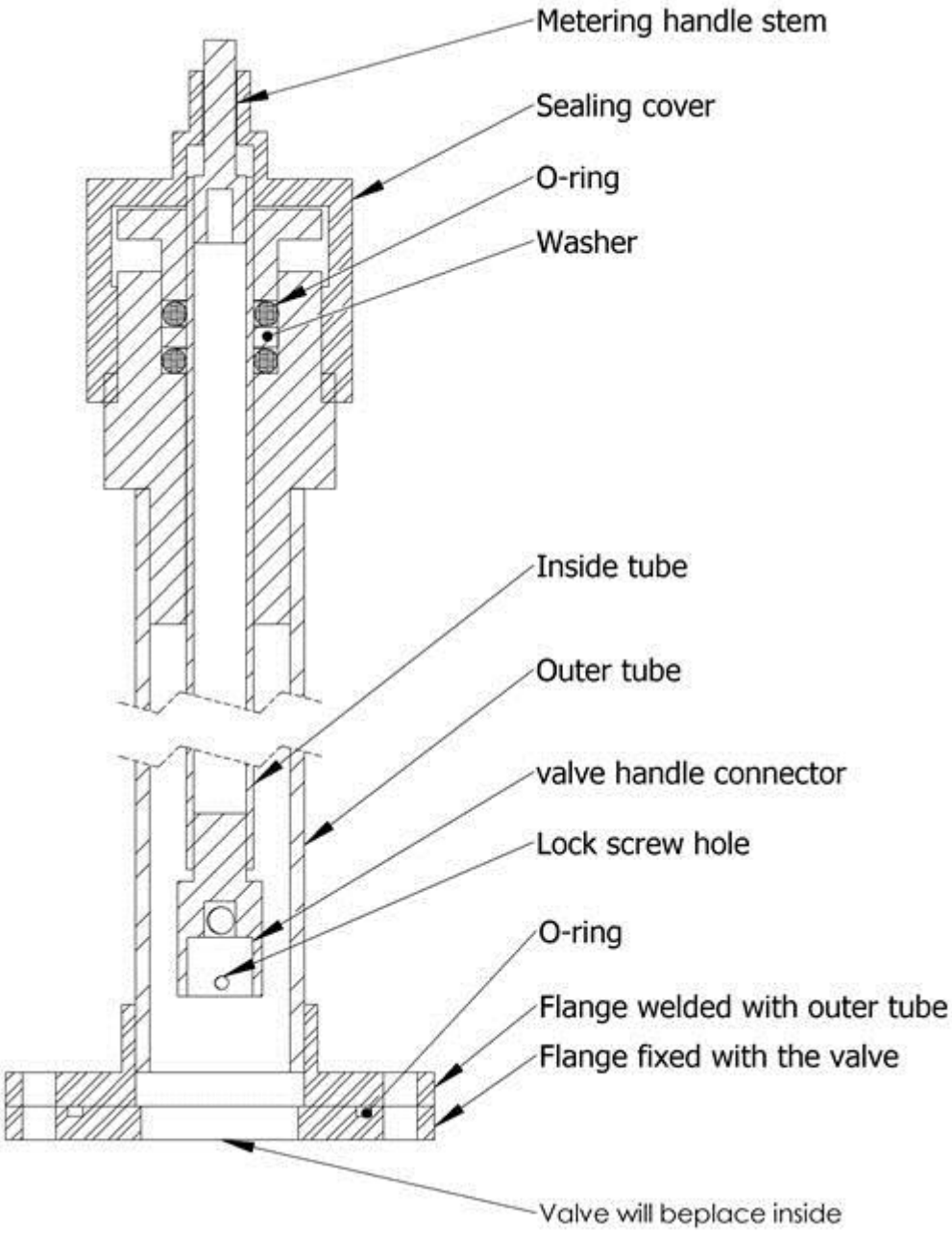

Figure 6-5 Long stem handle assembly for the J-T expansion valve

Figure 6-6 Photograph of expansion valve

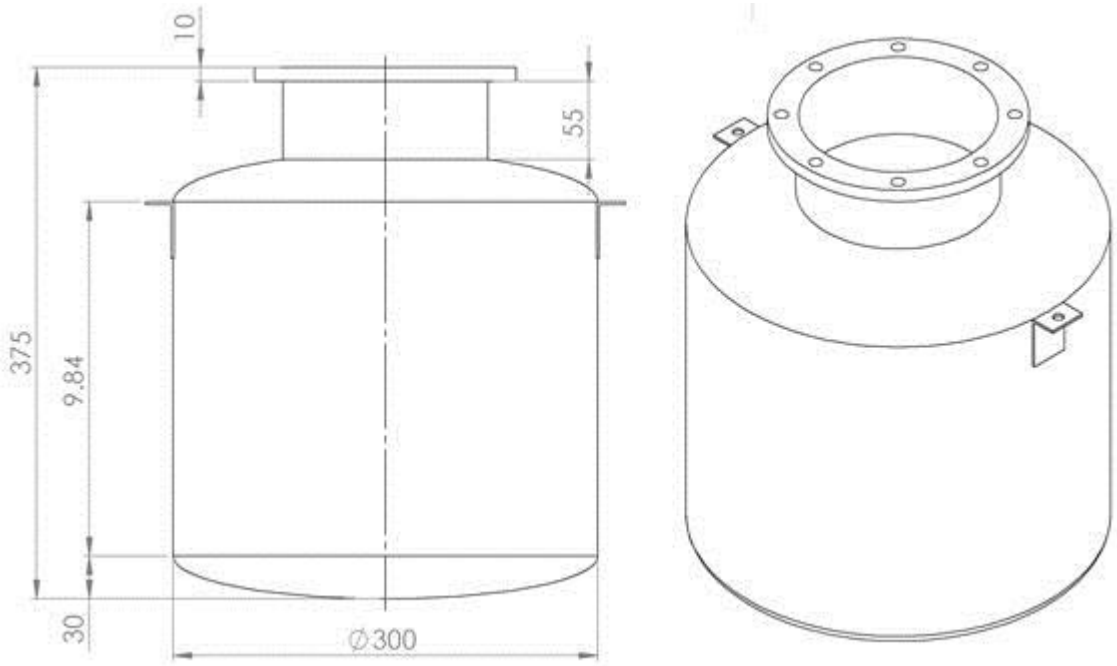

Figure 6-7 Dimensions of phase separator

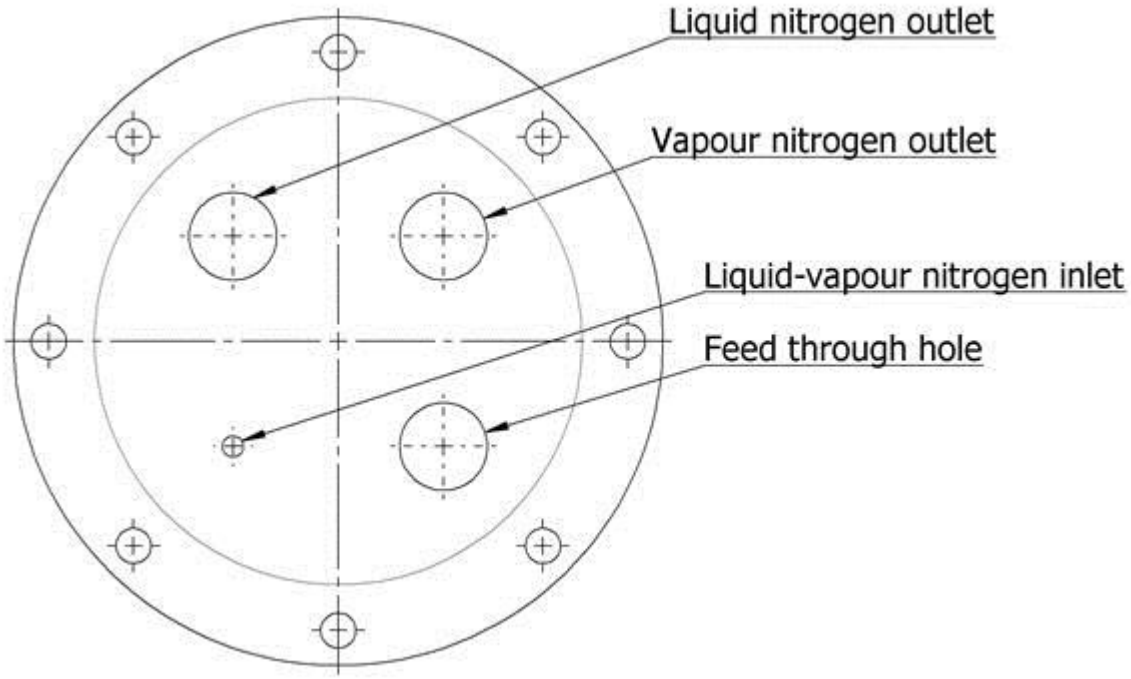

Figure 6-8 Cover plate of phase separator

(v) Cold box

All the equipment need to be housed in a vacuum vessel to reduce the cold loss. The vessel is called cold box. A double walled cold box is fabricated with a height of 1800 mm and diameter of 850 mm. A lower vacuum maintained inside the main chamber while high vacuum is maintained at the annular space provided at the double wall. On the flange of the cold box holes are drilled for the outlet of process gas pipes and also to accommodate the turboexpander.

Figure 6-9 Photograph cold box

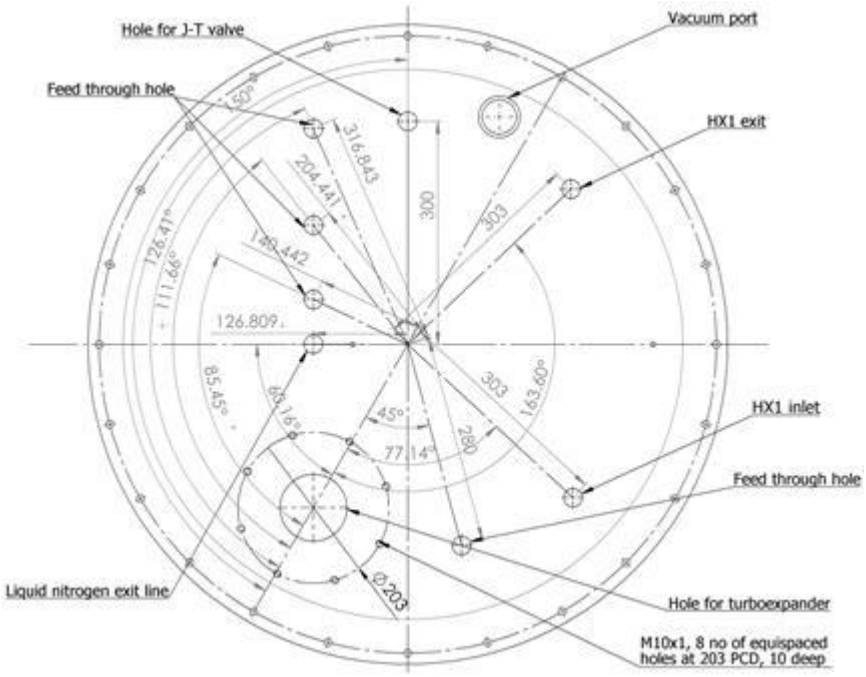

Figure 6-10 Holes on the cold box flange

6.3 Instrumentation

(i) Temperature measurement

To study the performance of the liquefier and to monitor the cool down behavior, it is necessary to measure the temperature. So temperature is measured by using Platinum Resistance Temperature Detector (RTD). It is the most linear and stable temperature sensor. The Pt-100 type RTDs is fitted at different locations to measure the temperatures. Prior to the using of the RTD all of them are calibrated by dipping inside liquid nitrogen. ADAM-4015 data acquisition modules are used and it provides data output as RS-485. This is again converted to RS-232 to view in PC by using ADAM-4520 converter.

Figure 6-11 Photograph of the RTD

(ii) Pressure measurement

The pressure is measured by using WIKA make dial pressure gauges. For high pressure stream, 0-16 bar (g) and for low pressure stream 0-4 bar (g) range pressure gauges are used.

(iii) Measurement of flow rate

An orifice type flow meter is used to measure the flow rate of liquid or gas. Its working is based on the Bernoulli's principle which relates the pressure and the

velocity of a fluid stream. When the velocity increases, the pressure drop across the orifice plate increases and vice versa.

The volumetric and mass flow rates are obtained from the Bernoulli's equation by measuring the difference in fluid pressure between the normal pipe section and at the vena contracta of the orifice plate. The pressure difference is measured by mercury u-tube manometer. The orifice plate is calibrated with a rotameter as shown in photograph before use.

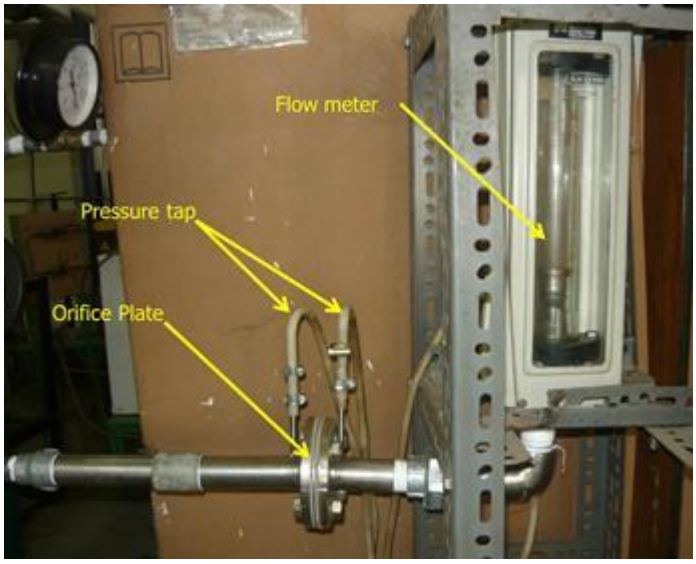

Figure 6-12 Orifice plate calibration

(iv) Turbine speed measurement

Turbine rpm is measured by a Brüel & Kjær make piezoelectric Miniature DeltaTron™ Accelerometers. It has high sensitivity, low mass and small physical dimensions and easy to mount on the turboexpander body using supplied glue. The photograph and specification is shown in Figure 6-13 and Table 6-3 respectively.

Figure 6-13 Photograph of the accelerometer used for speed measurement

Table 6-3 Specification of the accelerometer

Model No.	4507
Frequency	0.3 - 6000 Hz
Sensitivity	100 mV/g
Temperature	-54 - 121 ºC
Residual Noise Level in Spec Freq Range (rms) ±	0.35 mg
Maximum Operational Level (peak)	70 g
Maximum Shock Level (± peak)	5000 g
Resonance Frequency	18 kHz

6.4 *Assembly of components*

The 3-D model of the cold box assembly is shown in Figure 6-16 . The two heat exchanger and phase separator are hanged from the cold box flange using tie rod. The one end of tie rod is inserted inside a welded socket on the cold box flange and bolted. The other end is fixed with nut and bolt arrangement with the component. Slight movement of the component could be done with adjusting the nuts. After hanging the components, pipes are connected by TIG welding as per the process diagram shown in Figure 6-15.

Figure 6-14 Connection of turboexpander with the pipelines

The critical connection is the turboexpander with the process pipelines. As the turboexpander is to be taken out for maintenance, it could not be connected permanently. So it is connected by brass connector with proper sealing as shown in Figure 6-14.

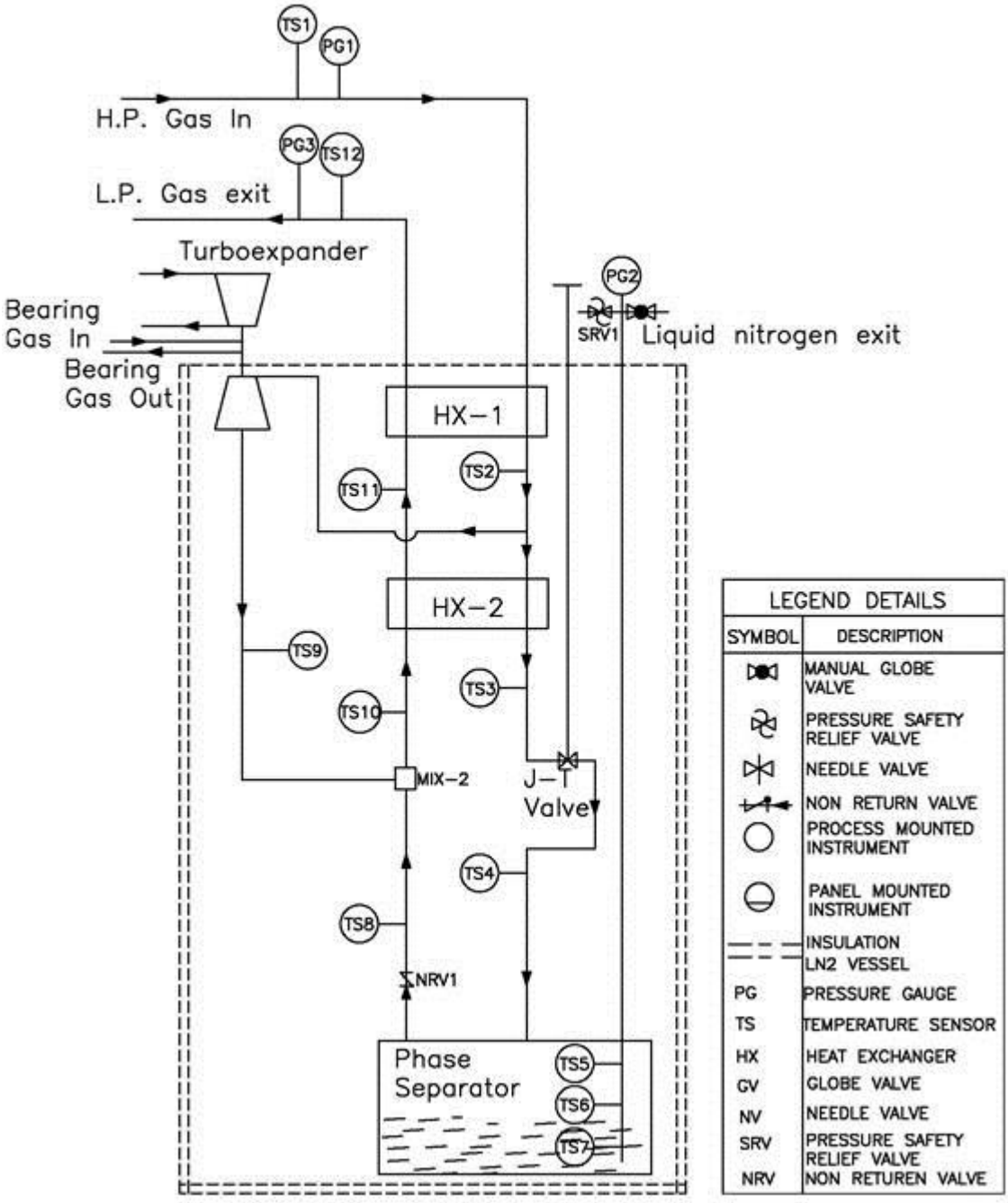

Figure 6-15 P & I diagram of Nitrogen liquefier

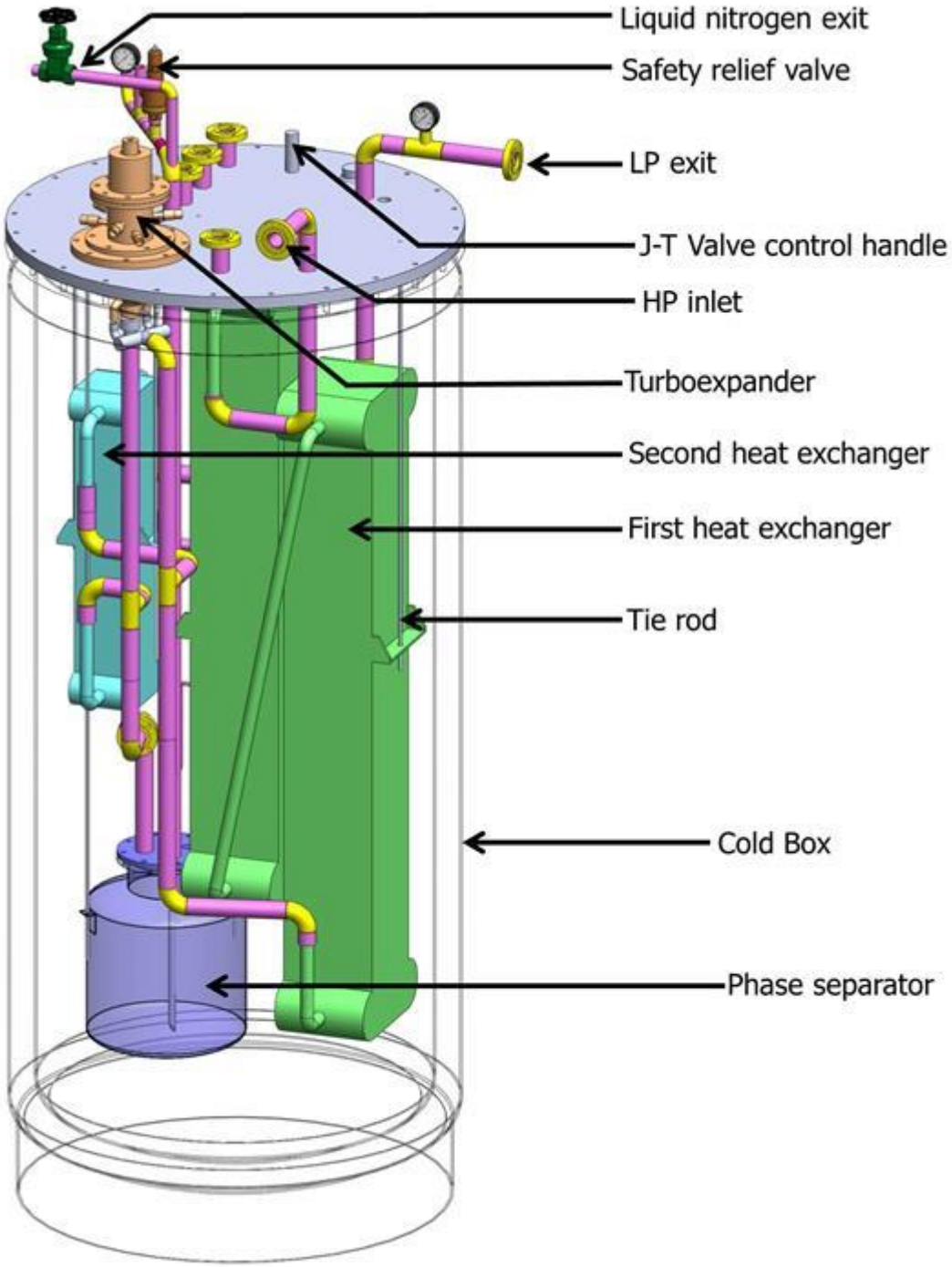

Figure 6-16 3-D model assembly of nitrogen liquefier inside cold box

Figure 6-17 Assembly photograph of nitrogen liquefier

Figure 6-18 Photograph of cold box flange

Chapter VII

Testing and Commissioning of the Liquefier

7.1 Introduction

The assembled cold box is required to be connected with other components with proper pipeline. To study the experimental performance of the plant, it is required run the plant. Before running the plant to study the performance, the turboexpander is to be tested by the trial run of the plant. After completing the trial run of the plant successfully, vacuum is to be created inside the annular space of the cold box and all the components inside the cold box have to be covered by super insulation. Then the plant will be ready for the experimental performance evaluation.

7.2 Testing of turboexpander

The turboexpander is the heart of the liquefaction plant. So the turboexpander should run at rated speed and able to lower the temperature having required efficiency. This is evaluated by doing trial run of the turboexpander before using it on liquefaction plant. By doing trial run of the turboexpander, the performance is evaluated as well as the knowledge on operation is achieved.

(i) Turboexpander trial run set up

The testing of the turboexpander has been done with air as the process fluid. The trial run set up consists of a compressor to supply the compressed air to the turboexpander. The photograph of the test setup is shown in Figure 7-1. Some fraction of the high pressure gas is supplied to the turbine inlet and some to the turboexpander bearing. To make the flow smooth and to avoid flow fluctuation the turboexpander bearing gas supply is made through a H.P. pressure vessel. The bearing supply gas from the H.P. pressure vessel is divided into two streams. One is

supplied to the upper thrust bearing and other is feed to the lower thrust bearing through two valves to control the flow rate. The exit air from the turboexpander is discharged to atmosphere. The exit bearing gas also vent to the atmosphere. The brake compressor of the turboexpander sucks the atmospheric air and also its compressed hot air leaves to the atmosphere.

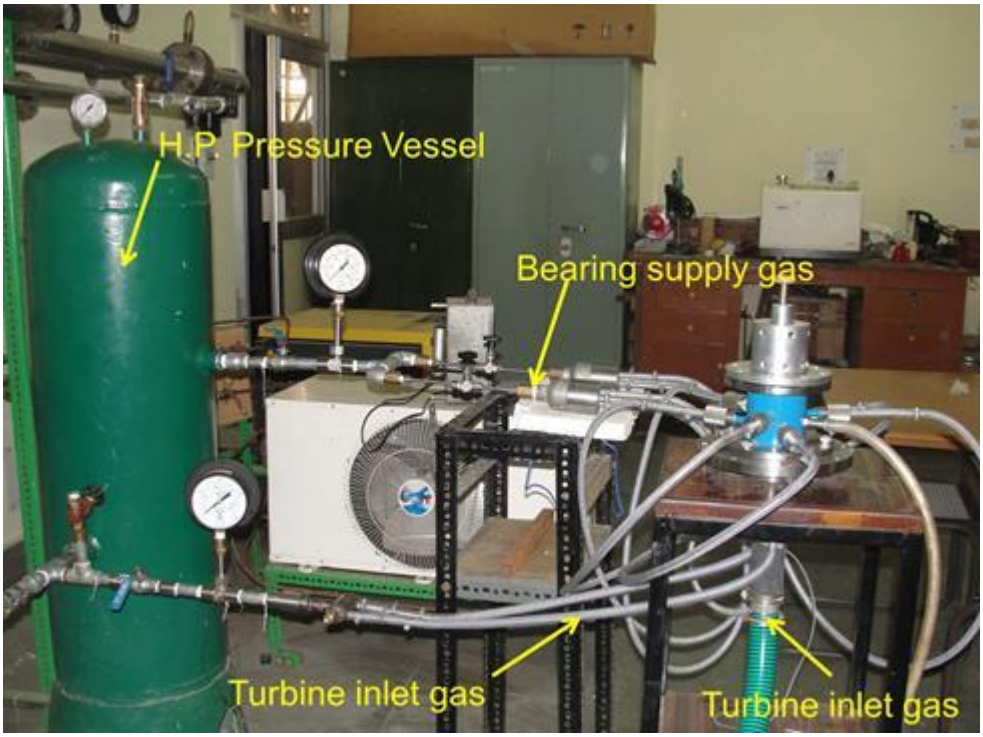

Figure 7-1 Turboexpander test set up

(ii) Problems occurred during turboexpander trial run

Trial run of the turboexpander has done using the compressed air from the compressor. After assembly, at the fresh start of the turboexpander, it rotates smoothly and steadily. But after some start and stop the rotation is not smooth as compared to the first run. After disassembly of the turboexpander, it is found that the thrust bearing surface has been damaged along with surface of the shaft and shaft collar. The photo graph of the damaged surface is shown in Figure 7-2, Figure 7-3 and Figure 7-4. The damage occurs due to the small dust particles that come from the compressor. The dust particles are rubbed with graphite pads of the journal bearing and also in between the collar and the thrust bearing. This is resulting wear in the surfaces. To avoid this, filters are provided with micron size of SS mesh as shown in Figure 7-5.

(iii) Performance of the turboexpander

The bearings surfaces are buffed and made mirror finished. Due to this the shaft rotates smoothly without any friction for a long time after several starts and stops. The turbine speed is measured by placing the accelerometer on the flange of the bearing housing. The rotating speed of turbine is about 1,04,760 rpm (1.746 kHz). It is observed that at an inlet pressure of 5 bar, it is able to decreases temperature of 18 °C by expanding the gas to the atmosphere. The FFT graph is shown in Figure 7-7.

Figure 7-2 Damaged surface of the thrust bearing

Figure 7-3 Damaged surface of the shaft collar

Figure 7-4 Damaged shaft surface by rubbing with tilting pad bearing

Figure 7-5 Filter used to remove micron dust particles

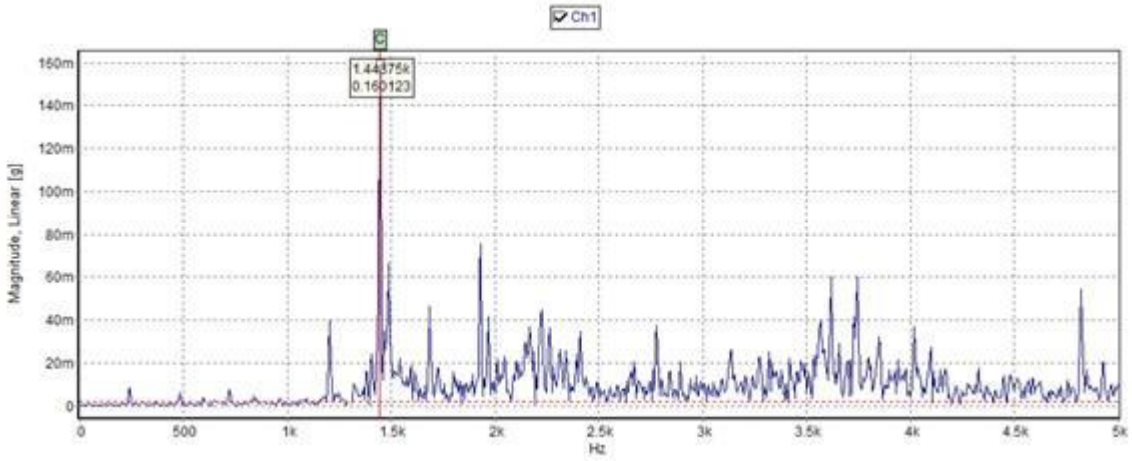

Figure 7-6 FFT diagram for the speed of turbine wheel at 5 bar of inlet pressure

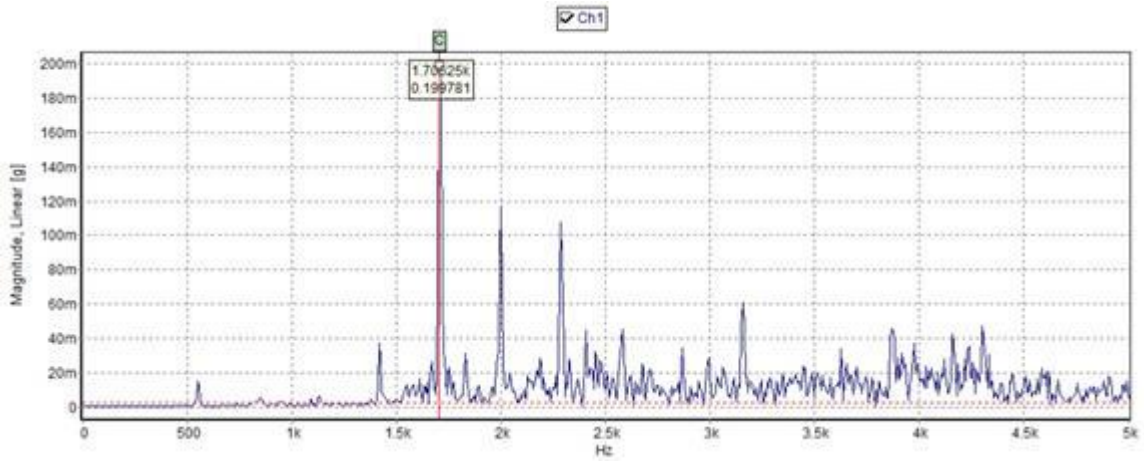

Figure 7-7 FFT diagram for the speed of turbine wheel at 6 bar of inlet pressure

7.3 Plant pipeline setup

Pure nitrogen gas is required for the nitrogen liquefier. The air contained nitrogen but it also contained objectionable amount of moisture, carbon dioxide and oxygen. At low temperatures the small quantity of moisture will form ice and block the flow passage. Hence for the experiment, the pure nitrogen is supplied from a liquid nitrogen Dewar. From the Dewar the liquid goes to the nitrogen vaporizer by just opening and pressurising the Dewar (Figure 7-8). Vapour nitrogen comes out from the nitrogen vaporizer is feed to the gas bag. For the safety of the gas bag, it is equipped with a level indicator and oil safety valve. The maximum and minimum level of the gas bag is marked and controlled manually to maintain the level. The secondary safety is the oil safety valve and it is shown in Figure 7-10. It is filled with compressor oil up to the required level. The oil remains inside till it sustains the pressure of the gas bag. When the pressure become access the oil comes out, this indicates that the bag is over filled. The gas bag is connected with the suction of the compressor.

The discharge gas from the compressor is connected to coil type small heat exchanger for pre-cooling and moisture removal from the process gas. The precooling is done by using liquid nitrogen from a LN2 cylinder. The photograph of the pre-cooler is shown in Figure 7-11.

The pre-cooled gas divided into two streams. One is supplied to the high pressure end of the cold box through a orifice type flow meter and a dust filter. Another stream is supplied to bearings of the turboexpander through a buffer. The buffer is meant for the smooth supply of the gas to the bearing without any flow fluctuation.

The cold box flange has one high pressure inlet to HX1 and one low pressure exit end from the HX1. The exit from the HX1 is connected to the suction side of the compressor. In this way the process is made a closed cycle one. The process gas is coming in to the cold box, again return to the compressor. If some liquefaction occurs then the makeup gas is supplied by the gas bas connected through a non-return valve. If there is some decrease in pressure in suction side, the non-return valve gets opened and gas flows from the gas bag to the compressor.

The top flange of the cold box has liquid nitrogen transfer valve along with burst disk and safety relief valve. The flange has also four number of feed through connections and these are connected to temperature sensor mounted on components inside the cold box. The other end of the feed through connection is connected to the data acquisition system. The data is sent to the PC through a converter. The detail pipeline assembly drawing is shown in Figure 7-13.

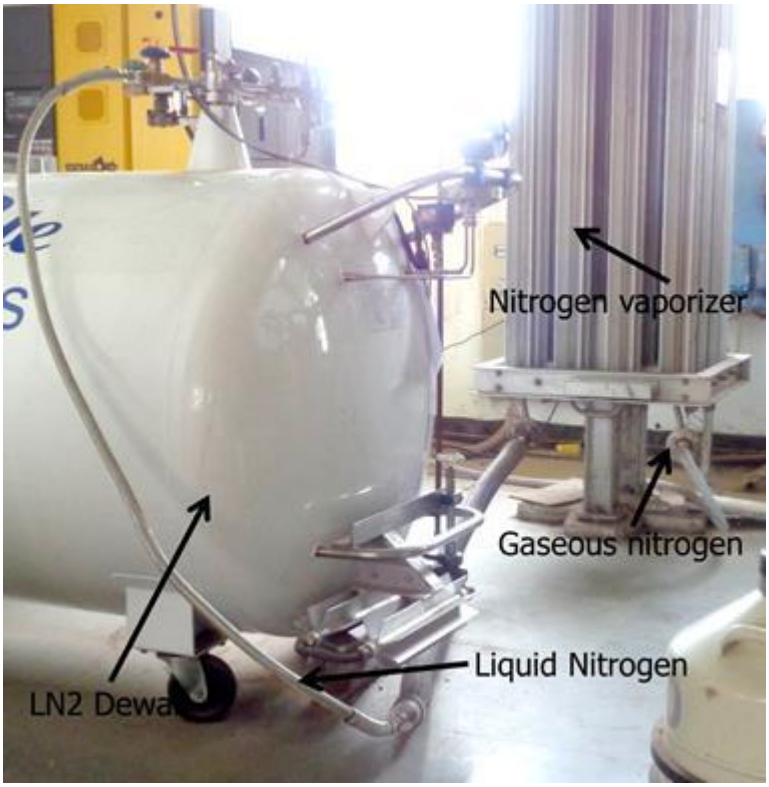

Figure 7-8 LN2 Dewar to vaporizer

Figure 7-9 Gas bag for gaseous nitrogen

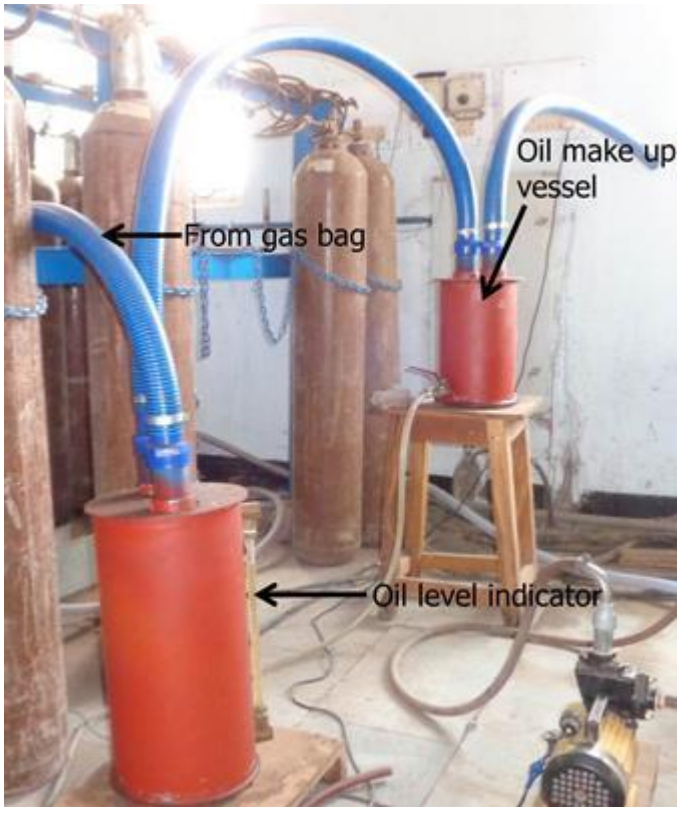

Figure 7-10 Oil safety valve

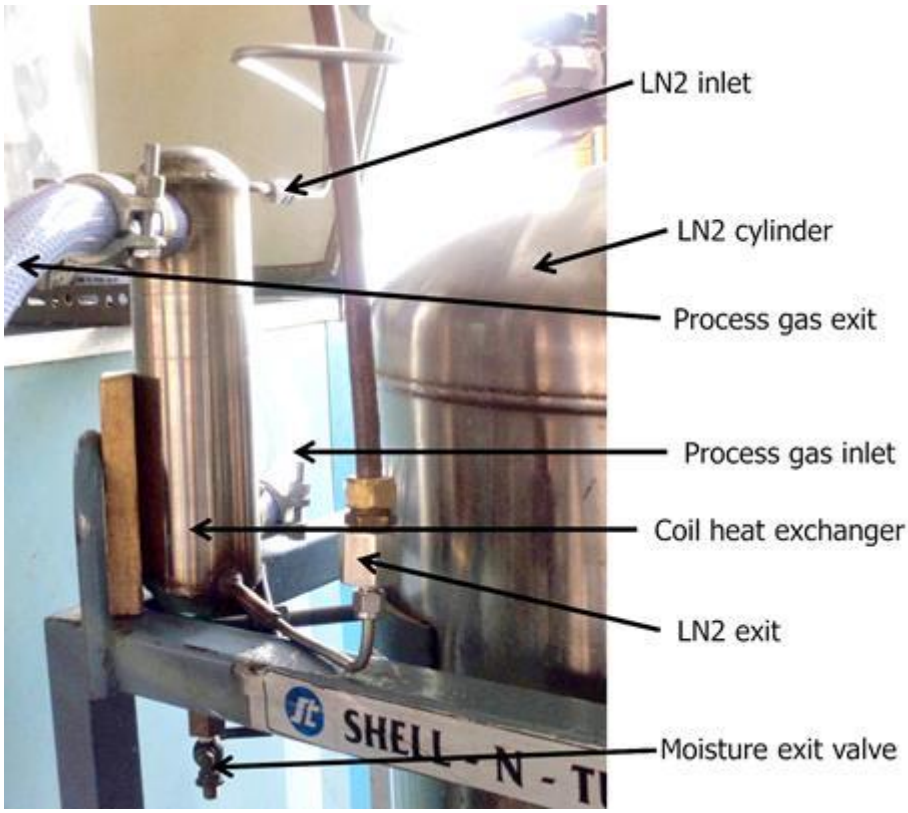

Figure 7-11 Coil heat exchanger for pre-cooling

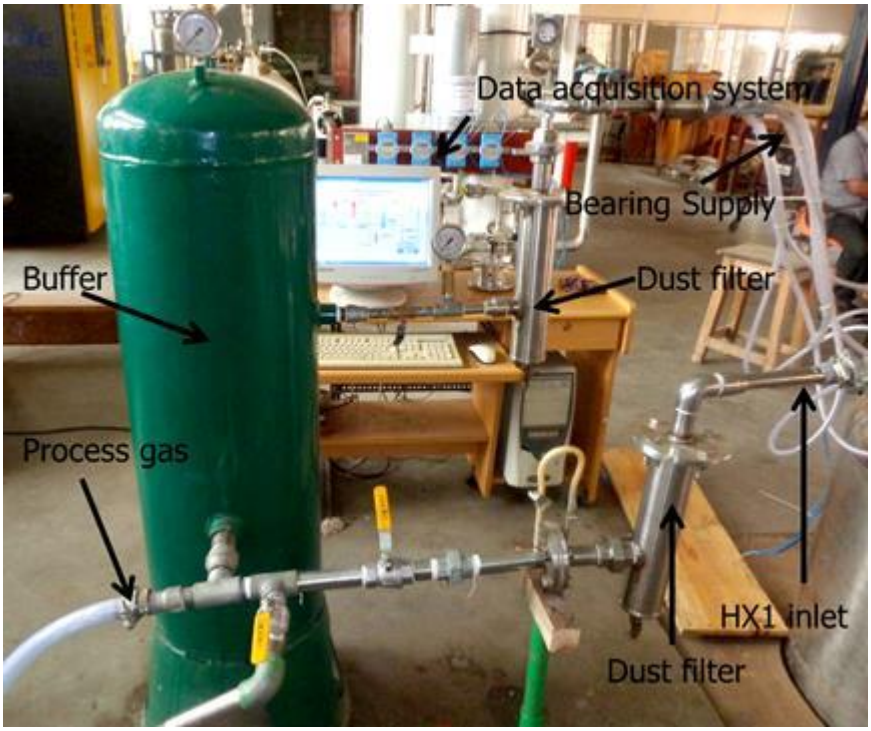

Figure 7-12 Arrangement for supply of process gas to cold box and turbine bearing

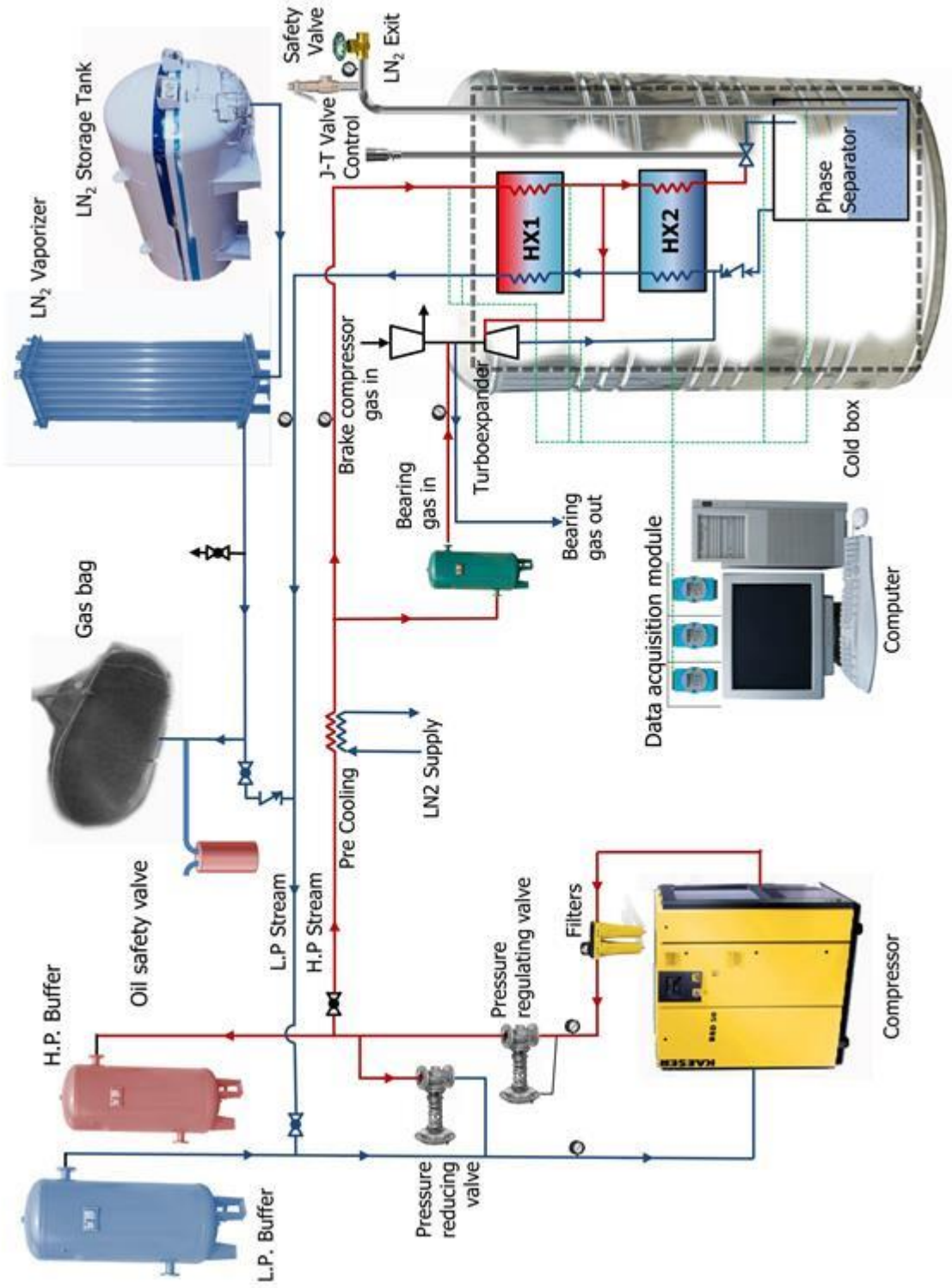

Figure 7-13 P & I Diagram of the liquid nitrogen plant

7.4 Commissioning of the plant

The plant starts with filling the gas bag with nitrogen gas up to a marked level. This is done by opening the valve of liquid nitrogen Dewar. After filling the gas bag, the compressor is started and the valve of the bearing supply is opened first. Then cold box inlet valve is opened slowly. At this time the exit valve from the cold box is also opened. The whole system is filled with air. By supplying nitrogen to remove the air from the system is called purging. It took some hours to purge completely. The coil heat exchanger present for pre-cooling removes the condensed moisture and also filters present at the supply end of the cold box and bearing supply removes the moisture. After ensuring the all gas are purged the cold box exit valve is closed so that the process becomes closed cycle. The nitrogen gas is circulated in closed cycle.

7.5 Performance of the plant

The plant performance is observed from the temperature sensor mounted at the node locations of the components. A graphical user interface is developed in PC to monitor and also to record the temperature at different nodes of the liquefier. The PC along with the data acquisition system is shown in Figure 7-14.

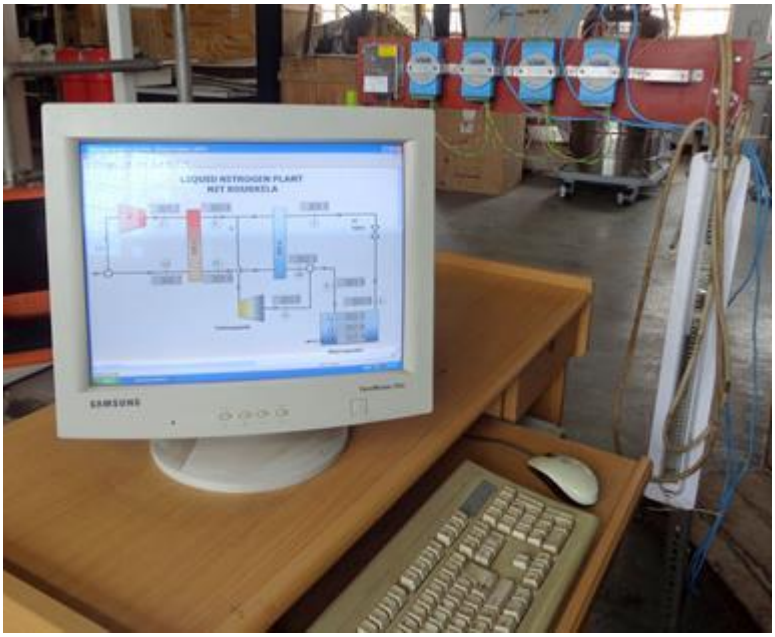

Figure 7-14 Temperature monitoring and recording using data acquisition system

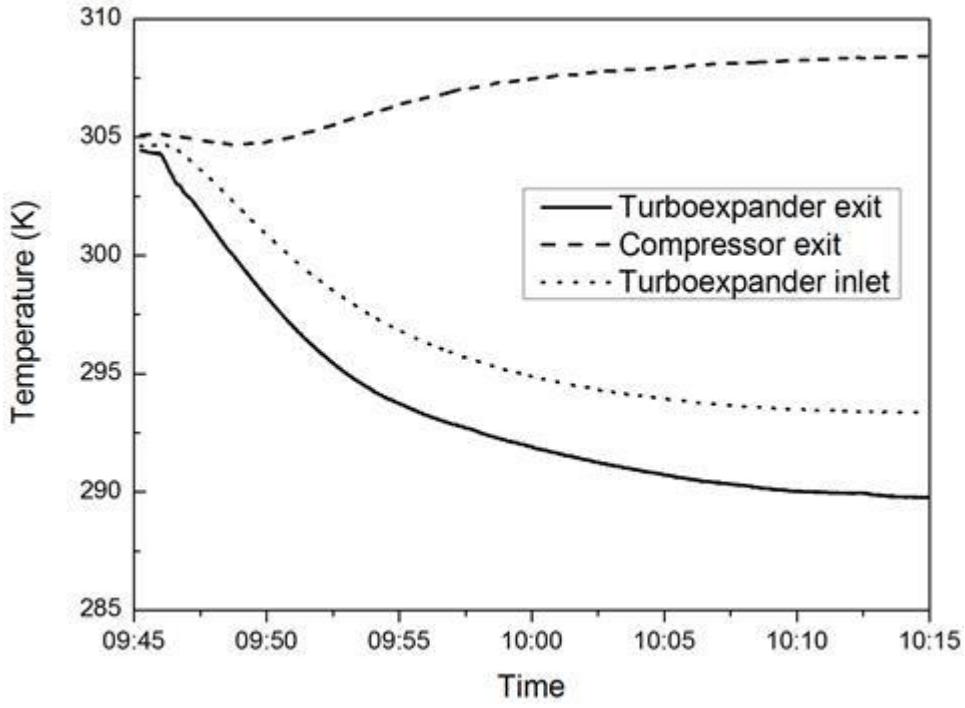

Figure 7-15 Turboexpander exit temperature with time

The plant is required to run continuously for several hours for cool down the entire mass of the system and produce liquid nitrogen. Figure 7-15 shows the graph of the turboexpander exit temperatures with time. It took around 30 minutes to decrease the temperature from 305 K to 289 K.

Chapter VIII

Conclusions

The work reported in this thesis is an attempt to design and construct a turboexpander based nitrogen liquefier. The development includes turboexpander, heat exchanger, J-T valve etc. During this period a lot of important technological ideas are implemented. A liquefier is built which will produce liquid nitrogen. The following are the significant contributions of the thesis.

1. Process design of the liquefaction cycle has been done by equation oriented method and optimization of the cycle has been done by using the software Aspen Hysys. Finally process design parameters and component specifications are fixed. This will produce 17.44 liter of liquid nitrogen per hour by supplying 296 kg/hr of gaseous nitrogen.

2. The First heat exchanger has been designed for maximum effectiveness (0.99) and second heat exchanger has been designed to give minimum pinch temperature (1 K). Due to the large length of the first heat exchanger, it is divided into two halves and joined together. Again the analysis is carried out to split heat exchanger using the software Aspen MUSE. After successful design of the heat exchangers, these are fabricated.

3. The turboexpander has been designed for an efficiency of 75%. All the parts of the turboexpander have required dimensional accuracy. So these parts are designed and manufactured carefully considering thermal, design and production points of view. The turboexpander is tested in the test rig before using in the liquefier. It is found that the turboexpander rotates at around 1,02,375 rpm and results a temperature drop of 18 K at room temperature in an open cycle.

4. Modification in the JT valve has been done for ease of its operation from the top of the cold box flange.

5. Other components like cold box and phase separator have been designed and fabricated. Apart from these oil safety valve is fabricated for the safety of the gas bag. Two dust filters are made to avoid the dust as well as moisture. A small coil type heat exchanger is developed for pre cooling of the process gas.

6. Assembly of the components carried out inside cold box by TIG welding. Piping and instrumentation have been done for complete plant.

7. The commissioning of the plant has been done and 16 K temperature drop has been obtained in just 30 minutes. The plant is required to run for several hours with proper insulation of the system and vacuum inside the cold box, so that it will produce liquid nitrogen.

The present development of turboexpander based liquid nitrogen plant is not sufficient. Further a lot work can be carried out. Further to improve the plant, the following are major works that could be considered,

1. The performance study of the liquid nitrogen plant could be done with optimization of the plant parameters.

2. The dynamic analysis of the plant could be done using the process simulation software Aspen Hysys. This can be compared with the real existing system.

3. The experimental study of the heat exchanger and comparing the effectiveness with the rating programs or software Aspen MUSE.

4. Similarly the second heat exchanger is important because it is two phase heat exchanger. Attention can be focused on experimental validation.

5. The main focus could be given to the heart of the system, the turboexpander. As it rotates smoothly, but further modification is necessary to decrease the bearing gas consumption.

A lot of efforts are given for developing liquid nitrogen plant. A complete design methodology is provided along with the production drawing. This will be fruitful to develop another plant indigenously with in-house development of turboexpander and heat exchanger.

References

1. **Barron, R. F.,** *Cryogenic Systems*. Oxford University Press (1985),

2. **Wolfgang, F.,** History of cryogenics: the epoch of the pioneers from the begining to the year 1911. *Int. J. refrigeration* (2002), *25*, 283-292.

3. **Flynn, T. M.,** *Cryogenics Engineering*. Marcel-Dekker Inc (1996),

4. **Timmerhaus, K. D., and Flynn, T. M.,** *Cryogenic Process Engineering*. Plenum Press (1989),

5. **Scott, R. B.,** *Cryogenic Engineering*. (1959),

6. **Scurlock, R. G.,** *History and Origins of Cryogenics*. Oxford, Clarendon Press. (1993),

7. **White, F. M.,** *Fluid mechanics*. 2nd ed.; McGraw-Hill BookCompany,

8. **Simms, J.,** *Fundamentals of the turboexpander " Basic Theory and Design"*. SIMMS Machinery international,Inc (2009),

9. **Sulaiman, M. Y.,** *Turbomachinery*. (2005),

10. **Collins, S. C., and Cannaday, R. L.,** *Expansion Machines for Low Temperature Processes*. Oxford University Press (1958),

11. **Sixsmith, H.,** Miniature cryogenic expansion turbines - a review. *Adv Cryo Eng* (1984), *29*, 511-523.

12. **Kapitza, P. J.** *Phys. Ac. Sci. USSR.1, No.7,*; (1939); p 29.

13. **Swearingen, J. S.,** Turbo-expanders. *Trans AIChE* (1947), *43* (2), 85-90.

14. **Land, M. L.,** Expansion turbines and engines for low temperature processes. *Advances in Cryogenic Engineering* (1957), *V2*, 251-260.

15. **Linhardt, H. D.,** *Cryogenic turboexpanders in Vance, R. W. (Ed)*. Vol. 4, 89-117,

16. **Linhardt, H. D.,** Process application and design of large power output turboexpanders. *J Engg. for Industry,Trans ASME* (1973), 227-232.

17. **Clarke, M. E.,** A decade of involvement with small gas lubricated turbine. *Adv Cryo Eng* (1974), *19*, 200-208.

18. **Beasley, S. A., and Halford, P. ,** Development of a High Purity Nitrogen Plant using Expansion Turbine with Gas Bearing. *Advances in Cryogenic Engineering* (1965), *10B*, 27-39.

19. **Trepp, C.,** Refrigeration system for temperatures below 25 K with turboexpanders. *Adv Cryo Eng* (1962), *7*, 251-261.

20. **Schmid, C.** In *Gas bearing turboexpanders for cryogenic plant*, *6th International Gas Bearing Symposium University of Southampton England*, *University of Southampton England*, (Year), 131 B1:1-8.

21. **Eber, N., Quack, H. and Schmid, C.,** Gas bearing turbines with dynamic gas bearings. *Cryogenics* (1978), *18*, 585-588.

22. **Blackford, J. E., Halford P. and Tantam, D. H.,** Expander and Pumps in G G Haselden (Ed). In *Cryogenic Fundamentals*, Academic Press London: (1971); pp 403-449.

23. **Colyer, D. B.,** Miniature cryogenic refrigerator alternators. *Adv Cryo Eng* (1968), *13*, 405-415.

24. **Colyer, D. B., and Gessner, R. L.,** Miniature cryogenic refrigerator Turbomachinary. *Adv Cryo Eng* (1968), *13*, 484-493.

25. **Izumi, H., Harada, S. and Matsubara, K.,** Development of small size Claude cyclehelium refrigerator with micro turbo-expander. *Adv Cryo Eng* (1986), *31*, 811-818.

26. **Yang, K. J., He, H. B., Ke, G., and Li, G. Y. ,** Application and test of miniature gas bearing turbines. *Advances in Cryogenic Engineering* (1990), *V35*, 997-1003.

27. **Yang, K. J., and He, H. B.,** Miniature expansion turbine with grooved self-acting gas bearings. In *Proc Tenth Inti Cryo Eng Conf*, Butterworth, Guildford, UK, (1984); pp 660-663.

28. **Yang, K. J., and He, H. B.,** Design and test of a novel miniature cryogenic expansion turbine. *Adv Cryo Eng* (1986), *31*, 829-833.

29. **Yang, K. J., and Munday, A. J.,** A grooved self-acting gas bearing for use in cryogenic expansion turbines. *Cryogenic Process and Engineering 1982, AIChE Symposium Series* (1983), *79*, 90-101.

30. **Kato, T., Yamaura, H., Kawno, K., Hiyama, T., Tada, E., Kakayama, Y.,Kawashina, Sato, M., Yoshida, J., Ito, N., Sato, S. and Shimamato, S. A.,** Large scale turboexpander d velopment and its performance test result. *Adv Cryo Eng* (1990), *35*, 1005-1012.

31. **Kato, T., Kamiyauchi, Y., Tada, E., Hiyama, T.,· Kawano, K., Sugimoto, M., Kawageo, E., Ishida, H., Yoshida, J., Tsuji, H., Sato, S., Xakayama, Y., Kawashima I,** Development of a large helium turbo-expander with variable capacity. *Adv Cryo Eng* (1992), *37B*, 827.

32. **Kato, T., Miyake, A., Kawno, K., Hamada, K., Hiyama, T., Iwamoto, S., Ebisu, H., Tsuji, H., Saji, N., Kaneko, Y., Asakura, H., Kuboto, M. and Nagai, S. ,** Design and test of wet type turbo-expander with an alternator as a brake. *Advances in Cryogenic Engineering* (1994), *39*, 917.

33. **Ino, N., Machida, A.,Ttsugawa, K. and Arai, Y.,** Development of high expansion ratio Helium turbo expander. *Advances in Cryogenic Engineering* (1992), *V37B*, 835-844.

34. **Ino, N., Machida, A. and Ttsugawa, K.,** Development of externally pressurized thrust bearing for high gas expansion ratio expander. *Adv Cryo Eng* (1992), *37B*, 817-825.

35. **Davydenkov, I. A., Davydov, A. B. and Perestoronin, G. A.,** Hydrogen and nitrogen turboexpanders with high gas expansion ratios. *Cryogenics & 32 (1992) ICEC supplement* (1992), 84-86.

36. **Davydenkov, I. A., Ravikorichy, Yu A., Davydov, A. B., Ermilov, Yu., Zakharova, N. E., Adler, Yu. R and Schedukhin,** Development of cryogenic turboexpanders with gas dynamic foil bearings. *Cryogenics* (1992), *32*, 80.

37. **Baranov, A., Duzev, V., Kashirskikh, G., Mikhailov, A., Ugrovatov, A. and Zhulkin, V.,** An experience in the maintenance of a liquefier from the T-15 cryogenic system, results of its reliability and capacity enhancement. *Adv Cryo Eng* (1996), *41 a*, 737-743.

38. **Polishchuk, E. L., Shariklankin V. I. and Lyapin. V. I.,** Self-contained microcryogenic system with a turboexpander *Khimicheskoe I Neftyanoe Mashinostroenie Trans: Chemical & Petroleum Engg* (1991), *27 (3/4)*, 217.

39. **Kun, L. C.,** Expansion turbines and refrigeration for gas separation and liquefaction. *Adv Cryo Eng* (1988), *33*, 963-973.

40. **Kun, L. C., and Hanson, T. C.,** High efficiency turboexpander in a N_2 liquefier. In *AIChE Spring meeting*, Houston, Texas, (1985).

41. **Kun, L. C., and Sentz, R. N.,** High efficiency expansion turbines in air separation and liquefaction plants. In *International Conference on Production and Purification of Coal Gas & Separation of Air*, Beijing, China (1985); pp 1-21.

42. **Sixsmith, H., Valenjuela, J. and Swift, W. L. ,** Small Brayton cryocoolers *Adv Cryo Eng* (1988), *34*, 827-836.

43. **Jadeja, H. T., Mitter, A. and Chakrabarty, H. D.,** Turboexpander application for cryoprocessing of nitrogen and related gases. In *Proceedings of INCONCRYO85 Indian Cryogenic Council*, Tata McGraw: (1985); pp 85-101.

44. **Jadeja, H. T., Kundu, K. M.,Chakrabarty, H. D. and Mitter, A. ,** IFR expansion turbine for cryogenic plants. *Institution of Engineers (India) J. Ill Mech Eng* (1987), *67*, 106 -112.

45. **Jadeja, H. T., Chakrabarty, H. D. Nidhi, S. C. and Mitter, A.,** Mechanical reliability and manufacturing process for indigenous development of turboexpander In *Proceedings of INCONCRY0-88 Indian Cryogenic Council*, (1988); pp 331-337.

46. **Aghai, R. R., Lin, M.C. and Ershaghi, B.,** High Performance cryogenic turboexpanders. *Adv Cryo Eng* (1996), *41*, 941-947.

47. **Aghai, R. R., Lin, M.C. and Ershaghi, B.,** Improvements of the efficiency of the turboexpanders in cryogenic applications *Adv Cryo Eng* ((1996)), *41*, 933-940.

48. **Ghosh, P.** Analytical and Experimental Studies on Cryogenic Turboexpanders. (2002).

49. **Ghosh, S. K.** Experimental and Computational Studies on Cryogenic Turboexpander. (2008).

50. **Chakravarty, A., and Singh, T.,** High speed miniature cryogenic turboexpander impellers at BARC. *Indian Journal of Cryogenics* (2011), *36*, 1-9.

51. **Menon, R., Chakravarty, A.,Goyal, M., Jadav, M., Arun, S.,Bharti, S. K., and Singh, T.,** High speed cryogenic turboexpander rotor for stable operation upto 4.5 kHz rotational speed. *Indian Journal of Cryogenics* (2012), *37* (1-4), 40-45.

52. **Barron, R. F.,** *Cryogenic Heat Transfer*. (1985),

53. **Robertson, J.,** Heat exchnager equipment for cryogenic process industry. *Heat exchnager theory and practice* (1983), 469-561.

54. **Abadzic, E. E., and Scholz, H. W.,** Coiled Tubular heat exchangers. *Adv. Cryogenics Engg.* (1973), *18*, 42-51.

55. **McKeever, J., Pillarella, M., and Bower, R.,** An ever evolving technology. *LNG Ind Spring* (2008), 44–52.

56. **Tariq, S.,** LNG technology selection. *Hydrocarb Eng* (2004), *9* (2), 71-76.

57. **Venkatarathnam, G., and Sarangi, S.,** Matrix heat exchangers and their application in cryogenic systems. *Cryogenics* (1990), *30* (11), 907-918.

58. **Venkatarathnam, G.,** Effectiveness-Ntu relationship in perforated plate matrix heat exchangers. *Cryogenics* (1996), *36* (4), 235-241.

59. **Pavan, K., and G. Venkatarathnam,** Optimization of Matrix Heat Exchanger Geometry. *Journal of Heat Transfer, ASME* (200), *122*, 579-586.

60. ALPEMA. The Standards of the Brazed Aluminium Plate-Fin Heat Exchanger Manufacturers' Association. (2000).

61. Chart Energy & Chemicals Inc. www.chartindustries.com.

62. Fives Cryo. www.fivesgroup.com/fivescryogenie.

63. Kobe Steel, Ltd. www.kobelco.co.jp.

64. Linde AG, Germany. http://www.linde-engineering.com.

65. Sumitomo Precision Products Co., Ltd. www.spp.co.jp.

66. **Kays, W. M., and London, A. L.,** *Compact Heat exchangers*. McGraw-Hill New York, (1984),

67. **Kern, D. Q., and Kraus, A. D.,** *Extended Surface Heat Transfer*. McGraw-Hill New York, (1972),

68. **Ozisik, M. N.,** *Heat Transfer-A Basic Approach*. McGraw-Hill (1985),

69. **Frank, P. I., David P. DeWitt., Theodore L. Bergman., and Adrienne S. Lavine,** *Fundamentals of Heat and Mass Transfer 6th ed.* John Wiley New York, (2006),

70. **Frass, A. P.,** *Heat Exchanger Design, 2nd ed.* Wiley-Interscience (1989),

71. **Shah, R. K.,** *Cmpact Heat Exchangers & Enhancement Technology*. Begell House Publication (1999),

72. **Smith, E. M.,** Plate Fin Surface OptimisationUsing Direct-Sizing. *Advances in Enhanced Heat Transfer, ASME,* (2000), *4*, 105–115.

73. **Shah, R. K., Subbarao, E. C., and Mashelkar, R. A.,** *Heat Transfer Equipment Design edited by R.K.Shah*. Publishing Corporation Washington DC, (1988),

74. **Taborek, J., Hewitt, G. F., and Afgtan, N,** *Heat Exchangers-Theory and Practice*. Hemisphere Publishing New York, (1983),

75. **Taylor, M. A.,** *Plate Fin Heat Exchangers: Guide to their Specification and Use HTFS*. Oxon UK, (1987),

76. **Aslam, B., Hayat, M. M., Nasir, Bashir., Khan, M. H.,Ahmad, A. R., and Khan, A. N.,** CFD applications in various heat exchangers design: A review. *Applied Thermal Engineering* (2012), *32* (0), 1-12.

77. **Das, P. K., and Ghosh, I.,** Thermal Design of Multistream Plate Fin Heat Exchangers—A State-of-the-Art Review. *Heat Transfer Engineering* (2011), *33* (4-5), 284-300.

78. **Pacio, J. C., and Dorao, C. A.,** A review on heat exchanger thermal hydraulic models for cryogenic applications. *Cryogenics* (2011), *51* (7), 366-379.

79. **Kakac, S., Bergles, A. E., and Mayinger, F.,** *Heat Exchangers, Thermal-Hydraulic Fundamentals and Design*. Hemisphere Publication (1988),

80. **Kuppan, T.,** *Heat exchanger design handbook. Mechanical engineering. A series of textbooks and reference books*. Marcel Dekker Inc. New York, (2000); Vol. 126,

81. **Shah, R. K., Dusan,P., and Sekulic,D. P.,** *Fundamentals of Heat Exchanger Design*. John Wiley & Sons (2003),

82. **Taborek J.,** Evolution of heat exchanger design techniques. *Heat Transfer Eng* (1979), *1* (1), 19-25.

83. **Mueller, A.** In *New charts for true mean temperature difference in heat exchangers.*, AIChE paper 10, 9th National Heat Transfer Conference, (Year).

84. **Roetzel, W., and Spang, B.,** Verbessertes diagramm zur berechnung von wärmenbertragern. *Heat Mass Transfer* (1990), *25*, 259–64.

85. **Iu, I.** Development of air-to-air heat pump simulation program with advanced heat exchanger circuitry algorithm. Ph.D., Oklahoma State University, (2007).

86. **Orth, L., Zietlow, D. C., and Pedersen, C. O.** *Predicting refrigerant inventory of HFC 134a in air cooled condensers. Technical Report ACRCTR-34.*; Air Conditioning and Refrigeration Center, University of Illinois: (1993).

87. ASPENTech, MUSE. http://www.aspentech.com/products/aspen-plate-fin.cfm.

88. *Aspen Muse Reference guide*. Aspen Technology, Inc. Cambridge, Massachusetts, Vol. V2006,

89. **Venkatarathnam, G.,** *Cryogenic Mixed Refrigerant Processes*. Springer-Verlag New York Inc (2008),

90. **Sekwang, Y., Habin, C., Dong-H, L., and Jin-Kuk, K,** Process Design and Optimization of Natural Gas Liquefaction Processes. *Chemiical Engiineeriing Transactiions* (2012), *29*, 1585-1590.

91. **Atrey, M. D.,** Thermodynamic analysis of Collin's helium liquefaction cycle. *Cryogenics* (1998), *38*, 1199-1206.

92. **Narinsky, G. B., Temirova, V. V., and Chernokov, L. V. ,** Influence of thermodynamic parameters on main characteristics of helium liquefaction and refrigeration plant. *Cryogenics* (1995), *35*, 483-487.

93. **Jianlin, Y.,** Improving the performance of small Joule–Thomson cryocooler. *Cryogenics* (2008), *48*, 426-431.

94. **Nandi, T. K., and Sarangi, S. ,** Performance And Optimization Of Hydrogen Liquefaction Cycles. *Int. J. Hydrogen Energ* (1993), *18* (2), 131-139.

95. **Harvey, S., and Kane, N'Diaye,** Analysis of a reheat gas turbine cycle with chemical recuperation using Aspen. *Energy Conversion and Management* (1997), *38* (15–17), 1671-1679.

96. **Melaaen, E., Owren, G.,Wadahl, A., and Wagner, U.,** Simulation Program for Cryogenic Plants at CERN. In *Proceedings of the Sixteenth International Cryogenic Engineering Conference/International Cryogenic Materials Conference*, Haruyama, T.; Mitsui, T.; K. YamafujiA2 - T. Haruyama, T. M.; Yamafuji, K., Eds. Elsevier Science Oxford, (1997); pp 99-102.

97. **Maekawa, R., Ooba, K., Nobutoki,M., and Mito,T,** Dynamic Simulation of a Helium Liquefier. *Advances in Cryogenic Engineering* (2004), *49*, 192-199.

98. **Deschildre, C., Barraud, A., Bonnay, P., Briend, P., Girard, A., Poncet, J. M., Roussel,P., and Sequeira, S. E.,** Dynamic Simulation of an Helium Refrigerator. *Advances in Cryogenic Engineering* (2008), *53*, 475-482.

99. **Rogez, E., Bradu B.,Moraux, A.,Pezzetti, M.,Gayet, Ph., and Coppier, H.** In *A simulation study for the virtual commissioning of the CERN central helium liquefier*, ICEC 22 - ICMC 2008 Conference, Seoul, Korea, Seoul, Korea, (Year), 1-5.

100. **Bradu, B., Gayet, Philippe., and Niculescu, Silviu-Iulian.,** A process and control simulator for large scale cryogenic plants. *Control Engineering Practice* (2009), *17* (12), 1388-1397.

101. **Maekawa, R., Ooba, Kouki.,Nobutoki, Minoru., and Mito, Toshiyuki.,** Dynamic simulation of the helium refrigerator/liquefier for LHD. *Cryogenics* (2005), *45* (3), 199-211.

102. Stirling Cryogenics. http://www.stirlingcryogenics.com/.

103. Linde Cryoplants. http://www.lindecryoplants.com/en.php.

104. Pacific Consolidated Industries. http://www.pci-intl.com/.

105. Cryomech Inc. www.cryomech.com/.

106. Kelvin International Corporation http://www.kelvinic.com.

107. *Aspen Hysys User's Guide*. Aspen Technology, Inc. Cambridge, Massachusetts,

108. **Moon, J. W., Lee, Y. P., Jin, Y. W., Hong, E. S., and Chang, H. M.,** Cryogenic Refrigeration Cycle for Re-Liquefaction of LNG Boil-Off Gas. In *International Cryocooler Conference, Inc.*, Boulder, (2007); pp 629-635.

109. Lemmon, E. W., Jacobsen, R. T., Penoncello, S. G., and Beyerlein, S. W., *ALLPROPS 4.2 – Computer Programs for Calculating Thermodynamic Properties*

of Fluids of Engineering Interest, Centre for Applied Thermodynamic Studies: University of Idaho (1995).

110. **Seshaiah, N.** Experimental and computational studies on oil injected twin screw compressor. NIT Rourkela, (2006).

111. **Maiti, D. K.** Heat Transfer and Flow Friction Characteristics of Plate Fin Heat Exchanger Surfaces – A Numerical Study. (2002).

112. **Manglik, R. M., and Bergles, A. E,** Heat Transfer and Pressure Drop Correlations for the Rectangular Offset Strip Fin Compact Heat Exchanger *Experimental Thermal Fluid Science* (1995), *10*, 171-180.

113. **Joshi, H. M., and Webb, R. L.,** Heat Transfer and Friction of the Offset Strip-fin Heat Exchanger. *Int. J. Heat Mass Transfer* (1987), *30* (1), 69-84.

114. **Frost, W.,** *Heat Transfer At Low Temperatures*. Plenum Press New York, (1975); 208,

115. **Denton, J. D.,** The turboexpander - a design, make and test student project. *ASME-96-GT- 191* (1996).

116. **Jekat, W. K.,** An Impulse Type Expansion Turbine. *Advances in Cryogenic Engineering* (1957), *V2*, 250-260.

117. **Whitfield, A., and Baines, N. C. ,** *Design of Radial Turbomachines*. Longman Scientific & Technical (1990),

118. **RohliK, H. E.,** Analytical determination of radial inflow turbine geometry for maximum efficiency. *NASA TN D-4384* (1968).

119. **Hasselgruber, H.,** Stromungsgerechte gestaltung der laufrader von radialkompressoren mit axialelaufradeintrict. *Konstruction* (1958), *10 (1)* 22 (in German).

120. **Balje, O. E.,** *Turbomachines*. John Wiley and Sons (1981),

121. **Sixsmith, H., and Swift, W. L.,** *Cryogenic turbines and pumps in Hands, B. A: (Ed.)*. Academic Press (1986),

122. **Dixion., S. L.,** *Fluid Mechanics and Thermodynamics of Turbomachinery* 3rd ed.; Pergamon Press (1978),

123. **Chakravarty, A.** Analytical and Experimental Studies on Gas Bearings for Cryogenic Turboexpanders (2000).

124. **Muhammad, S., Malik M. Nazeer, and Abdul, Qayyum,** Balancing of a cryogenic turbo-expander assembly. In *15th International Congress on Sound and Vibration*, Daejeon, Korea, (2008); pp 2381-2386.

Appendix A

Production Drawings of Turboexpander

Turboexpander Part List :

SL. NO	PART NO	PART NAME	MATERIAL	QUANTITY
1	1	Shaft	Monel K-500	1
2	2	Aerostatic thrust plate	SS304	2
3	3	Aerostatic thrust plate	SS304	2
4	4	Exhaust gas plate (lower)	SS304	2
5	5	Exhaust gas plate (upper)	SS304	2
6	6	Tilting pad housing	Monel K-500	2
7	7	Pad	High density metal impregnated graphite	6
8	8	End pad plate	SS304	4
9	9	Spacer	SS304	1
10	10	Bearing block	SS304	1
11	11	Lock nut (Turbine side)	SS304	1
12	12	Lock nut (Ccompressor	SS304	1
13	13	Nozzle diffuser	Brass	1
14	14	Cold end housing	SS304	1
15	15	Cover T nozzle	SS304	1
16	16	Nozzle brake compressor	Al Alloy	1
17	17	Heat exchanger	Al Alloy	1
18	18	Stem	Brass	1
19	19	Stem tip	Brass	1
20	20	Thermal Insulator-1	Nylon-6	1
21	21	Thermal Insulator-2	Nylon-6	1
22	22	Thermal Insulator-3	Teflon	1

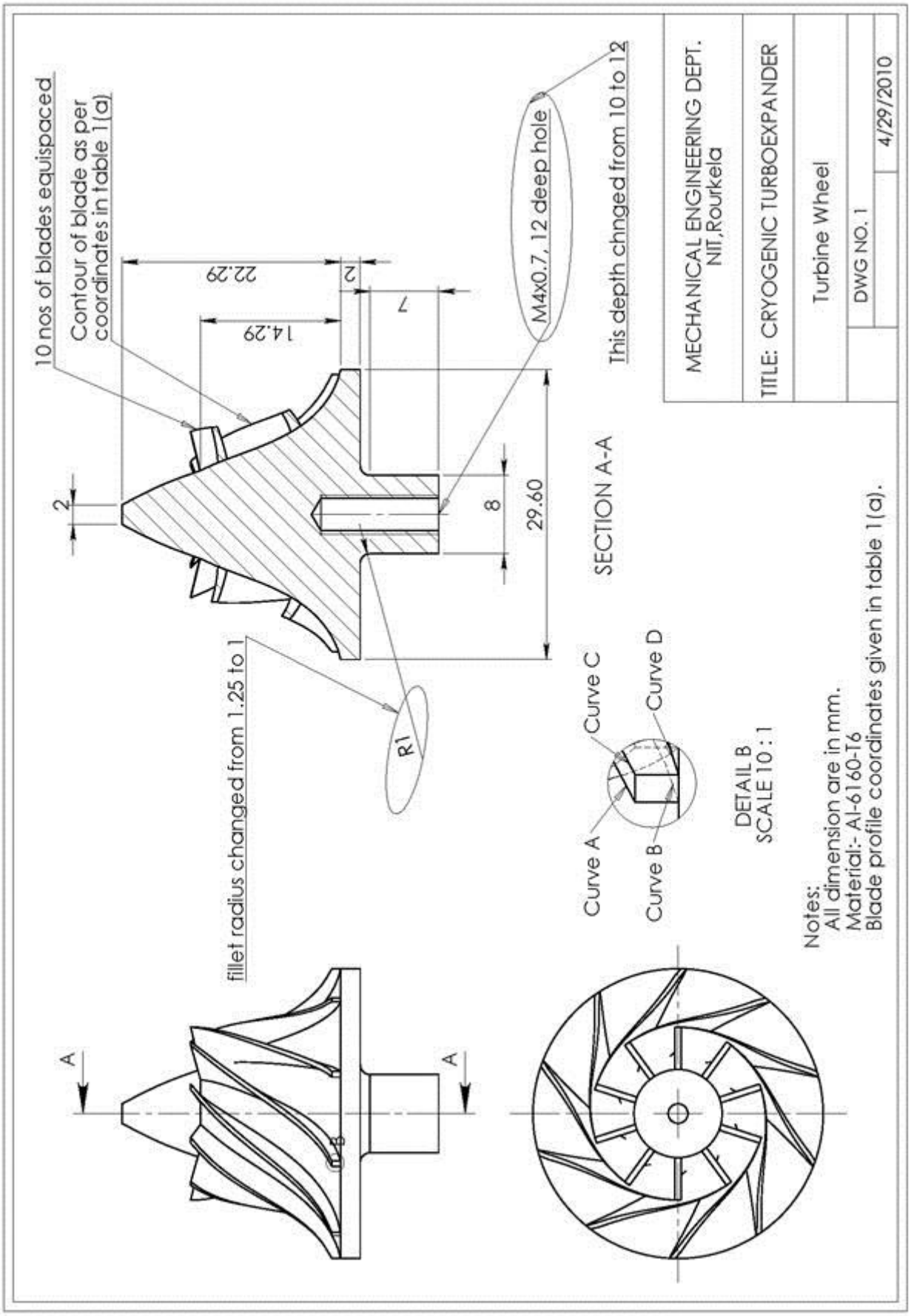

Figure A-1 Turbine wheel

Table 1(a) Blade Profile coordinates of Turbine wheel

Curve-A			Curve-B			Curve-C			Curve-D		
Radius r	Angle θ	Height z	Radius r	Angle θ	Height z	Radius r	Angle θ	Height z	Radius r	Angle θ	Height z
8.8434	1.9437	0.0000	4.5066	3.8141	1.0012	8.8434	358.0563	0.0000	4.5066	356.1859	1.0012
8.8459	8.7875	0.8446	4.8746	10.3705	1.7614	8.8459	4.9012	0.8446	4.8746	3.3181	1.7614
8.8804	14.9109	1.6794	5.2106	16.2741	2.5313	8.8804	11.0397	1.6794	5.2106	9.6765	2.5313
8.9404	20.4272	2.5037	5.5230	21.6167	3.3113	8.9404	16.5820	2.5037	5.5230	15.3924	3.3113
9.0217	25.4335	3.3175	5.8205	26.4814	4.1004	9.0217	21.6230	3.3175	5.8205	20.5751	4.1004
9.1222	30.0126	4.1210	6.1113	30.9410	4.8967	9.1222	26.2440	4.1210	6.1113	25.3157	4.8967
9.2414	34.2339	4.9143	6.4030	35.0584	5.6982	9.2414	30.5139	4.9143	6.4030	29.6894	5.6982
9.3796	38.1550	5.6974	6.7031	38.8867	6.5026	9.3796	34.4899	5.6974	6.7031	33.7582	6.5026
9.5384	41.8231	6.4700	7.0188	42.4700	7.3071	9.5384	38.2190	6.4700	7.0188	37.5721	7.3071
9.7197	45.2756	7.2314	7.3568	45.8436	8.1087	9.7197	41.7387	7.2314	7.3568	41.1707	8.1087
9.9262	48.5416	7.9805	7.7236	49.0354	8.9036	9.9262	45.0782	7.9805	7.7236	44.5844	8.9036
10.1612	51.6425	8.7157	8.1253	52.0663	9.6873	10.1612	48.2593	8.7157	8.1253	47.8354	9.6873
10.4284	54.5938	9.4349	8.5674	54.9518	10.4545	10.4284	51.2973	9.4349	8.5674	50.9392	10.4545
10.7322	57.4059	10.1351	9.0550	57.7025	11.1986	10.7322	54.2027	10.1351	9.0550	53.9060	11.1986
11.0770	60.0855	10.8128	9.5921	60.3258	11.9119	11.0770	56.9820	10.8128	9.5921	56.7418	11.9119
11.4676	62.6370	11.4629	10.1813	62.8264	12.5855	11.4676	59.6392	11.4629	10.1813	59.4499	12.5855
11.9085	65.0633	12.0796	10.8234	65.2080	13.2097	11.9085	62.1765	12.0796	10.8234	62.0318	13.2097
12.4033	67.3670	12.6556	11.5166	67.4737	13.7743	12.4033	64.5953	12.6556	11.5166	64.4886	13.7743
12.9543	69.5510	13.1830	12.2563	69.6266	14.2700	12.9543	66.8973	13.1830	12.2563	66.8217	14.2700
13.5611	71.6194	13.6534	13.0353	71.6706	14.6894	13.5611	69.0844	13.6534	13.0353	69.0333	14.6894
14.2209	73.5774	14.0596	13.8441	73.6103	15.0286	14.2209	71.1601	14.0596	13.8441	71.1272	15.0286
14.8000	75.4414	14.3970	14.8000	75.4414	15.2881	14.8000	73.1186	14.3970	14.8000	73.1186	15.2881

(All are in cylindrical coordinate system)

Table 1(b) Turbine wheel Blank profile coordinates

Radius r	Height z
8.8434	0.0000
8.8459	0.8446
8.8804	1.6794
8.9404	2.5037
9.0217	3.3175
9.1222	4.1210
9.2414	4.9143
9.3796	5.6974
9.5384	6.4700
9.7197	7.2314
9.9262	7.9805
10.1612	8.7157
10.4284	9.4349
10.7322	10.1351
11.0770	10.8128
11.4676	11.4629
11.9085	12.0796
12.4033	12.6556
12.9543	13.1830
13.5611	13.6534
14.2209	14.0596
14.8000	14.3970

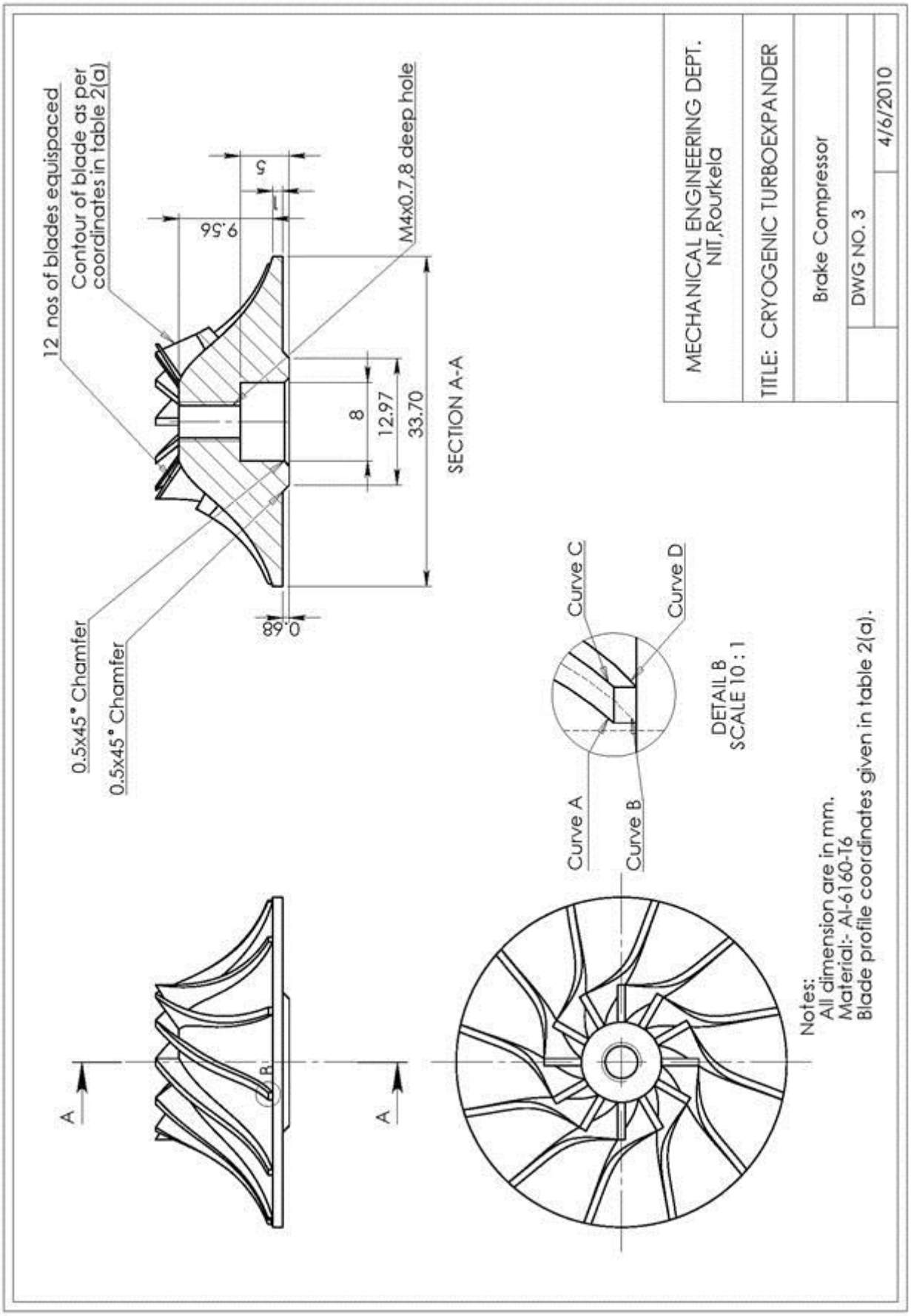

Figure A-2 Brake compressor

Table 2(a) Blade Profile coordinates of Brake compressor

Curve-A			Curve-B			Curve-C			Curve-D		
Radius r	Angle θ	Height z	Radius r	Angle θ	Height z	Radius r	Angle θ	Height z	Radius r	Angle θ	Height z
7.9049	2.7181	0.0000	4.0951	5.2467	2.3806	7.9049	357.2819	0.0000	4.0951	354.7533	2.3806
7.9187	10.2395	0.8616	4.8635	11.9440	2.7707	7.9187	4.8129	0.8616	4.8635	3.1084	2.7707
8.0488	16.3428	1.6485	5.5156	17.5689	3.2356	8.0488	11.0039	1.6485	5.5156	9.7779	3.2356
8.2481	21.3070	2.3879	6.0999	22.2244	3.7470	8.2481	16.0971	2.3879	6.0999	15.1798	3.7470
8.4947	25.3475	3.0935	6.6425	26.0528	4.2887	8.4947	20.2888	3.0935	6.6425	19.5835	4.2887
8.7771	28.6337	3.7732	7.1603	29.1865	4.8493	8.7771	23.7378	3.7732	7.1603	23.1851	4.8493
9.0893	31.3012	4.4311	7.6660	31.7401	5.4201	9.0893	26.5735	4.4311	7.6660	26.1346	5.4201
9.4285	33.4602	5.0696	8.1690	33.8115	5.9938	9.4285	28.9025	5.0696	8.1690	28.5512	5.9938
9.7939	35.2020	5.6891	8.6768	35.4845	6.5642	9.7939	30.8144	5.6891	8.6768	30.5320	6.5642
10.1858	36.6036	6.2894	9.1951	36.8309	7.1259	10.1858	32.3848	6.2894	9.1951	32.1575	7.1259
10.6048	37.7309	6.8694	9.7284	37.9134	7.6737	10.6048	33.6787	6.8694	9.7284	33.4962	7.6737
11.0516	38.6407	7.4274	10.2797	38.7867	8.2031	11.0516	34.7524	7.4274	10.2797	34.6064	8.2031
11.5268	39.3825	7.9617	10.8507	39.4987	8.7099	11.5268	35.6545	7.9617	10.8507	35.5384	8.7099
12.0305	39.9986	8.4704	11.4422	40.0904	9.1909	12.0305	36.4267	8.4704	11.4422	36.3349	9.1909
12.5622	40.5239	8.9517	12.0538	40.5960	9.6432	12.5622	37.1032	8.9517	12.0538	37.0310	9.6432
13.1206	40.9859	9.4040	12.6845	41.0422	10.0651	13.1206	37.7108	9.4040	12.6845	37.6544	10.0651
13.7043	41.4045	9.8264	13.3329	41.4482	10.4556	13.7043	38.2688	9.8264	13.3329	38.2252	10.4556
14.3111	41.7930	10.2180	13.9972	41.8267	10.8142	14.3111	38.7903	10.2180	13.9972	38.7567	10.8142
14.9389	42.1597	10.5787	14.6755	42.1855	11.1411	14.9389	39.2831	10.5787	14.6755	39.2573	11.1411
15.5853	42.5090	10.9086	15.3658	42.5287	11.4372	15.5853	39.7518	10.9086	15.3658	39.7321	11.4372
16.2480	42.8437	11.2084	16.0663	42.8587	11.7034	16.2480	40.1990	11.2084	16.0663	40.1840	11.7034
16.8500	43.1708	11.4790	16.8500	43.1708	11.9412	16.8500	40.6206	11.4790	16.8500	40.6206	11.9412

(All are in cylindrical coordinate system)

Table 2(b) Blank profile coordinates of Brake compressor

Radius r	Height z
7.9049	0.0000
7.9187	0.8616
8.0488	1.6485
8.2481	2.3879
8.4947	3.0935
8.7771	3.7732
9.0893	4.4311
9.4285	5.0696
9.7939	5.6891
10.1858	6.2894
10.6048	6.8694
11.0516	7.4274
11.5268	7.9617
12.0305	8.4704
12.5622	8.9517
13.1206	9.4040
13.7043	9.8264
14.3111	10.2180
14.9389	10.5787
15.5853	10.9086
16.2480	11.2084
16.8500	11.4790

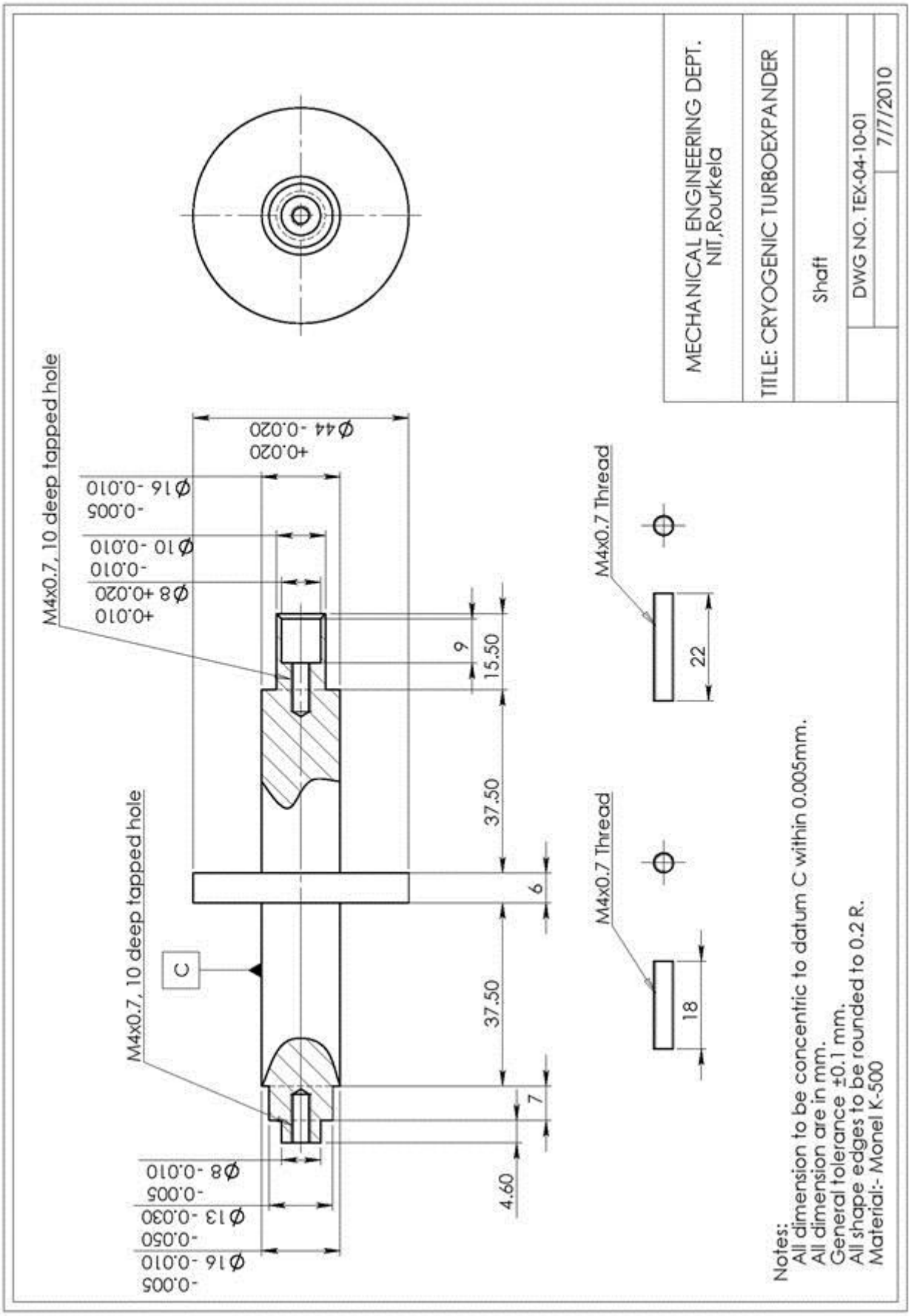

Figure A-3 Shaft

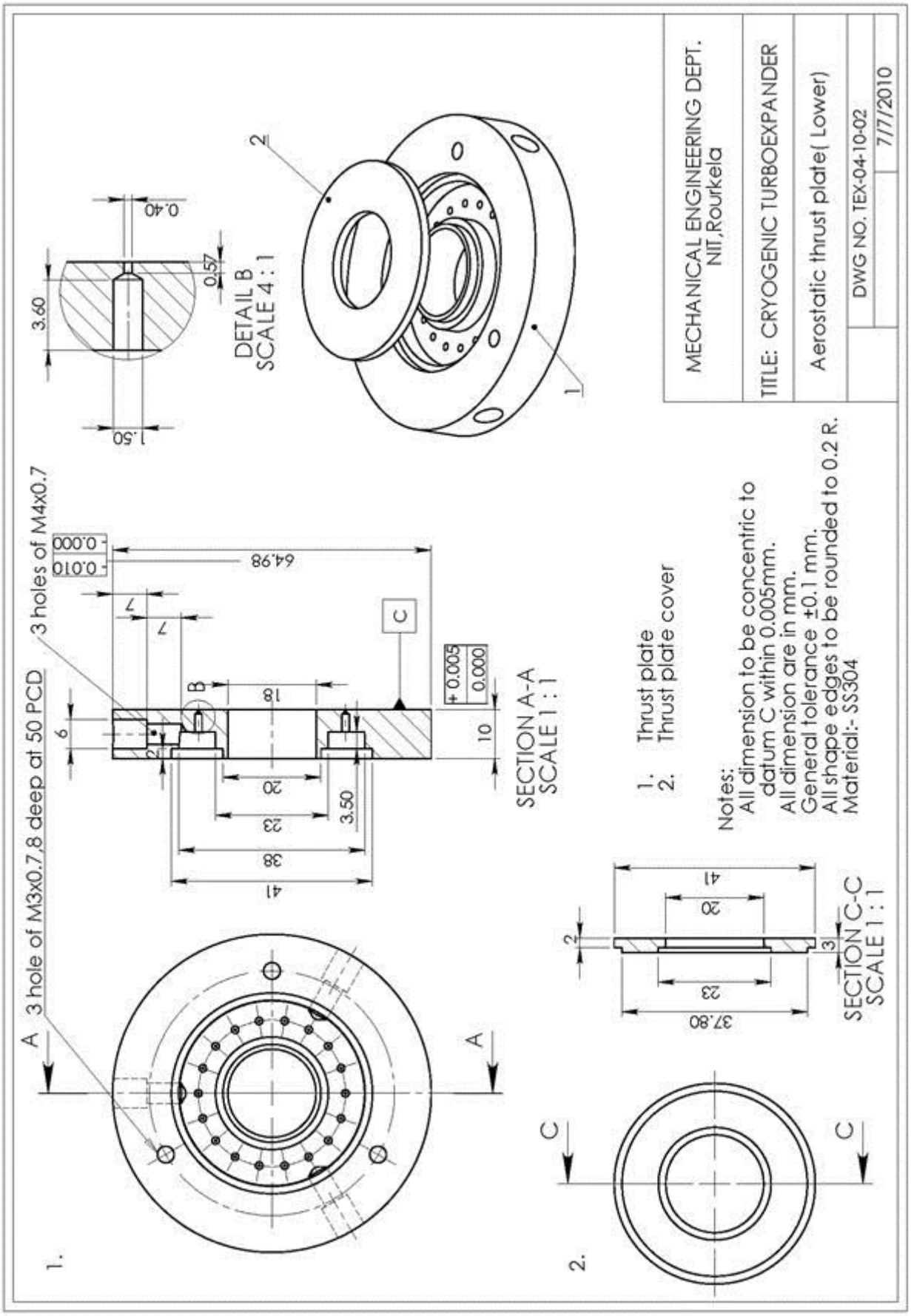

Figure A-4 Aerostatic thrust plate (lower)

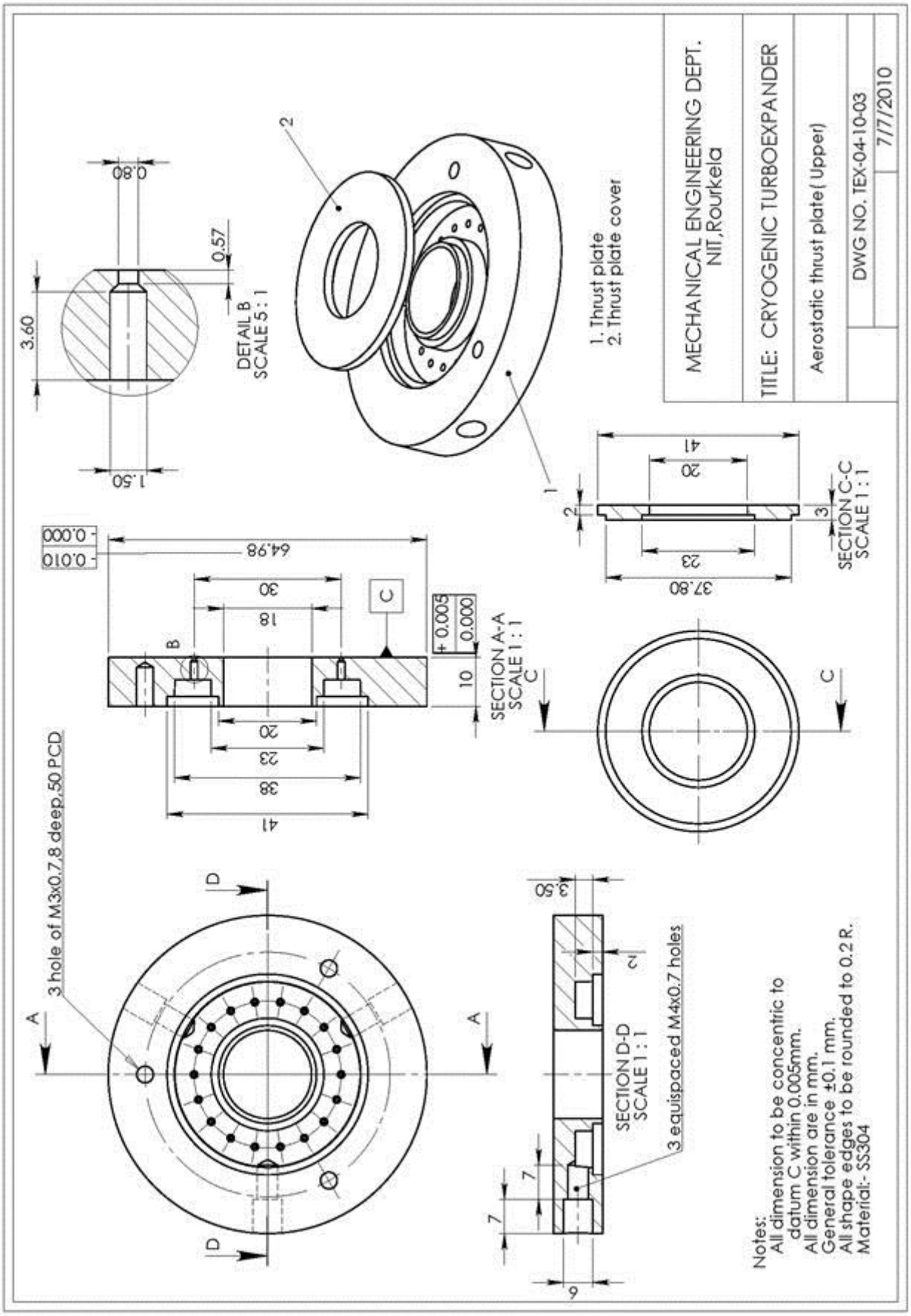

Figure A-5 Aerostatic thrust plate (upper)

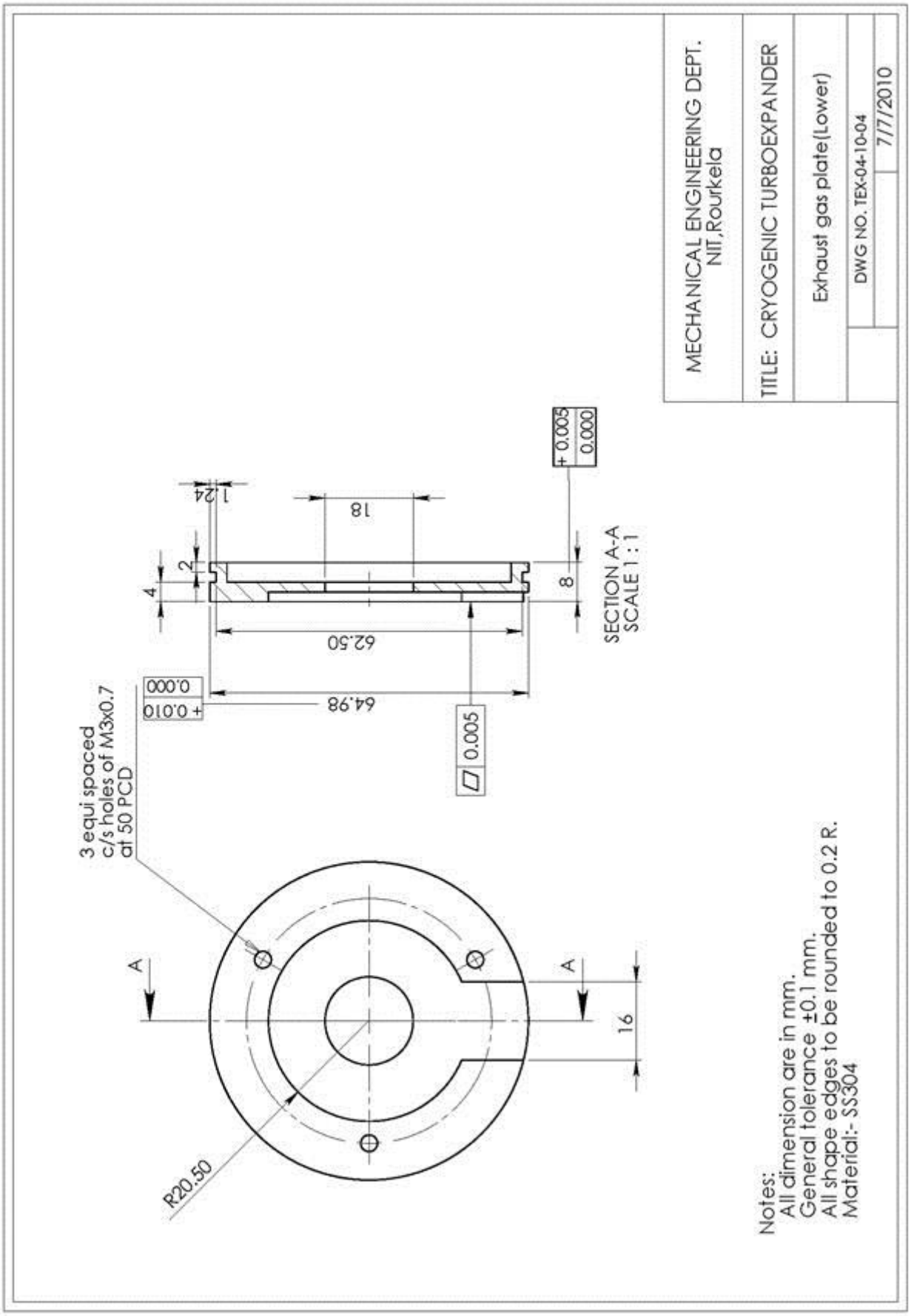

Figure A-6 Exhaust gas plate (lower)

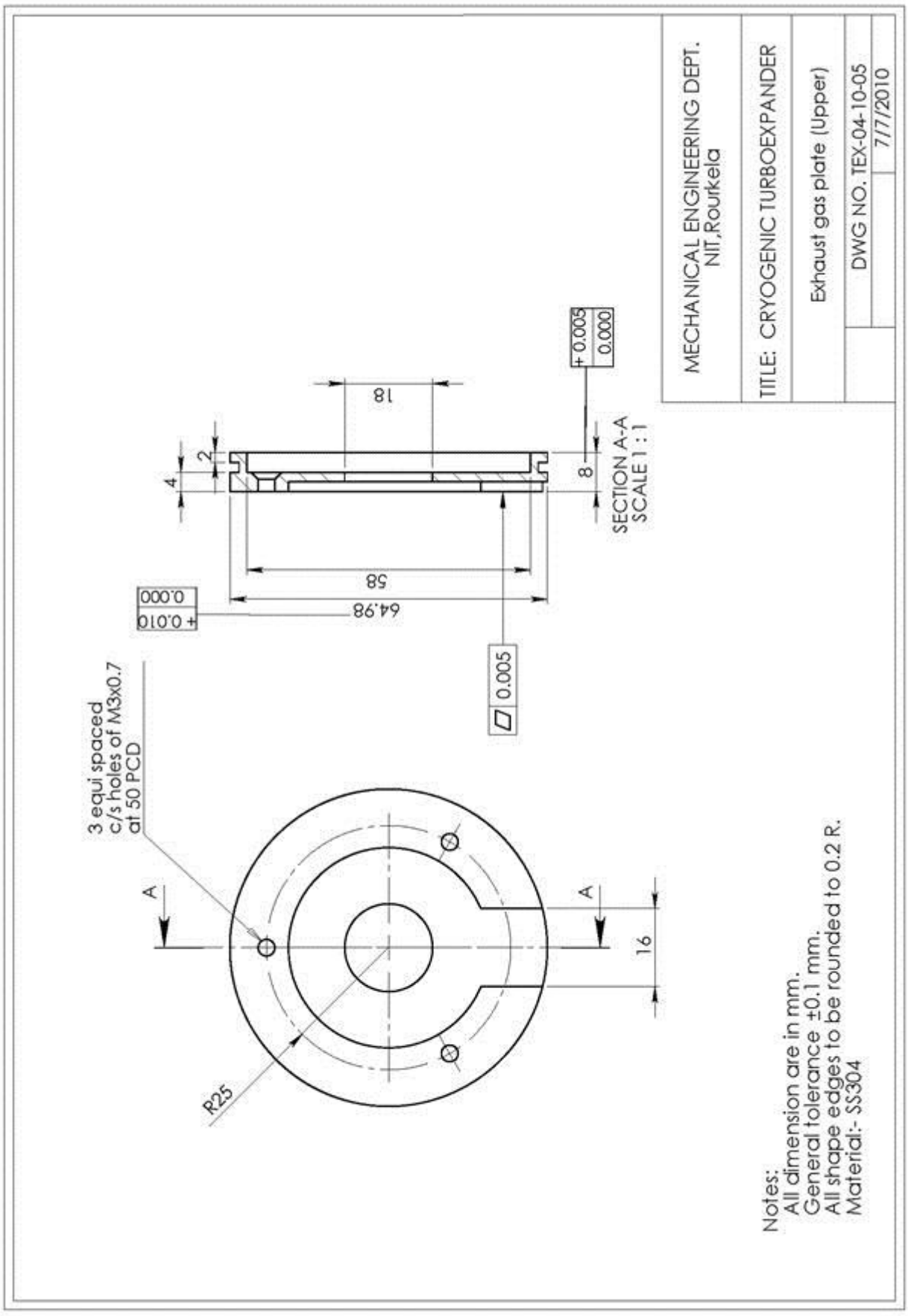

Figure A-7 Exhaust gas plate (upper)

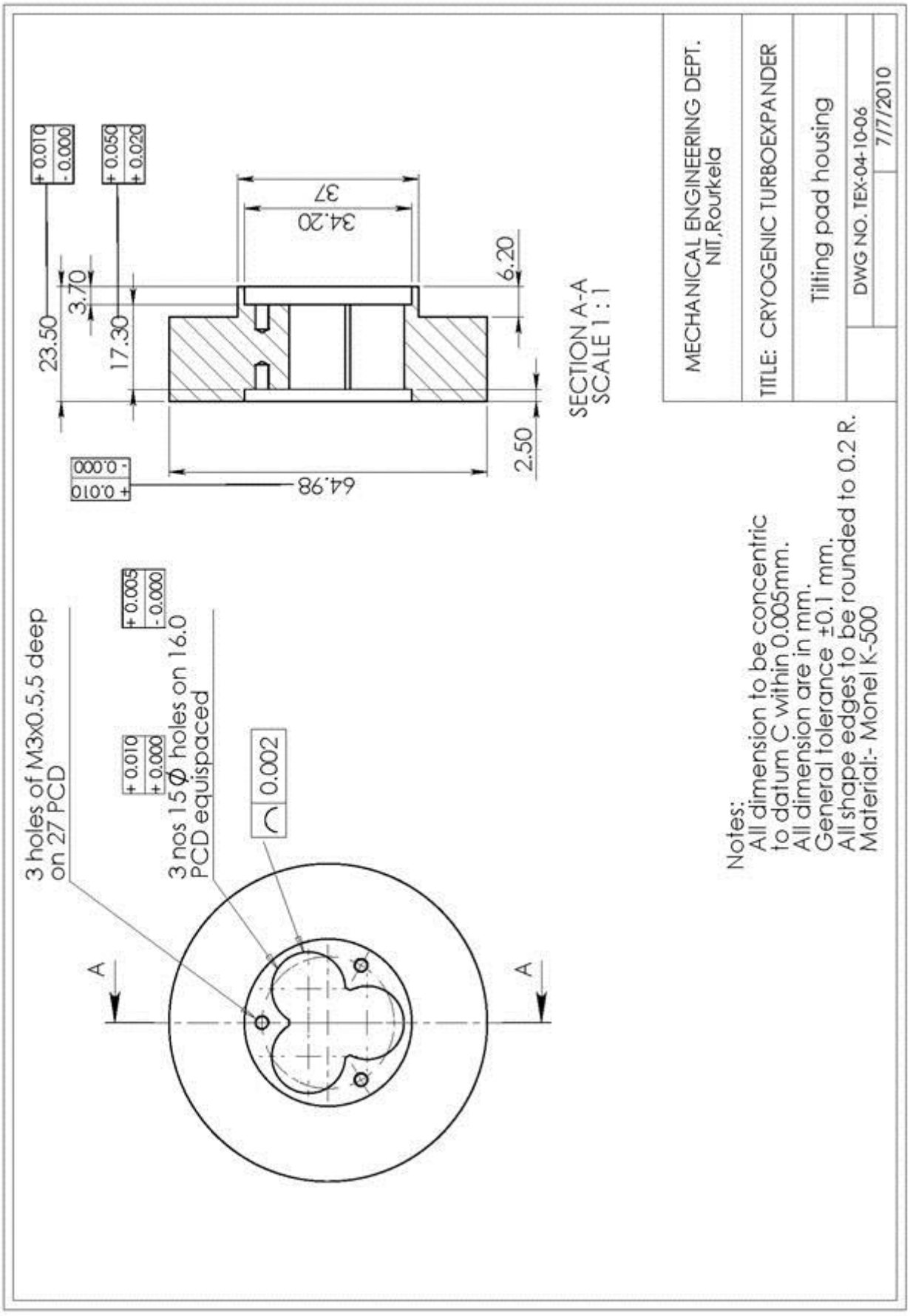

Figure A-8 Tilting pad housing

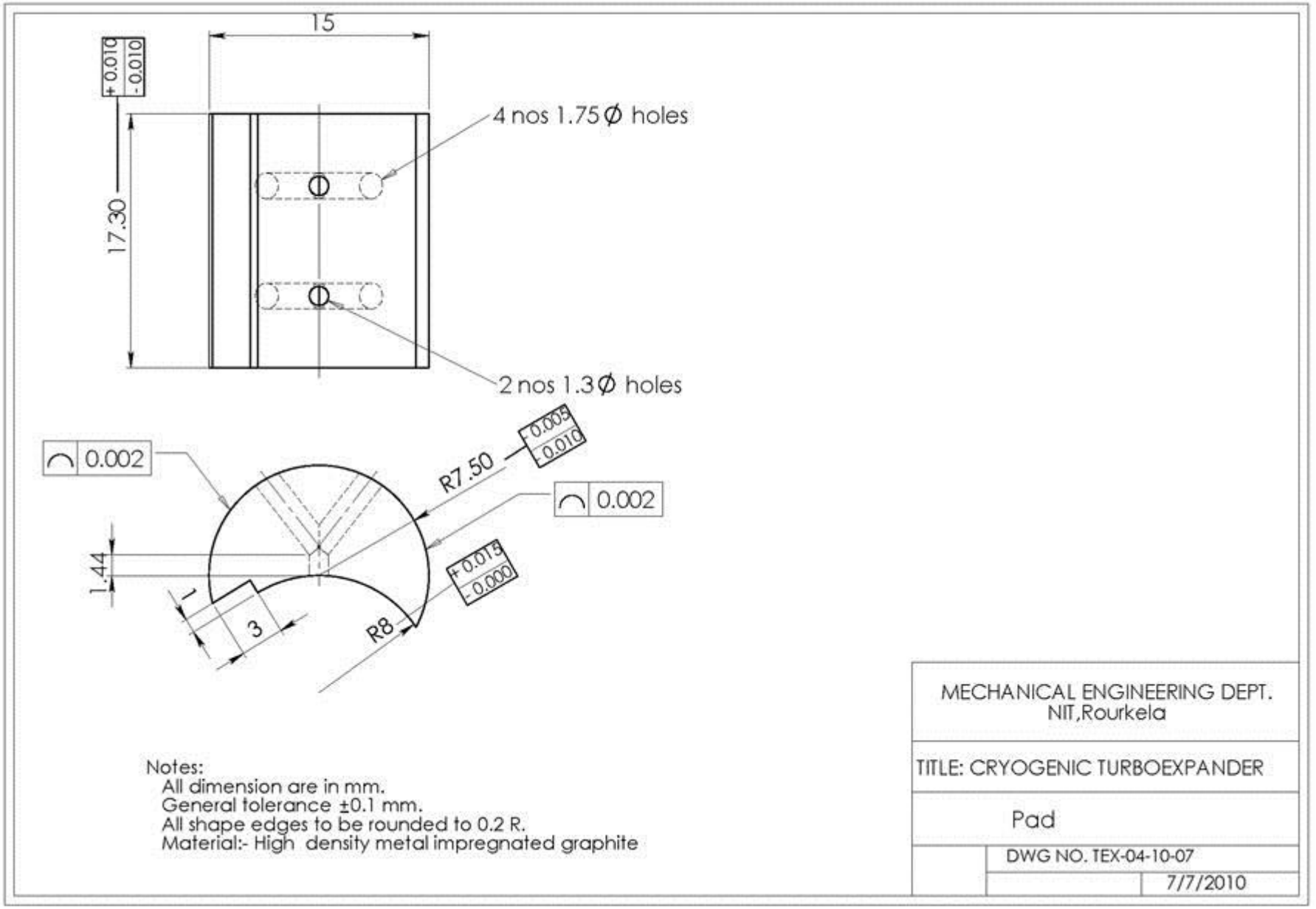

Figure A-9 Pad

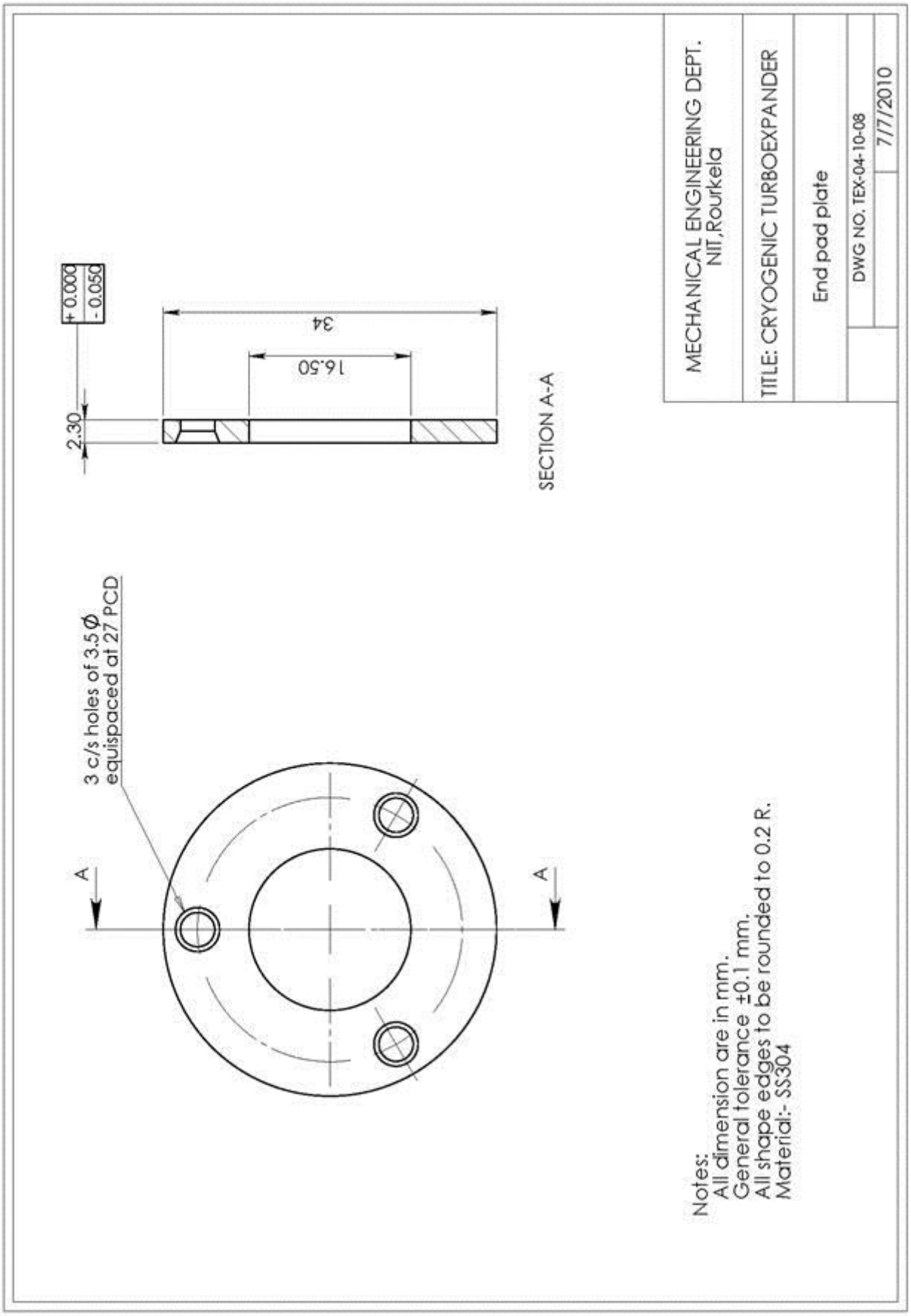

Figure A-10 End pad plate

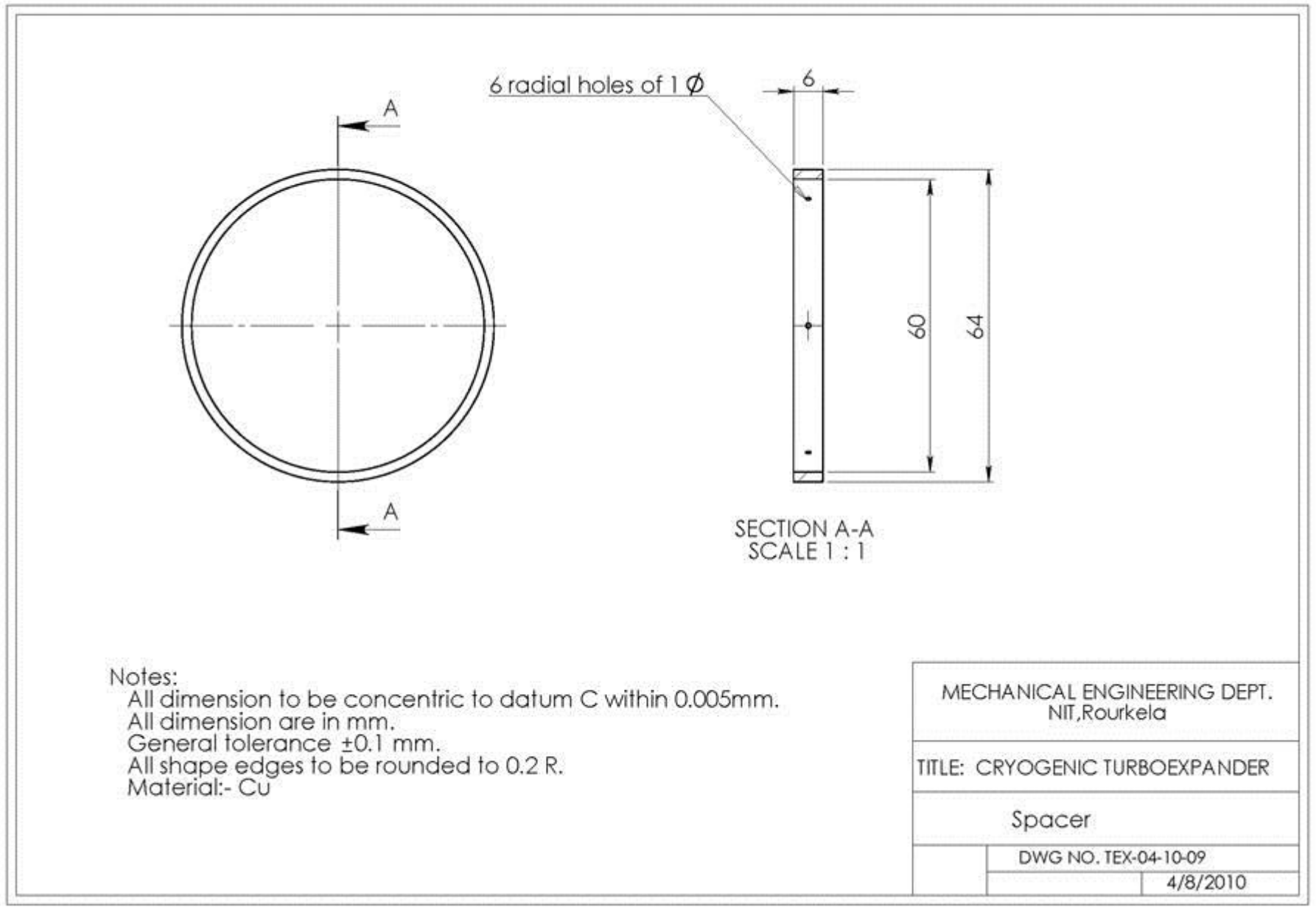

Figure A-11 Spacer

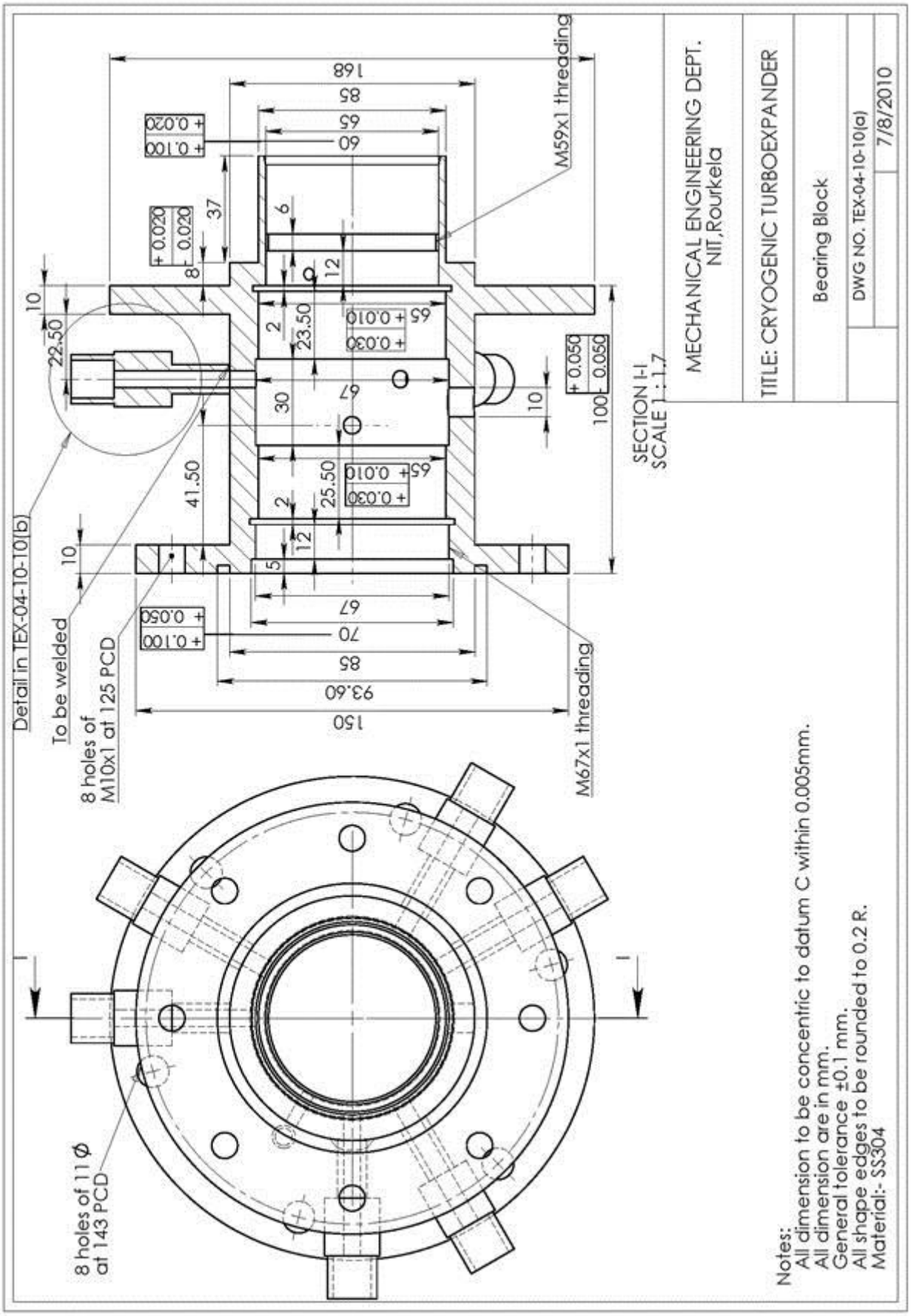

Figure A-12 Bearing block

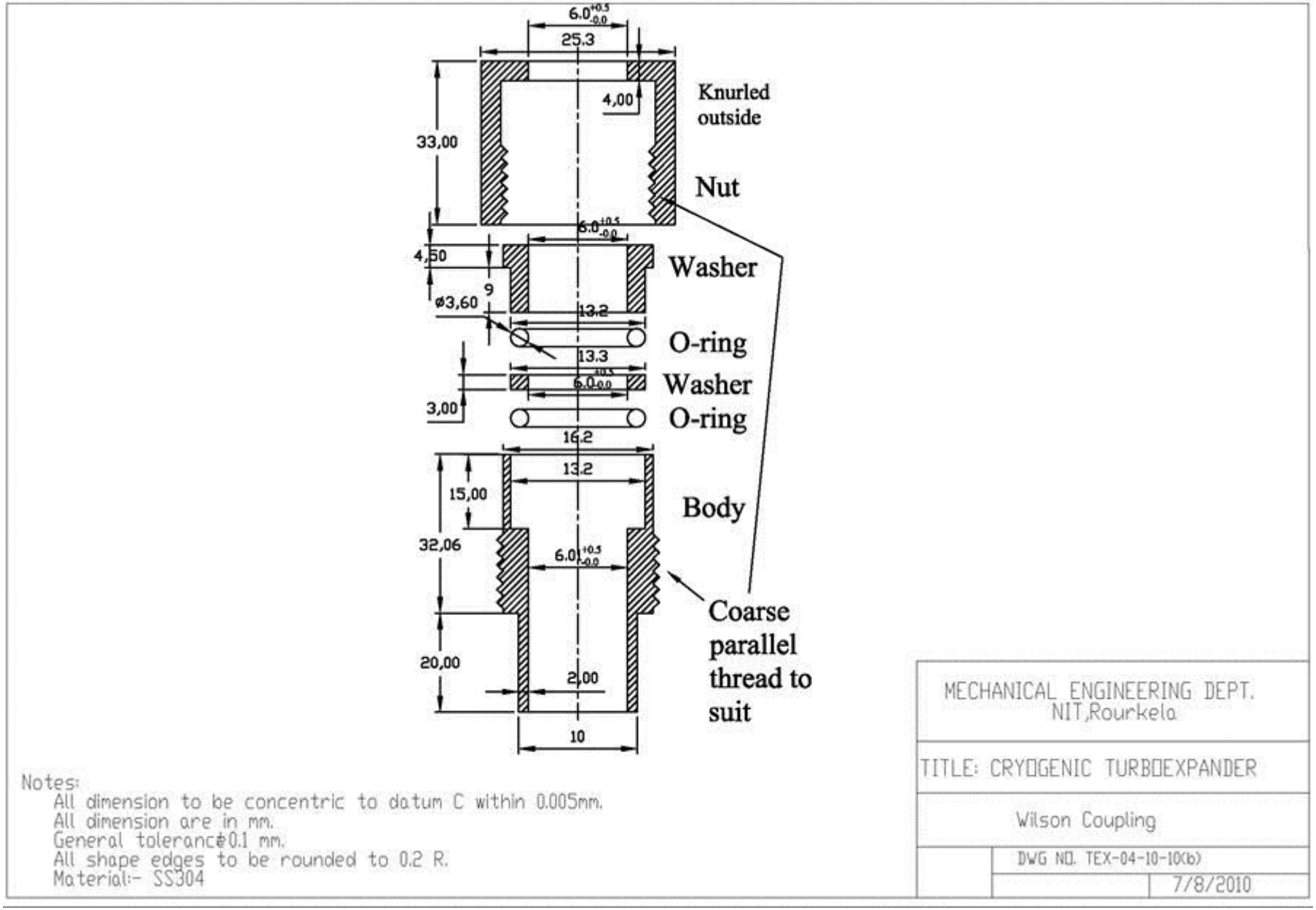

Figure A-13 Wilson coupling

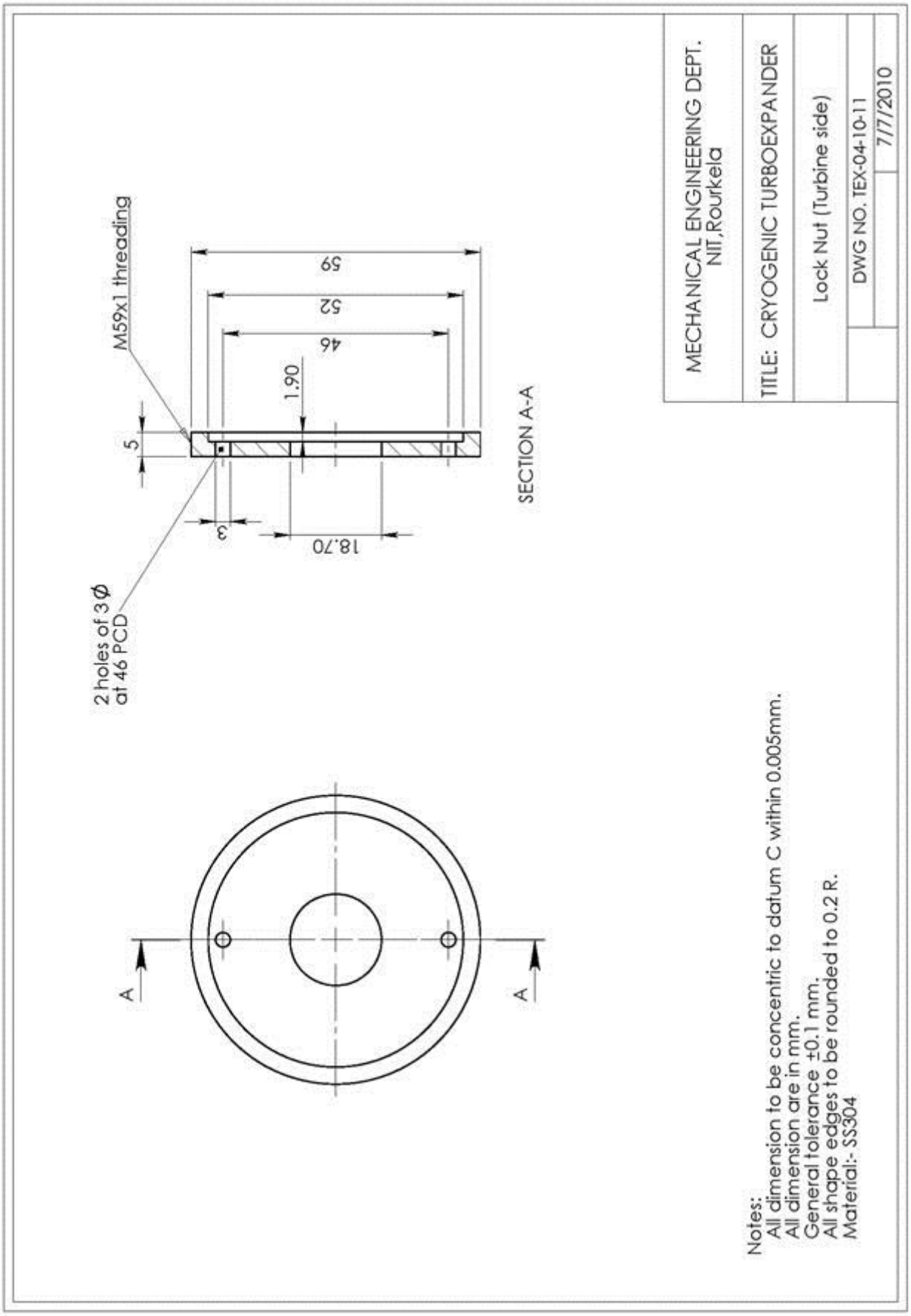

Figure A-14 Lock nut (Turbine side)

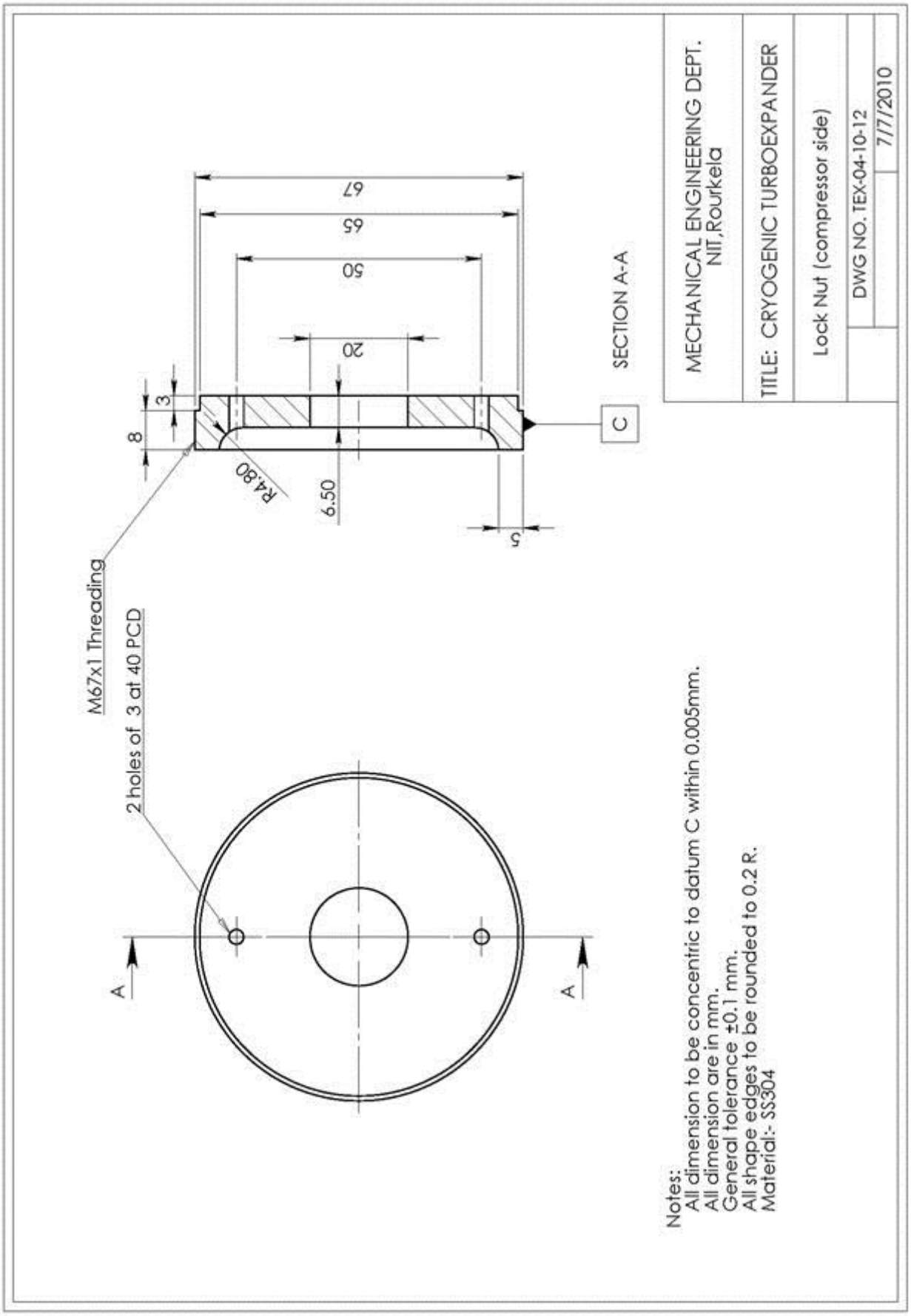

Figure A-15 Lock nut (compressor side)

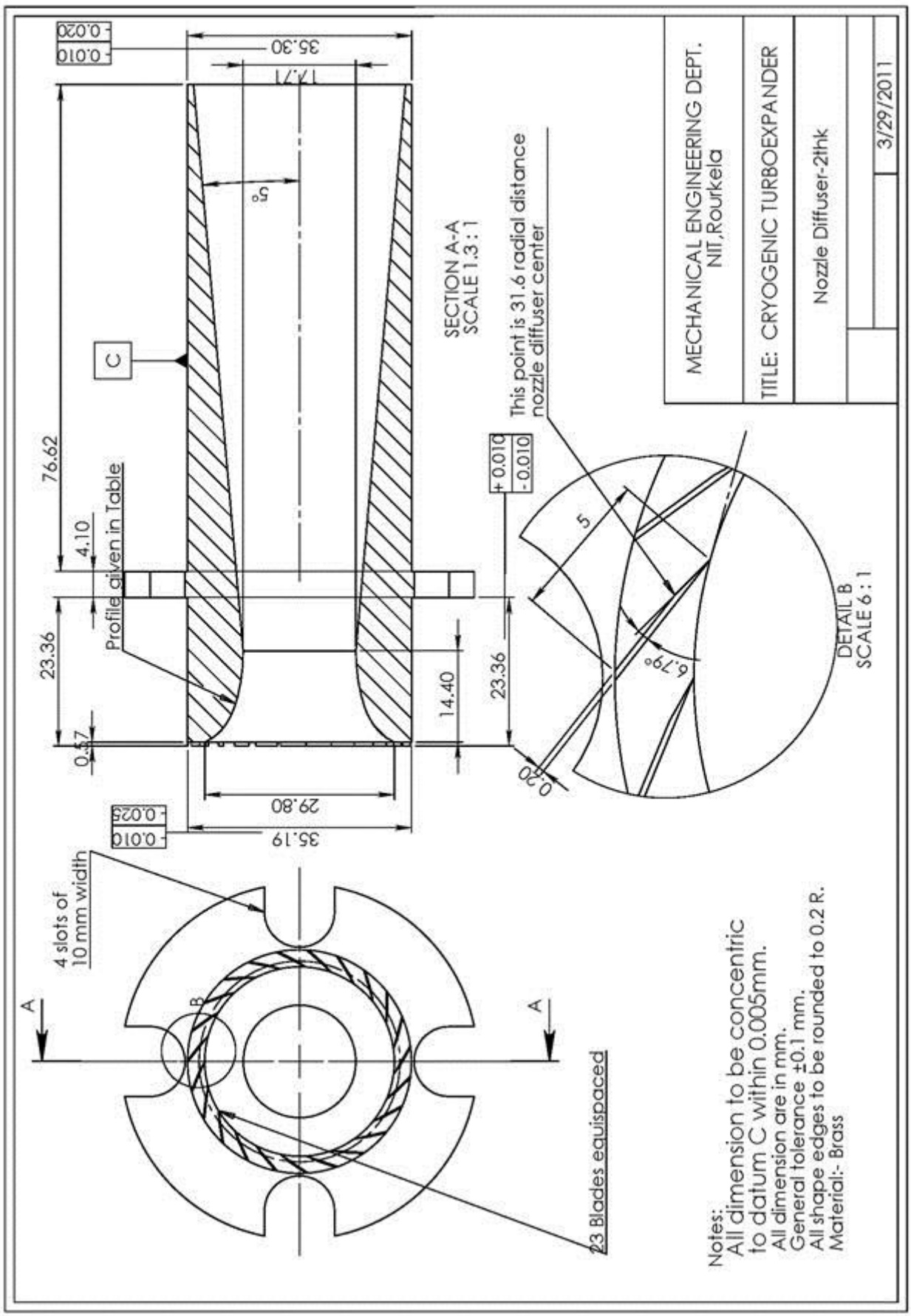

Figure A-16 Nozzle diffuser

Profile of Nozzle Diffuser
(DWG. No. TEX-04-10-13)

Radius r	Height z
8.8534	0
8.8559	0.8446
8.8904	1.6794
8.9504	2.5037
9.0317	3.3175
9.1322	4.121
9.2514	4.9143
9.3896	5.6974
9.5484	6.47
9.7297	7.2314
9.9362	7.9805
10.1712	8.7157
10.4384	9.4349
10.7422	10.1351
11.087	10.8128
11.4776	11.4629
11.9185	12.0796
12.4133	12.6556
12.9643	13.183
13.5711	13.6534
14.2309	14.0596
14.9	14.397

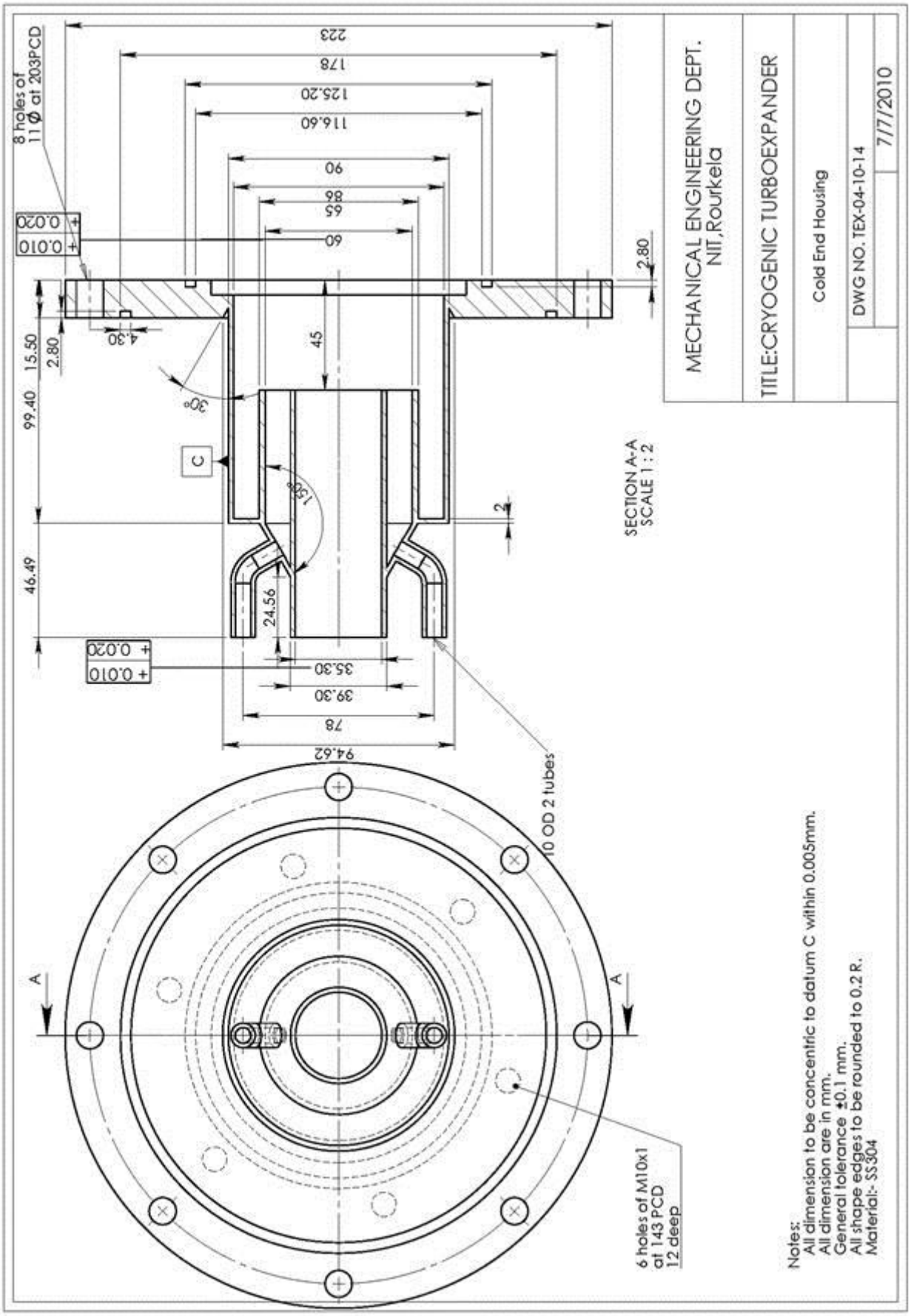

Figure A-17 Cold end housing

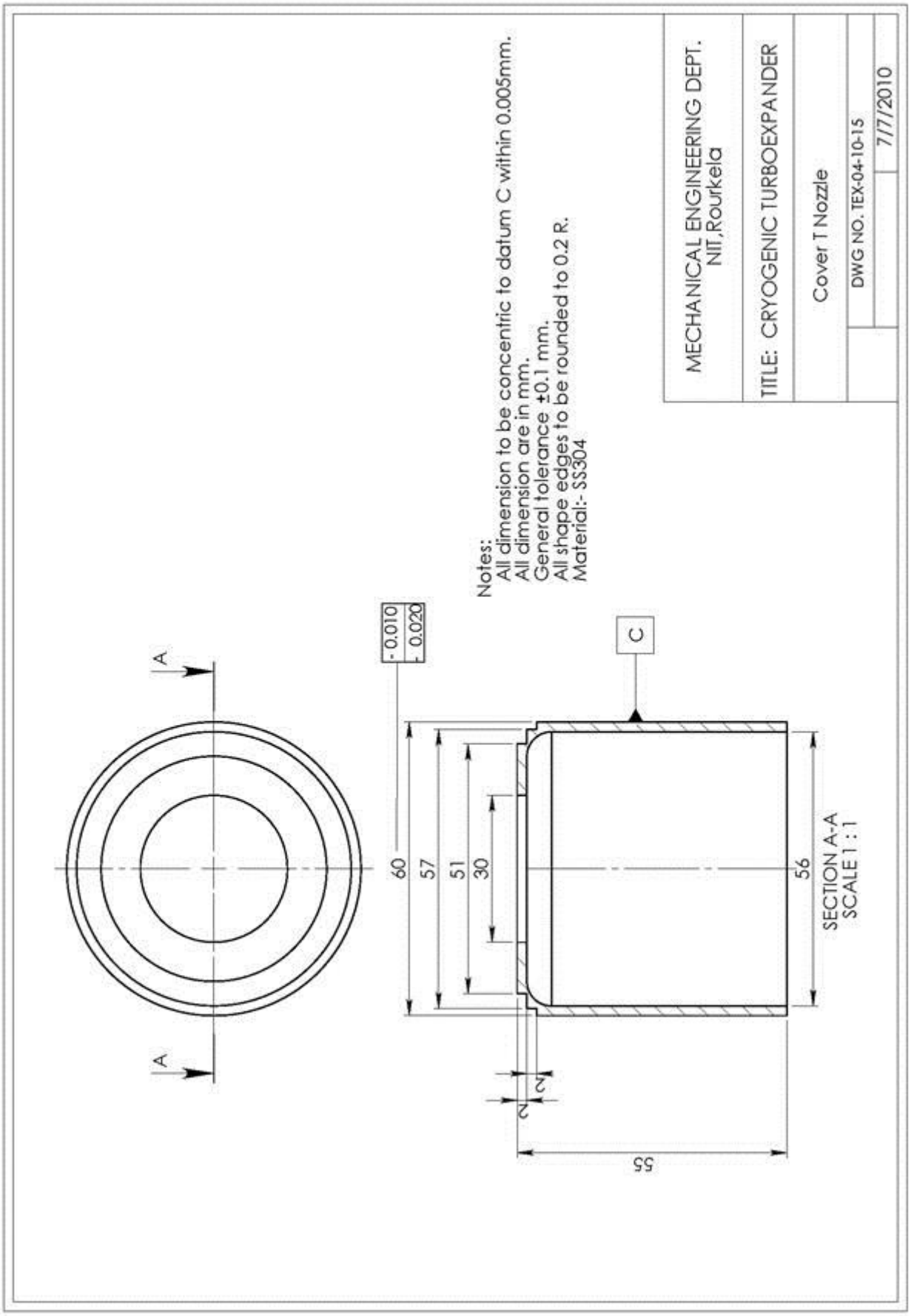

Figure A-18 Nozzle cover

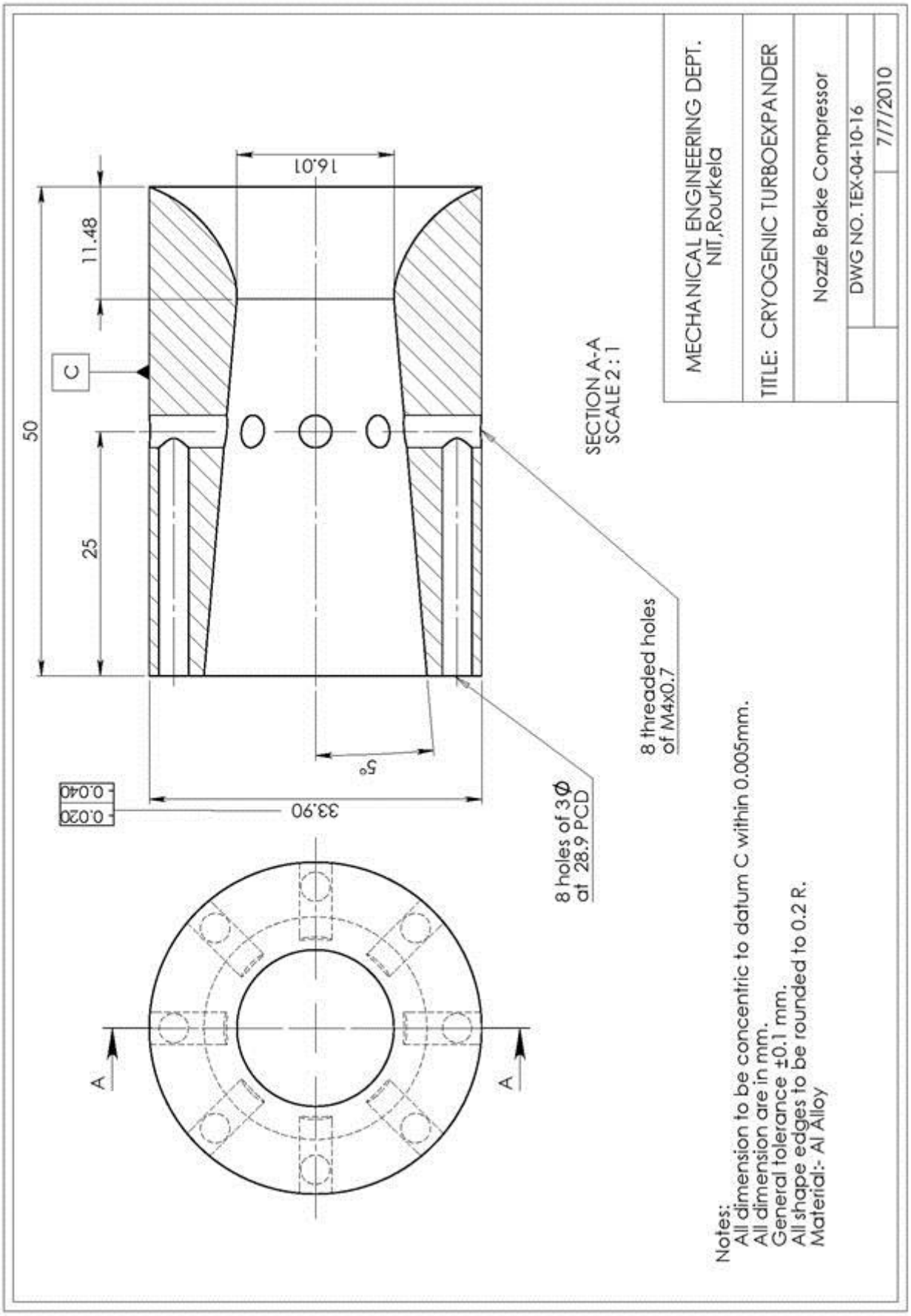

Figure A-19 Nozzle brake compressor

Profile of Nozzle Brake Compressor
(DWG. No. TEX-04-10-16)

Radius r	Height z
7.9149	0
7.9287	0.8616
8.0588	1.6485
8.2581	2.3879
8.5047	3.0935
8.7871	3.7732
9.0993	4.4311
9.4385	5.0696
9.8039	5.6891
10.1958	6.2894
10.6148	6.8694
11.0616	7.4274
11.5368	7.9617
12.0405	8.4704
12.5722	8.9517
13.1306	9.404
13.7143	9.8264
14.3211	10.218
14.9489	10.5787
15.5953	10.9086
16.258	11.2084
16.86	11.479

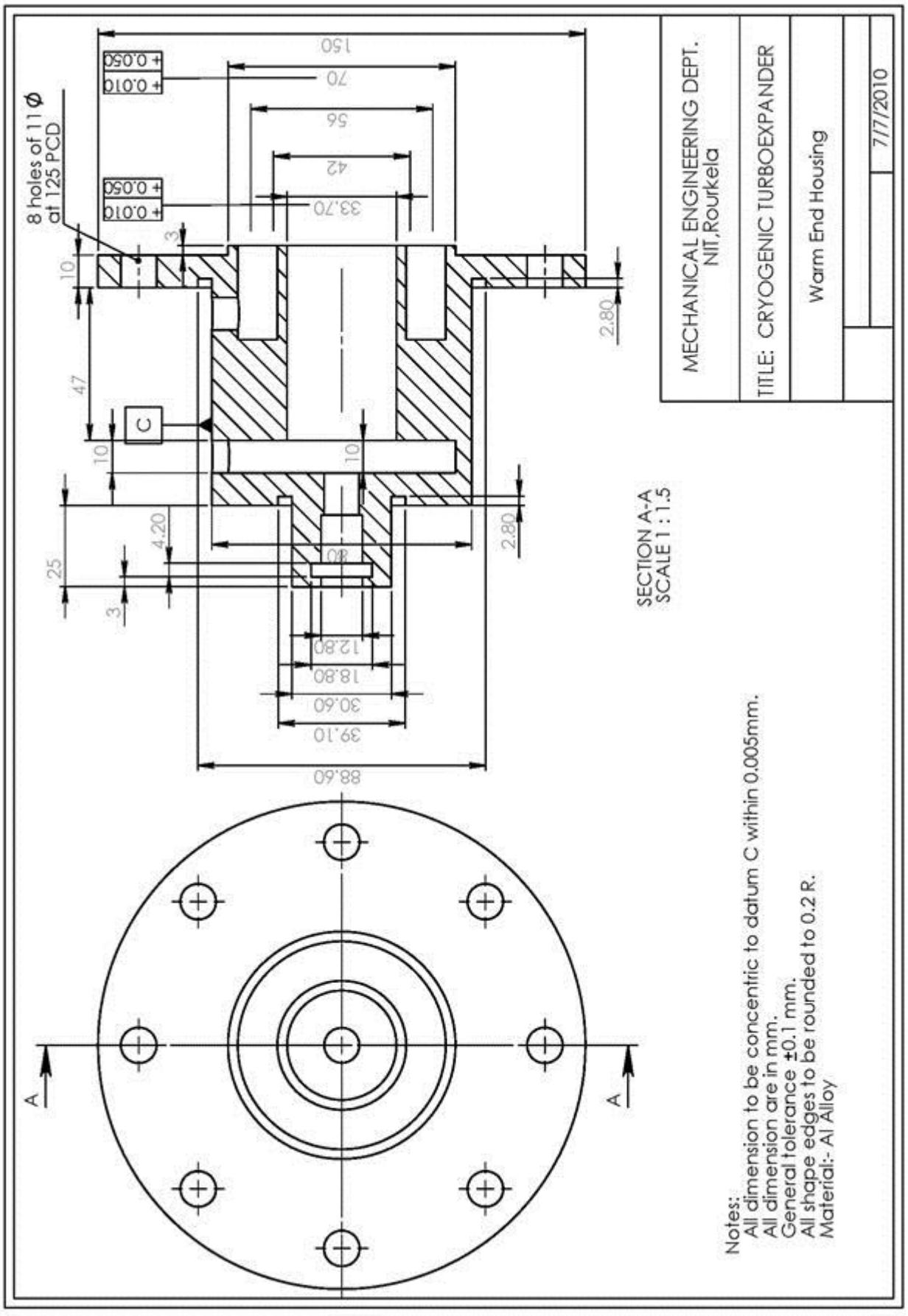

Figure A-20 Warm end Housing

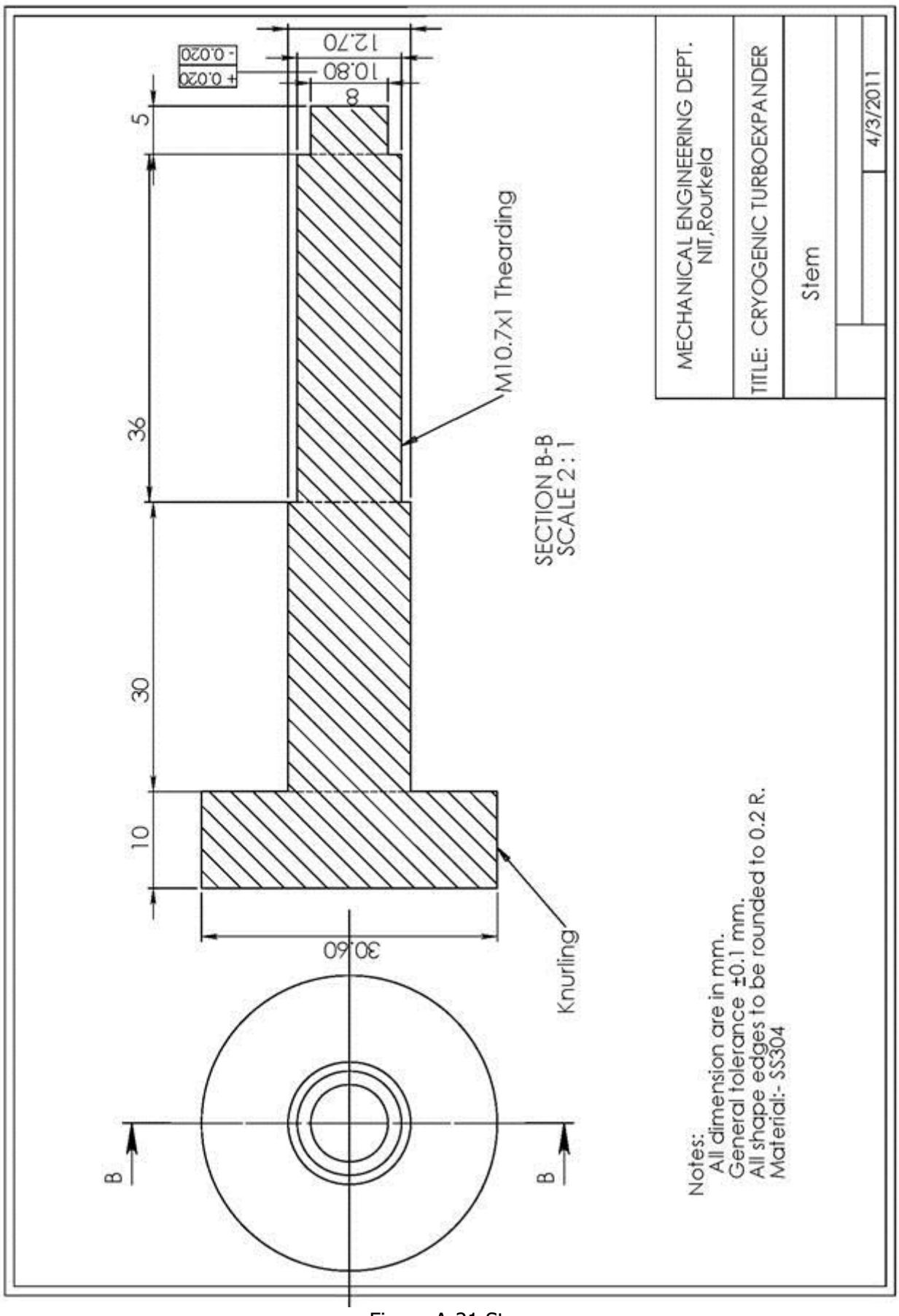

Figure A-21 Stem

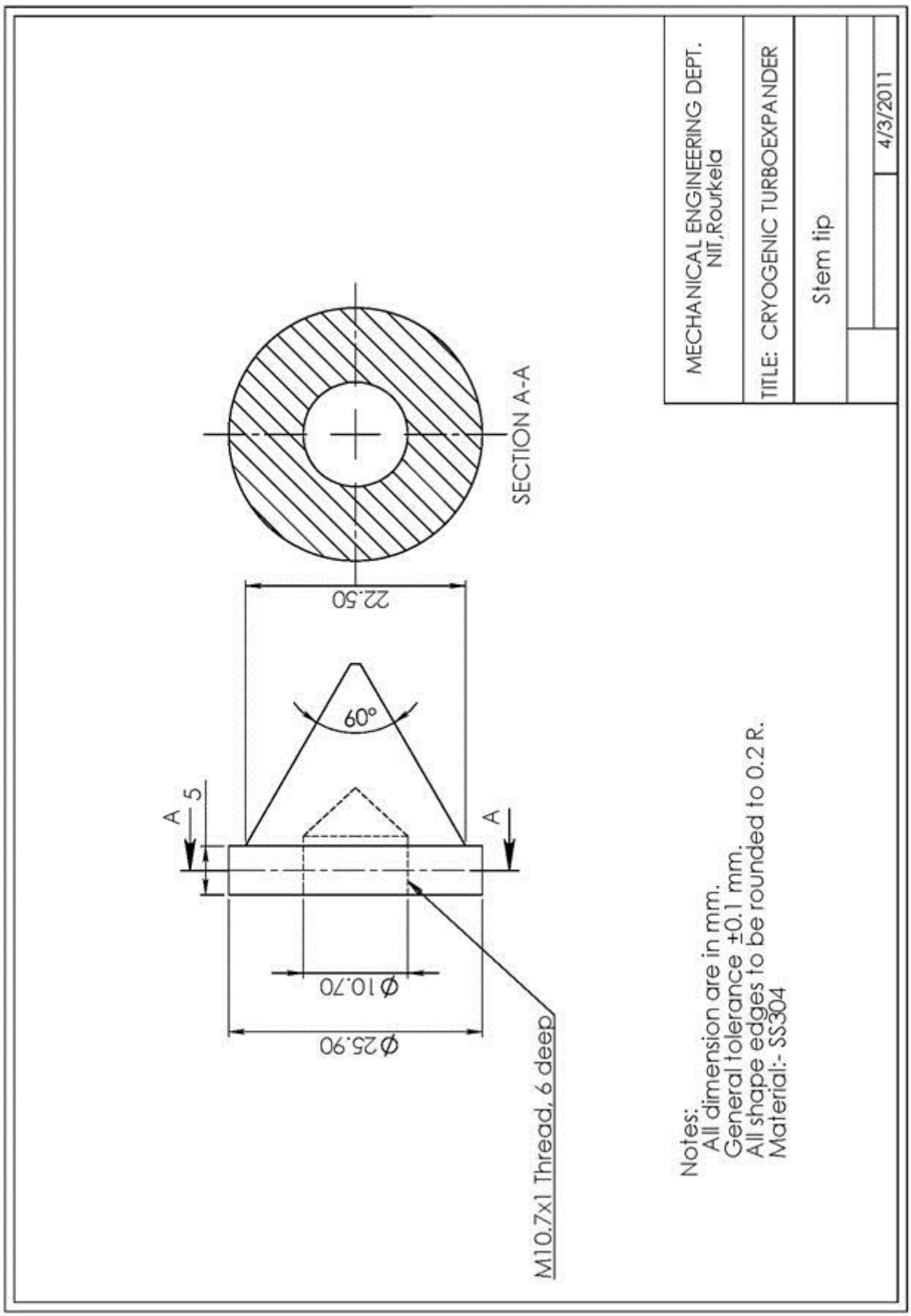

Figure A-22 Stem tip

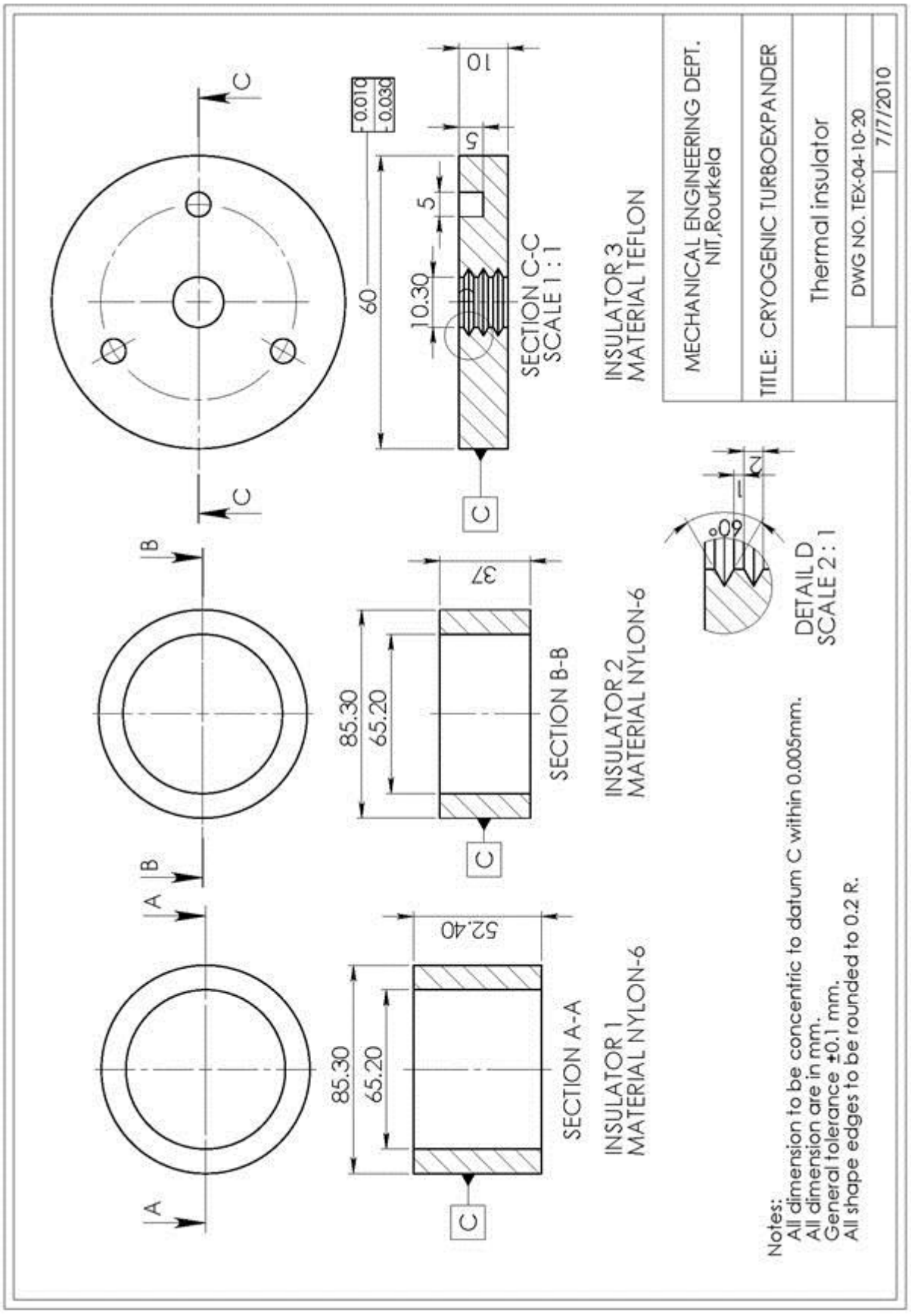

Figure A-23 Thermal insulators

Appendix B

Fabrication Drawings of Heat exchanger

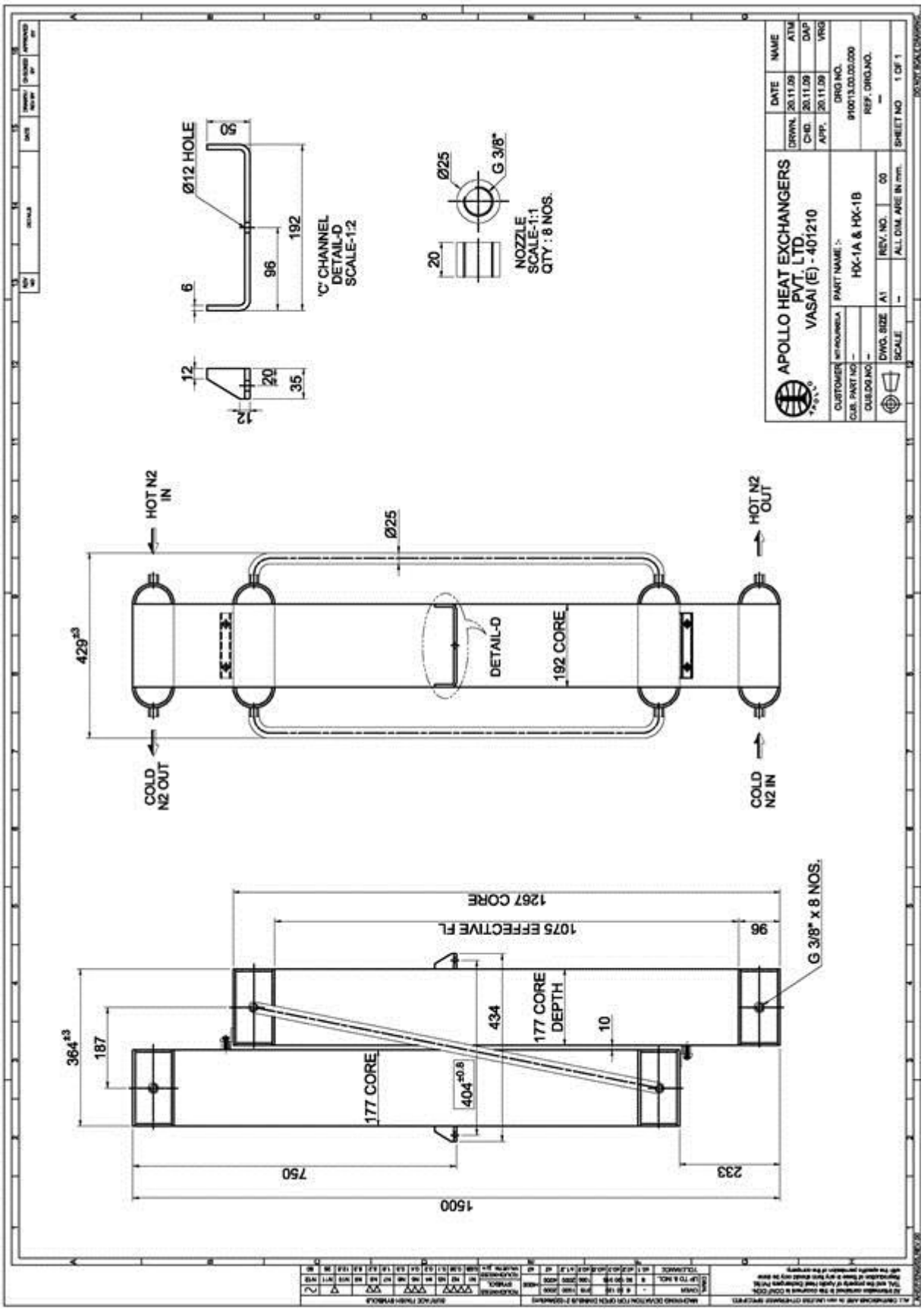

Figure B-1 HX1

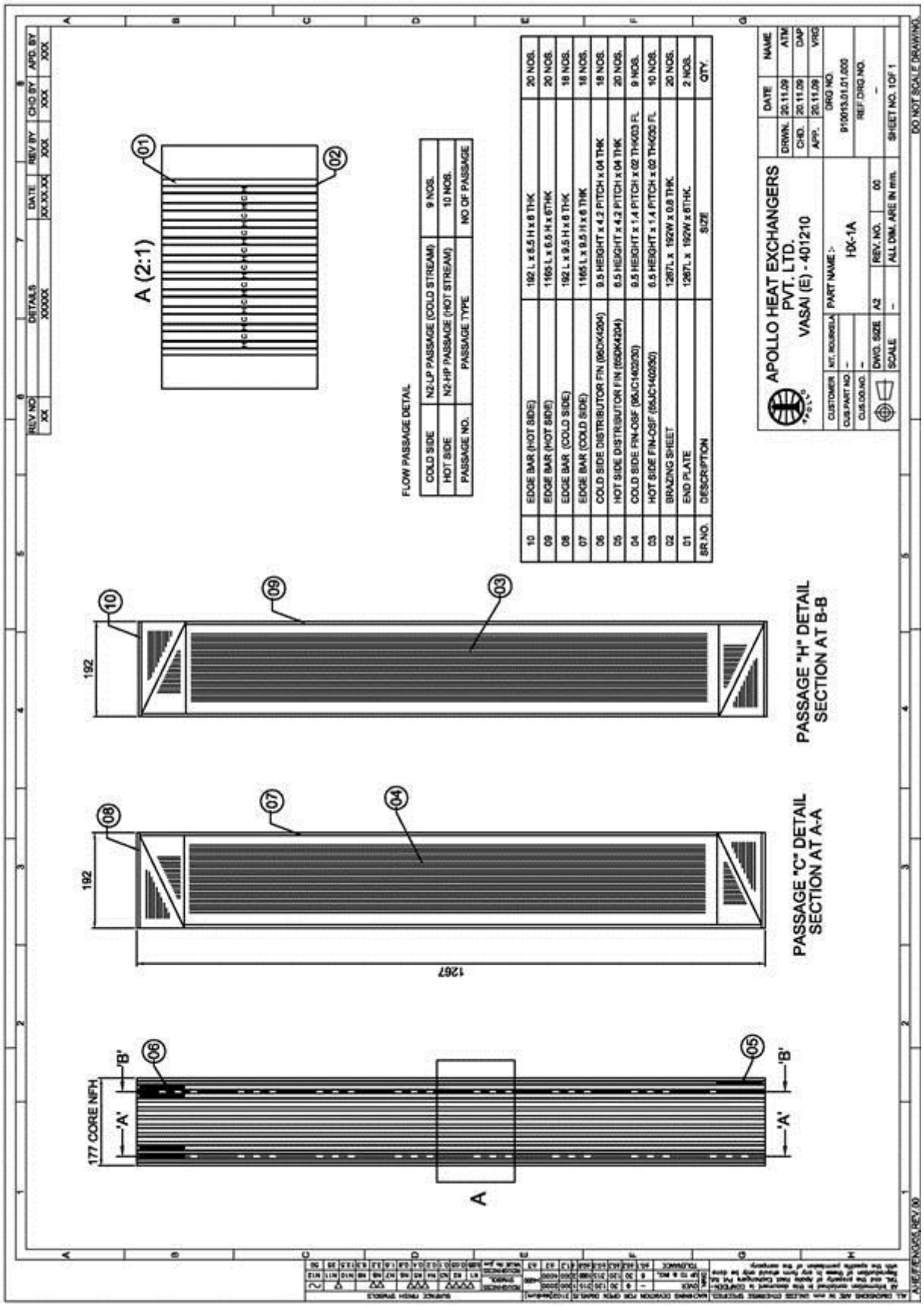

Figure B-2 HX1-A Passage Details

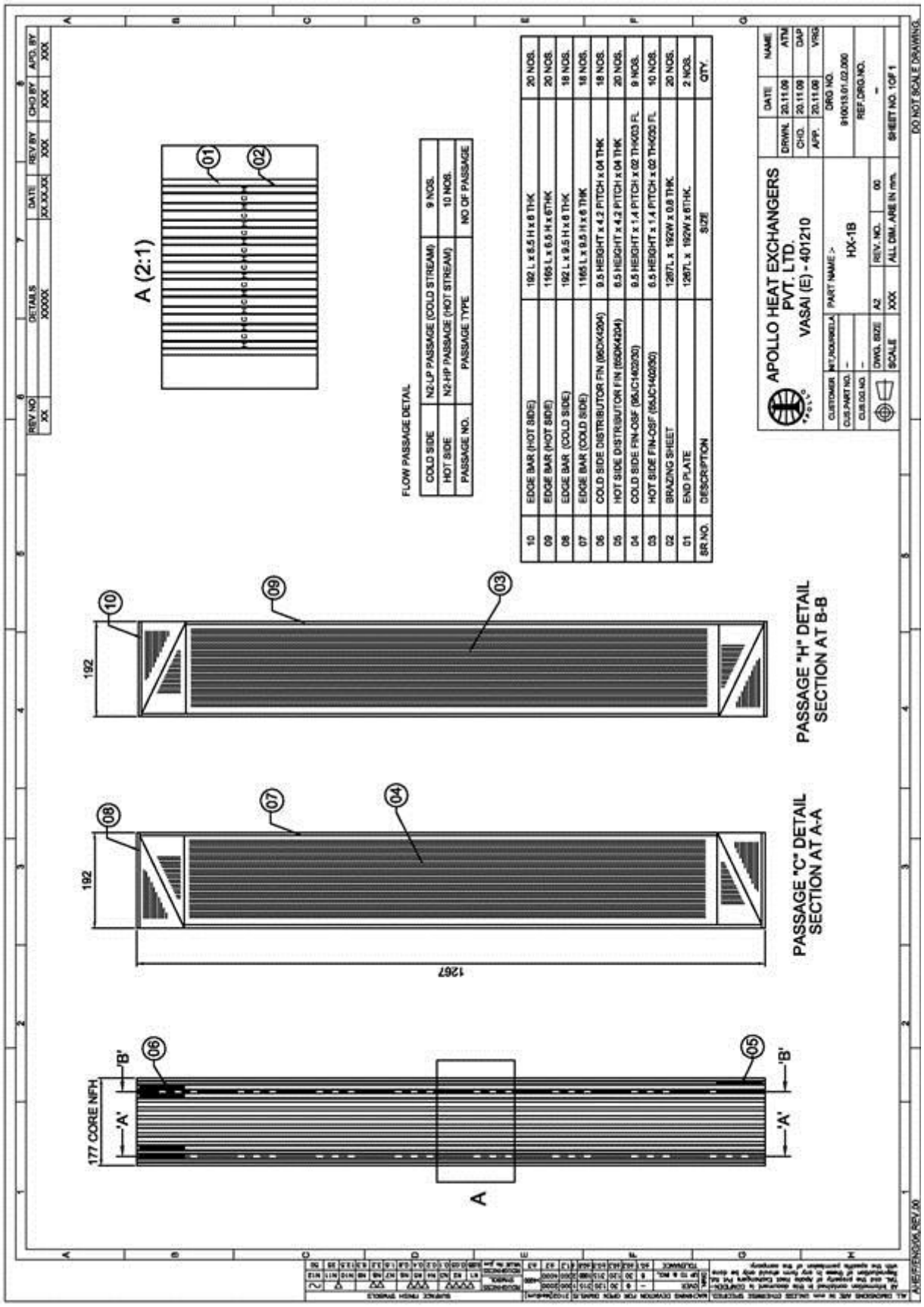

Figure B-3 HX1-B Passage Details

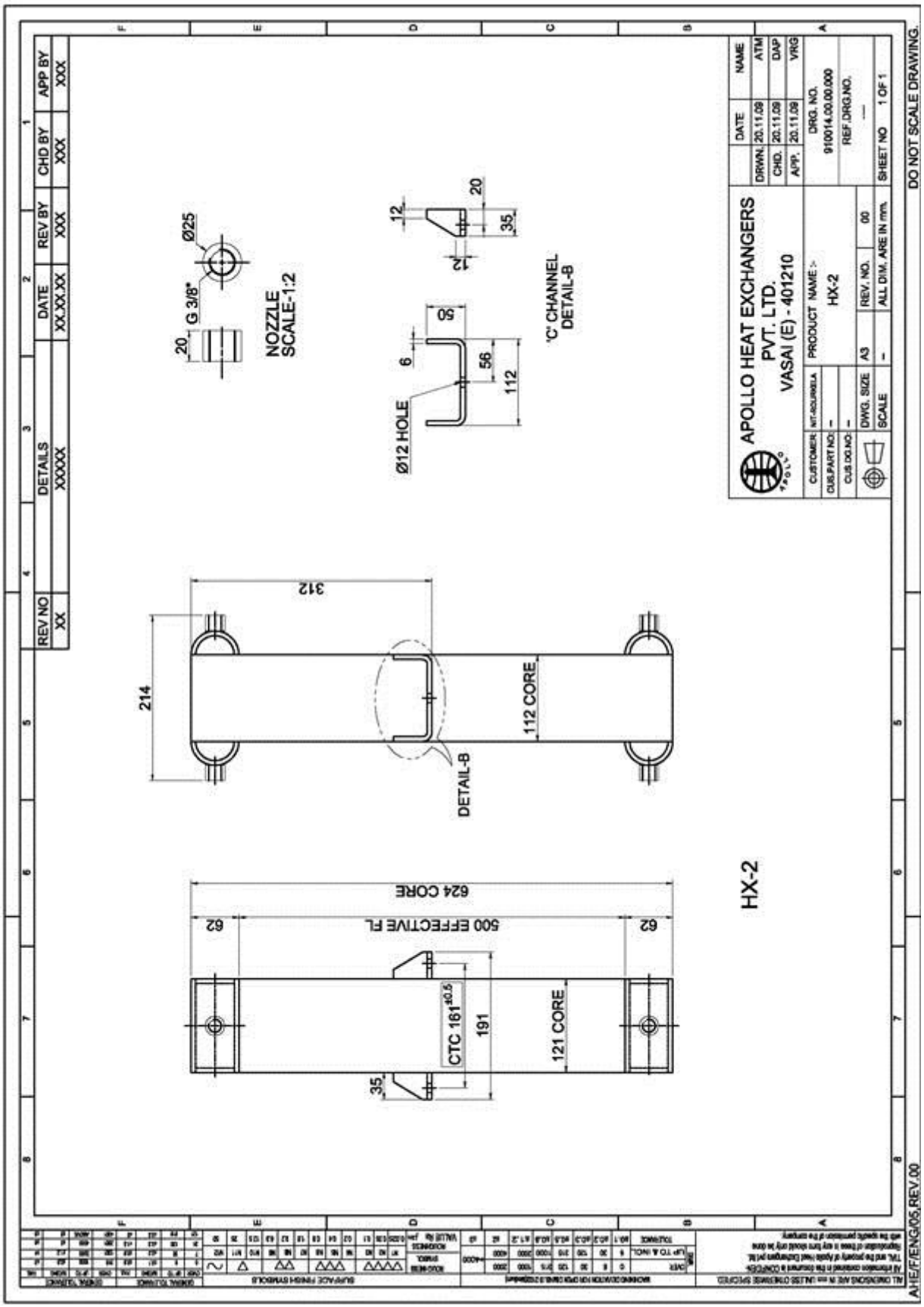

Figure B-4 HX2

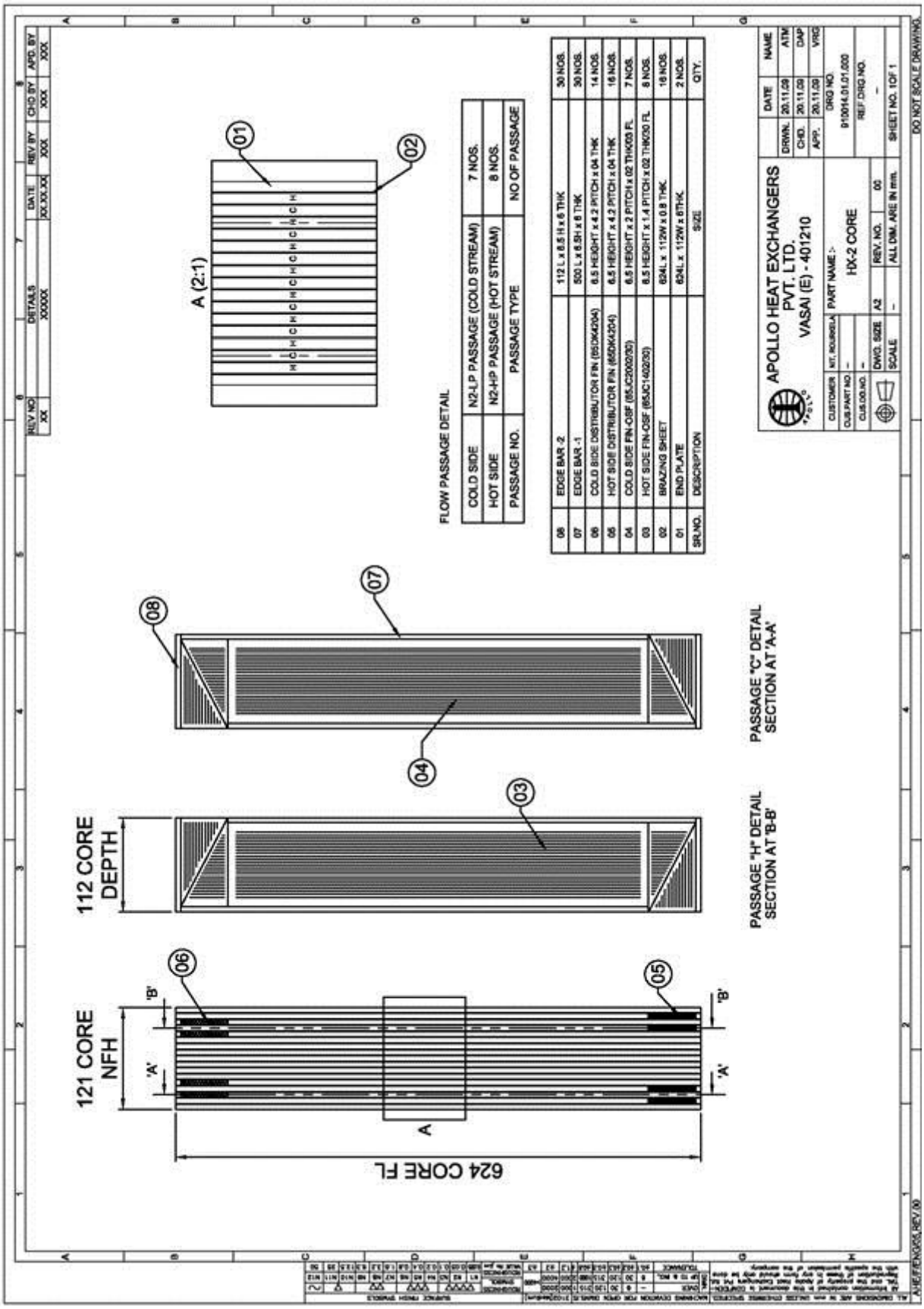

Figure B-5 HX2 Passage Details

Curriculum Vitae

NAME : BALAJI KUMAR CHOUDHURY

E-mail : balajichoudhury@gmail.com

Permenant Address : Salia bandha Street
Gosaninua Gaon
Berhampur-760003
Odisha,India

Education:

2013	Ph.D. Dissertation submitted, NIT Rourkela
2009	M.Tech., NIT Rourkela
2003	B.E., Degree Engg. College S.M.I.T., Ankushpur

Personal Information:

Date of Birth	01-06-1979
Nationality	Indian

Employment:

2006 – 2007 **Lecturer,** S.I.E.T. Dhenkanal

Publications:

1. **Choudhury, B. K., Sahoo, R. K., and Sarangi, S. K.,** Design of Backward Swept Turbine Wheel for Cryogenic Turboexpander, Journal of Engineering Science and Technology, V9(4),2014.
2. **Choudhury, B. K., Sahoo, R. K., and Sarangi, S. K.,** Dynamic Simulation of Modified Claude Cycle, Proceedings of the 24th National Symposium on Cryogenics, January 22-24, 2013., IPR, Ahmedabad, India.
3. **Choudhury, B. K., Alur, S. A., Sahoo, R. K., and Sarangi, S. K.,** Optimization Analysis of Liquefaction Cycles for Nitrogen, Indian Journal of Cryogenics, volume 37No(1-4), pp 34, 2012.
4. **Alur, S. A., Choudhury, B. K., Sahoo, R. K., and Sarangi, S. K.,** Performance Analysis of Plate Fin Heat Exchangers, Asian conference on Applied Super conductivity and Cryogenics November 16-18, 2011, I.U.A.C, .New Delhi.
5. **Alur, S. A., Choudhury, B. K., Sahoo, R. K., and Sarangi, S. K.,** Simulation of Turboexpander Based Nitrogen Liquefier. Proceedings of the 20th National and 9th International ISHMT-ASME Heat and Mass Transfer Conference, January 4-6, 2010, Mumbai, India.

6. **Choudhury, B. K., Alur, S. A., Sahoo, R. K., and Sarangi, S. K.,** Design of High Expansion Ratio Turboexpander for Nitrogen Liquefier. Proceedings of the 3rd International Conference on Advances in Mechanical Engineering, January 4-6, 2010., S.V. National Institute of Technology, Surat, India.
7. **Choudhury, B. K., Rout, S. K., Sahoo, R. K., and Sarangi, S. K.,** Optimization analysis of turbine wheel for cryogenic turboexpander, Experimental heat Transfer (Communicated)